COHERENT COOPERATIVE RADIATION PROCESSES IN SOLIDS

COLLEGE OF ENGINEERING

DEPARTMENT OF ELECTRICAL ENGINEERING AND COMPUTER SCIENCE

UNIVERSITY OF MICHIGAN, ANN ARBOR, MICHIGAN

FINAL TECHNICAL REPORT
(8/1/91 - 3/31/95)

Grant No. AFOSR-91-0369
Principal Investigator: Professor S. C. Rand

AIR FORCE OFFICE OF SCIENTIFIC RESEARCH
Program Manager
Dr. Howard R. Schlossberg

March 31, 1995

REPORT DOCUMENTATION PAGE

Form Approved
OMB No. 0704-0188

1. AGENCY USE ONLY (Leave blank)	2. REPORT DATE	3. REPORT TYPE AND DATES COVERED
	31 Mar 95	Final Report 1 Aug 91 - 31 Mar 95

4. TITLE AND SUBTITLE

Coherent Cooperative Radiation Processes in Solids

5. FUNDING NUMBERS

Grant AFOSR-91-0369

61102F
2301/CS

6. AUTHOR(S)

Stephen C. Rand

7. PERFORMING ORGANIZATION NAME(S) AND ADDRESS(ES)

The Regents of the University of Michigan
DRDA 3003 South State Street
Wolverine Tower, Room 1058
Ann Arbor, MI 48109-1274

8. PERFORMING ORGANIZATION REPORT NUMBER

DRDA 91-1296

9. SPONSORING/MONITORING AGENCY NAME(S) AND ADDRESS(ES)

United States Air Force
Air Force Office of Scientific Research
Building 410
Bolling AFB, DC 20332-0001

NE

10. SPONSORING/MONITORING AGENCY REPORT NUMBER

afosr 91-~~0396~~ 0369

11. SUPPLEMENTARY NOTES

12a. DISTRIBUTION/AVAILABILITY STATEMENT

Approved for public release; distribution unlimited.

12b. DISTRIBUTION CODE

13. ABSTRACT *(Maximum 200 words)*

This program is intended to explore cooperative interactions among rare earth dopants in dielectric solids, with upconversion lasers and nonlinear optical applications in mind. The focus is on fundamental studies of multi-atom upconversion and avalanche processes rather than multi-photon upconversion for new short wavelength lasers. Because of significant potential applications in the areas of short wavelength sources, optical memories, communications, and displays it is important to improve our understanding of cooperative dynamics in regard to their optical and spatial coherence, temporal evolution and relaxation mechanisms.

14. SUBJECT TERMS

upconversion, laser, nonlinear dynamics

15. NUMBER OF PAGES

16. PRICE CODE

17. SECURITY CLASSIFICATION OF REPORT	18. SECURITY CLASSIFICATION OF THIS PAGE	19. SECURITY CLASSIFICATION OF ABSTRACT	20. LIMITATION OF ABSTRACT
UNCLASSIFIED	UNCLASSIFIED	UNCLASSIFIED	UL

NSN 7540-01-280-5500

Standard Form 298 (Rev. 2-89)
Prescribed by ANSI Std. 239-18
298-102

DISCLAIMER NOTICE

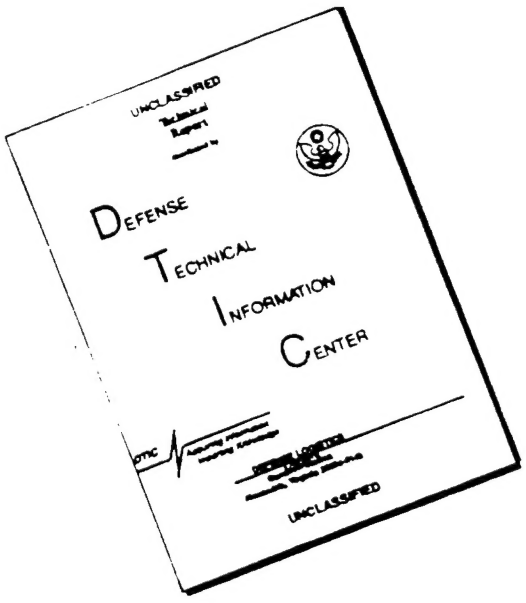

THIS DOCUMENT IS BEST QUALITY AVAILABLE. THE COPY FURNISHED TO DTIC CONTAINED A SIGNIFICANT NUMBER OF PAGES WHICH DO NOT REPRODUCE LEGIBLY.

FINAL TECHNICAL REPORT

"COHERENT COOPERATIVE RADIATION PROCESSES IN SOLIDS"
(November 1, 1993 - March 31, 1995)

PROJECT DESCRIPTION

This program is intended to explore cooperative interactions among rare earth dopants in dielectric solids, with upconversion lasers and nonlinear optical applications in mind. The focus is on fundamental studies of multi-atom upconversion and avalanche processes rather than multi-photon upconversion for new short wavelength lasers. Because of significant potential applications in the areas of short wavelength sources, optical memories, communications, and displays it is important to improve our understanding of cooperative dynamics in regard to their optical and spatial coherence, temporal evolution and relaxation mechanisms.

FINAL YEAR SUMMARY

In the final year of this three-year project, the first observations of ultrafast dephasing on cooperative transitions were made and optical switching mediated by both cooperative upconversion and avalanche interactions was reported for the first time. The latter work in particular represented a breakthrough in experimental control over nonlinear interactions in dense media, revealing that excited state dipole-dipole interactions can enhance the Lorentz local field in dense media in a very fundamental way, and even cause intrinsic bistability. The coherent transient experiments revealed previously unknown dynamics associated with the avalanche effect, important for a full understanding of the behavior of avalanche upconversion lasers.

Near the beginning of the third year of this project, the experimental and theoretical effort turned to the problem of careful characterization of nonlinear dynamics in cooperative interactions. Two main tasks were undertaken, namely direct measurements of dephasing on an avalanche transition using sub-picosecond pulses, and the observation of optical switching and instabilities mediated by electromagnetic coupling between atoms in dense media.

On the topic of dephasing it was shown that polarization of avalanche transitions in Tm:$LiYF_4$ and Tm:$YAlO_3$ decayed on an unexpectedly fast timescale. In $YAlO_3$, coherence decayed in 60 ps or less at low temperatures, and in $LiYF_4$ dephasing was too rapid to be resolved with 700 fs pulses below temperatures of 70K. Detailed measurements of T_2 versus temperature in Tm:$YAlO_3$ were analyzed using the known temperature dependences of various dephasing mechanisms to show that relaxation proceeded by a direct phonon emission process induced in the excited state by the avalanche itself. These dynamics have not been reported previously, and strongly affect the depletion of the lower avalanche level. For this reason our findings are important in the context of upconversion lasers. Similar considerations should apply to the dynamics responsible for fast decay in Tm:$LiYF_4$ but shorter pulses will be required in future measurements to verify this.

On the topic of optical switching, the first experiments attempting to demonstrate all-optical switching mediated by avalanche or other cooperative interactions were performed. A self-pulsing instability was generated in a thin disk of Tm:$LiYF_4$ when excited at the avalanche transition in the red spectral region inside an enhancement cavity. Losses in the external

cavity were minimized by working with a 100 μm thick sample mounted inside at Brewster's angle. A Drever-Pound frequency-offset locking scheme was implemented to permit observations at arbitrary detunings of the cavity from laser resonance, and transmission measurements versus time were then made. The periodic transmission maxima observed in these experiments were explained as arising from an avalanche nonlinearity opposed by a competing thermal nonlinearity. These results constitute the first reports of cavity-enhanced switching in an avalanche medium.

In parallel with these developments, it was also discovered that intrinsic bistability resulted from cooperative emission in crystals of Yb^{3+}:CsY_2Br_9 at low temperatures. Green upconversion luminescence intensity was measured versus temperature and versus input power. In this way abrupt steps in emission were noticed which were qualitatively reproduced by rate equations provided specific assumptions were made about temperature dependences of upconversion and migration coefficients. However this phenomenological approach gave no suggestions regarding the basic origin of the observed switching and considerable effort was expended developing a complete density matrix theory of this effect. One of the greatest successes of this program to date was the demonstration that a density matrix treatment, and more specifically a correct treatment of dephasing interactions, was necessary to obtain complete agreement with experiments. The density matrix theory revealed that fundamental roles of upconversion and migration interactions in the excited state were opposite. Resonant migration tended to suppress optical hysteresis, whereas upconversion generated it.

The data also confirmed that the mechanism responsible for intensity-dependent optical switching was an enhancement by upconversion of the implicit nonlinearity in optical response of all media caused by the difference between the local field and the input electric field of the light. That is, our experiments established for the first time that excited state dipole-dipole interactions can have a profound effect on the Lorentz field of all media, particularly dense media.

SECTION 1

PUBLICATIONS TO DATE

1. H. Ni and S. C. Rand, "Avalanche Upconversion in Tm:YALO," *Opt. Lett.* 16, 1424 (1991).

2. D. Redman, S. Brown, R. Sands and S. C. Rand, "Spin Dynamics and Electronic States of N-V Centers in Diamond," *Phys. Rev. Lett.* 67, 3420 (1991).

3. D. Redman, S. Brown and S. C. Rand, "Origin of Persistent Hole-Burning of N-V Centers in Diamond," *J. Opt. Soc. Am.* B 9, No. 5, (1992).

4. D. Redman, Q. Shu, S. W. Brown, A. Lenef, Y. Liu, J. Whitaker, S. C. Rand, S. Satoh, K. Tsuji and S. Yazu, "Electronic Structure of N-V Centers and Terahertz Spectroscopy of Diamond," AIP Proceedings Volume (1992).

5. D. Redman, Q. Shu, A. Lenef, and S. C. Rand, "Two-Beam Coupling by Nitrogen-Vacancy Centers in Diamond," *Opt. Lett.* 17, 175 (1992).

6. P. Xie and S. C. Rand, "Astigmatically-Compensated, High Gain Cooperative Upconversion Laser," *Appl. Phys. Lett.* 60, 3084(1992).

7. P. Xie and S. C. Rand, "Visible Cooperative Upconversion Laser," *Opt. Lett.* 17, (1992).

8. H. Hi, Q. Shu, and S. C. Rand, "Observation of the Cooperative Kerr Effect," *Phys. Rev. Lett.* (in preparation).

9. H. Ni and S.C. Rand, "Avalanche Phase Conjugation", Opt. Lett. 17, No. 17(1992).

10. P. Xie and S.C. Rand, "Cw Mode-locked Visible Upconversion Laser", Opt. Lett. 17, No. 16(1992).

11. P. Xie and S.C. Rand, "Nonlinear Dynamics of Cooperative Upconversion", J.O.S.A. B 11, 901(1994).

12. P. Xie and S.C. Rand, "Continuous-wave, four-fold Upconversion Laser", Appl. Phys. Lett. 63, 3125(1993).

13. Q. Shu, H. Ni and S.C. Rand, "Avalanche Two-beam Coupling", Optics Letters (submitted).

14. Q. Shu, S.W. Brown, J. Bretz, S.C. Rand, L.-Q. Zhang and M. Bretz, "Intersystem Crossing of C_{60}: Ulltrahigh Resolution Differential Transmission Spectroscopy", Opt. Lett. (submitted).

15. A. Lenef, S.W. Brown, and S.C. Rand, "Implications of Zeeman Coherence and Quantum Beats in Ultrafast Photon Echoes of N-V Centers in Diamond", Phys. Rev. Lett. (in preparation).

16. A. Lenef, D. Kreysar, K. Obermyer and S.C. Rand, "Laser-induced Collisional Avalanche in Atomic Cesium", Phys. Rev. Lett. (submitted).

17. S.C. Rand, A. Lenef, and S.W. Brown, "Zeeman coherence and quantum beats in ultrafast photon echoes of N-V centers in diamond", J. Luminescence 60&61, 739(1994).

18. A. Lenef and S.C. Rand, "Tunneling Dynamics of Squeezed States in a Potential Well", Phys. Rev. A 49, 32(1994).

19. M. Hehlen, H.U. Gudel, J. Rai, S. Rai Q. Shu and S. Rand, "Cooperative Bistability in Dense, Excited Atomic Systems", Phys. Rev. Lett. 73, 1103(1994).

20. M. Hehlen, H. Gudel, Q. Shu and S.C. Rand, Cooperative Bistable Dynamics in Yb^{3+}:CsY_2Br_9", Phys. Rev. B (in preparation).

21. H. Ni and S.C. Rand, "Avalanche Beam Propagation", Opt. Lett. (in preparation).

22. S.C. Rand (invited), Diamond Lasers", in *Properties and Growth of Diamond*, ed. G. Davies, Iinstitution of Electrical Engineers (Br.), London, United Kingdom, 1994, pp. 235-239.

23. I. McMichael, R. Saxena, T.Y. Chang, Q. Shu, S.C. Rand, J. Chen and H. Tuller, High Gain Nondegenerate Two-wave Mixing in Cr:$YAlO_3$", Opt. Lett. (submitted).

GRADUATE STUDENTS SUPPORTED:

(Fall '91 - Fall'93)
TOTAL NO. GRAD STUDENTS WHO RECEIVED AFOSR SUPPORT= 10
H. Ni-Physics-Ph.D. Degree 1994
A. Lenef-Applied Physics-Ph.D. Degree 1993
S. Brown-Applied Physics-Ph.D. Degree 1994
Qize Shu-Applied Physics-Candidate
Ping Xie-Applied Physics-Ph.D. Degree 1992
D. Kreysar-Applied Physics-M.Sc. Degree 1993
S. Kidner-Physics-Ph. D. 1994 (co-chair)
Lih-Mei Yang-Physics-Candidate
Dave Redman -EECS-Ph.D. Degree 1991
K. Obermyer-Physics-Pre-candidate

THESES:

1. D.A. Redman, "Electronic Structure of the Nitrogen-Vacancy Color Center in Diamond", Ph. D. Dissertation, University of Michigan, 1991.

2. P. Xie, "Continuous-wave Cooperative Upconversion Lasers", Ph. D. Dissertation, University of Michigan, 1992.

3. A. Lenef, "Ultrafast Photon Echo Spectroscopy of Luminescent Centers: N-V:Diamond and Tm^{3+}:$YAlO_3$", Ph. D. Dissertation, University of Michigan, 1993.

4. H. Ni, "Avalanche Upconversion in Tm:$LiYF_4$, Tm:$YAlO_3$ and Tm:YAG", Ph.D. Dissertation, University of Michigan, 1994.

5. S.W. Brown, "Electronic Structure of Luminescent Centers in Wide Bandgap Semiconductors", Ph. D. Dissertation, University of Michigan, 1994.

6. S. Kidner, "Ion-assisted, Sputter Deposition and Structural Characterization of Cubic Boron Nitride", Ph. D. Dissertation, University of Michigan, 1994.

PATENTS:

Continuous-wave, pair-pumped laser (Patent No.5,116,437).
Continuous-wave, trio-pumped laser (Patent No. 5,038,358).
Four-fold and Higher Order, Continuous-wave Upconversion Lasers (Patent No.5,289,481).
Mode-locked Upconversion Laser Source (Patent No.5,271,058).

INVITED CONFERENCE PRESENTATIONS:

S.C. Rand(invited), "Cooperative Upconversion Lasers and Nonlinear Dynamics", OSA Annual Meeting, Albuquerque, New Mexico, Sept. 20-25, 1992, paper MJ2.

S.C. Rand (invited), "A Hydrogenic Model of the N-V Center in Diamond", Annual Meeting of the American Physical Society, Indianapolis, March 16-20, 1992, paper O29-1.

S.C. Rand (invited), "Upconversion Lasers", French-US Symposium on Laser-Matter Interactions, University of Michigan, Ann Arbor, Michigan, April 29-30, 1993.

S.C. Rand (invited), "Spin Dynamics,Quantum Beats and Electronic States of Luminescent Centers in Diamond", Ann. Mtg. of Fed. Analyt. Chem. and Spectr. Soc. (FACSS'93), Detroit, Michigan, Oct. 17-22, 1993.

OTHER CONFERENCE PRESENTATIONS:

P. Xie and S.C. Rand, "Continuous-wave, pair-pumped Laser", in Advanced Solid State Lasers, Vol. 6, eds. H. Jenssen and G. Dube, Optical Society of America, 1991, pp. 190-191.

D.A. Redman, Q. Shu, S.W. Brown, A. Lenef, Y. Liu, J. Whitaker, S. Rand, S. Staoh, K. Tsuji and S. Yazu, "Electronic States of N-V Centers and Terahertz Spectroscopy of Diamond", Proc. of Mat. Res. Soc., Fall Meeting, Boston, Massachusetts, November 1991, paper G1.5.

P. Xie and S.C. Rand, "Cooperative Nonlinear Dynamics of the 2.8 μm pair-pumped erbium laser, Conference on Lasers and Electro-optics (CLEO'92), Anaheim, California, May 10-15, 1992, paper CFE4.

Q. Shu, S. Brown, A. Lenef, D. Redman, and S.C. Rand, "Nonlinear Dynamics and Electronic States of N-V Centers in Diamond", Ann. Mtg. American Physical Society, Indianapolis, Indiana, March 16-20, 1992, paper I26 8.

S.C. Rand, D. Redman, and S.W. Brown, "Origin of Persistent Hole-burning of N-V Centers in Diamond", American Physical Society, March Meeting, Indianapolis, Indiana, March 16-20, 1992.

A. Lenef and S.C. Rand, "Quantum Beats and Spin Coherences in N-V Centers in Diamond", Ann. Mtg. American Physical Society, Indianapolis, Indiana, March 16-20, 1992, paper I26 9.

S.C. Rand, D.A. Redman and S.W. Brown, "Origin of Persistent Hole-burning of N-V Centers in Diamond", Ann. Mtg. American Physical Society, Indianapolis, Indiana, March 16-20, 1992, paper I26 10.

H. Ni and S.C. Rand, "Spatial Ring Formation in Avalanche Optical Nonlinearities", Ann. Mtg. American Physical Society, Indianapolis, Indiana, March 16-20, 1992, paper O18 - 11.

S.C. Rand, "Nonlinear Dynamics of Upconversion Lasers", Program in Nonlinear Studies, Poster Conference, University of Michigan, Ann Arbor, Michigan, January 19, 1993.

I. McMichael, R. Saxena, T.Y. Chang, R. Neurgaonkar, and S.C. Rand, "High gain, non-degenerate Two-Wave Mixing in Cr:YAlO3", Conf. on Lasers and Electro-optics (CLEO'93), Baltimore, Maryland, May 2-7, 1993, paper CThS34.

H. Ni, Q. Shu and S.C. Rand, "Avalanche Phase Conjugation", Qu. Elect. and Laser Science Conf. (QELS'93), Baltimore, Maryland, May 2-7, 1993, paper QThD5.

A. Lenef, S. Brown, and S.C. Rand, "Quantum Beats in Diamond", Qu. Elect. and Laser Science Conf. (QELS'93), Baltimore, Maryland, May 2-7, 1993, paper QThH35.

S.C. Rand, A. Lenef, and S.W. Brown, "Zeeman Coherence and Quantum Beats in Ultrafast Photon Echoes of N-V Centers in Diamond", Int. Conf. on Lumin. (ICL'93), Storrs, Connecticut, Aug. 9-13, 1993.

S.C. Rand, A. Lenef, and S.W. Brown, "Excited State Structure and Dephasing of Point Defects in Widegap Semiconductors: Ultrafast Four-Wave Mixing Spectroscopy of N-V Centers in Diamond", Tech. Conf. 2041 of Soc. Photo-Optical Instrum. Eng. (S.P.I.E.), Quebec City, Canada, Aug. 16-20, 1993, paper 2041-18.

S.C. Rand, H. Ni, Q. Shu and P. Xie, "Mode-locking Applications of Nonlinear Cooperative Interactions", Tech. Conf. 2041 of Soc. Photo-Optical Instrum. Eng. (S.P.I.E.), Quebec City, Canada, Aug. 16-20, 1993, paper 2041-18.

A. Lenef, D. Kreysar, and S.C. Rand, "Collisional Avalanche in Atomic Cesium", Opt. Soc. of America (OSA'93), Toronto, Canada, Oct. 3-8, 1993, paper MTT7.

A. Lenef and S.C. Rand, "Tunneling Dynamics of Squeezed States in a Potential Well", Opt. Soc. of America (OSA'93), Toronto, Canada, Oct. 3-8, 1993, paper ThL3.

S.C. Rand and P. Xie, "Intrinsic Instabilities of Cooperative Upconversion Dynamics in Lasers", Opt. Soc. of America (OSA'93), Toronto, Canada, Oct. 3-8, 1993, paper WSS5.

S.C. Rand, A. Lenef and D. Kreysar, "Atomic Collisional Avalanche", Eleventh International Conference on Laser Spectroscopy, Hot Springs, Virginia, June 13-18, 1993, paper MP3.

M. Hehlen, H.U. Gudel, J. Rai, S. Rai and S.C. Rand, "Cooperative Bistability in Dense, Excited Atomic Sytems", Int. Qu. Elect. Conf. (IQEC'94), Anaheim, California, May 8-13, 1994, paper QME8.

A. Lenef and S.C. Rand, "Photon Echo Measurements of Optical Dephasing on a Thulium Avalanche Transition", Int. Qu. Elect. Conf. (IQEC'94), Anaheim, California, May 8-13, 1994, paper QMC3.

H. Ni and S.C. Rand, "Temperature Dependence of the avalanche threshold and the cross relaxation rate in Tm:$LiYF_4$", Int. Qu. Elect. Conf. (IQEC'94), Anaheim, California, May 8-13, 1994, paper QTuO5.

I. McMichael, R. Saxena, T.Y. Chang, Q. Shu, S.C. Rand, J. Chen, and H. Tuller, "high gain Non-degenerate Two-Wave Mixing in Cr:$YAlO_3$", OSA Conf. on Nonlinear Optics", Waikoloa, Hawaii, July 25-29, 1994, paper WA5.

INVITED COLLOQUIA:

S.C. Rand, "Coherent Cooperative Radiation Phenomena in Solids", General Colloquium, Dept. of Physics, Alabama A&M, Huntsville, Alabama, June 16, 1992.

S.C. Rand, "Ultrafast and Ultrahigh Resolution Spectroscopy of Diamond", General Colloquium, Dept. of Physics, Alabama A&M, Huntsville, Alabama, June 15, 1992.

S.C. Rand, "Cooperative Nonlinear Dynamics: Upconversion, Bistability, and Delocalization in Rare Earth Systems", General Colloquium, Dept. of Physics, Wayne State University, November 1993.

AWARDS:

1993- The thesis of Ping Xie on "Continuous-wave Cooperative Upconversion Lasers" was awarded the University of Michigan Distinguished Dissertation Award.

1993- The thesis of Ping Xie was awarded the Terwilliger Prize by the Department of Physics of the University of Michigan.

1994- Rackham Dissertation Fellowship for Hui Ni, awarded by the University of Michigan.

1994-PI named Fulbright Scholar by the Fulbright Foundation

1994-PI named a Fellow of the Joint Institute of Laboratory Astrophysics (University of Colorado and JILA).

SECTION 2

REPRINTS
(1993-1994 only)

Nonlinear dynamics of cooperative upconversion

P. Xie* and S. C. Rand

Division of Applied Physics, 1049 Randall Laboratory, University of Michigan, Ann Arbor, Michigan 48109-1120

Received July 15, 1993; revised manuscript received November 29, 1993

We describe several new aspects of light–matter interactions for solids in which interatomic coupling of impurity atoms plays a dominant role in population dynamics. We explore the implications of spatial coherence in such multiatom interactions by introducing a density-matrix theory of cooperative upconversion, focusing on pair systems for which analytic results can be obtained. We predict population pulsations in coherent cooperative upconversion, enhanced quantum efficiency, enhanced energy transfer, and pair-mediated instabilities, not only in cooperative upconversion media without external cavities but in upconversion lasers and conventional lasers in highly doped solids as well. These predictions are compared with rate equation solutions and observations in lasers with inversions sustained by cooperative processes, particularly the 2.8-μm Er laser. Rate equations fail to predict the observed steady-state instabilities of this laser, which are well reproduced by density-matrix theory, furnishing evidence of weak coherent delocalizations in a rare-earth system.

1. INTRODUCTION

Upconversion and energy-transfer processes that occur in solids as a result of nonlinear population dynamics, rather than parametric processes, have been studied for many decades.[1–3] Two classes of nonparametric upconversion that differ in the mechanism responsible for converting long-wavelength radiation incident upon a sample into short-wavelength emission are generally acknowledged. In the first, sequential absorption of incident photons by progressively higher energy levels of a single atom leads to emission from high-lying upconverted states, broadly designated as upconversion emission. In the second, each atom absorbs at most one photon, and energy transfer between atoms is required for upconversion emission. The latter type of process may proceed in one of three ways. In a cooperative process the pooled energy of several coupled atoms can become localized on one particular atom, which then emits light from a high-lying, upconverted state.[3] Or energy may be transferred in a sequence of discrete transfer steps.[1] Another possibility is an avalanche process in which upconversion results from field-induced cross-relaxation dynamics.[4,5] In this paper we confine our discussion to the cooperative upconversion process, highlighting novel experimental and theoretical dynamics that can result from spatial coherence among the coupled atoms or from the interaction of coupled atoms with radiation fields in optical cavities.

Early research on upconversion was motivated by the need to overcome the poor sensitivity of infrared detectors.[6] More recent research on upconversion has been stimulated by the realization that upconversion lasers have potential as practical, solid-state sources of visible and ultraviolet light.[7–13] However, to date, little discussion has been given to certain fundamental aspects of the upconversion processes themselves, such as basic limits to achievable degrees of upconversion and the inherent stability of these highly nonlinear interactions between light and matter.

In this paper we consider these topics, primarily in the context of new experiments with the pair-pumped Er laser, a laser with an inversion sustained purely by pair upconversion.[14] General predictions of enhanced quantum efficiency, enhanced energy transfer, population pulsations, and instabilities mediated by cooperative dynamics are compared with observations of nonlinear dynamics in twofold, threefold, and fourfold upconversion processes.

2. THEORY

A. Enhanced Quantum Efficiency

The general scheme of cooperative upconversion is illustrated in Fig. 1. Two atoms are depicted in an excited state undergoing a pair transition in which one atom is promoted to an upper state while the other descends to the ground state. Multipole or exchange coupling is presumed to furnish the interaction responsible for this pair transition, mediating evolution of the system in a manner somewhat analogous to coupled harmonic-oscillator dynamics. The energy transferred to the second atom rarely matches the precise transition energy required for gaining access to a real final state, but the energy defect can be accommodated in solids by the emission or the absorption of phonons. In solids doped heavily with rare earth or transition-metal impurities, transitions of this kind are common.[2]

A schematic representation of excitation and decay pathways involved in cooperative upconversion is given in Fig. 2. Excitation is initiated by a pumping process at wavelength λ_{in}, which populates level $|3\rangle$ with efficiency η_0. The system subsequently cascades to level $|1\rangle$ in steps with individual branching ratios η_i. Decay to the ground state $|0\rangle$ may then occur, or a cooperative transition of the type indicated in Fig. 1 may take place. The manner in which cooperative upconversion benefits the overall emission at λ_{out} is not immediately obvious because the maximum branching ratio for a single pair upconversion process is 0.5. This seems low from the outset. However, it can readily be appreciated from

0740-3224/94/050901-13$06.00

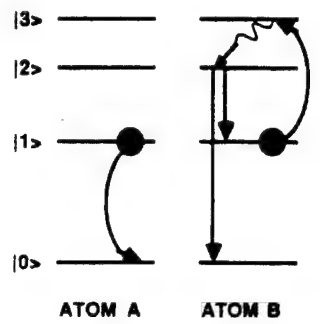

Fig. 1. Dynamics of cooperative upconversion in a system consisting of two four-level atoms initially occupying state $|1\rangle$, as indicated by filled circles. The system relaxes by promoting one atom to level $|3\rangle$ as the second decays to the ground state (curved arrows). In this fashion upconversion fluorescence from energy levels higher than the initial state becomes possible at several wavelengths (straight arrows). The correspondence between levels of the model and Er is as follows: $|0\rangle \leftrightarrow {}^4|_{15/2}$, $|1\rangle \leftrightarrow {}^4|_{13/2}$, $|2\rangle \leftrightarrow {}^4|_{11/2}$, $|3\rangle \leftrightarrow {}^4|F_{9/2}$.

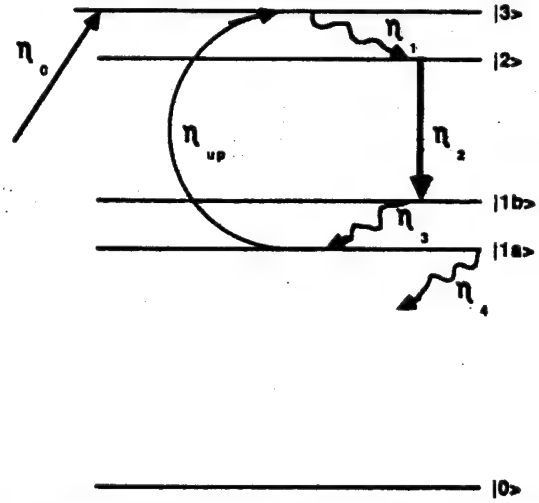

Fig. 2. Recycling by cooperative upconversion. The initial excitation of level $|3\rangle$, either by resonant optical excitation or by a cooperative process, occurs with quantum efficiency η_0. This is followed by a cascade of nonradiative decay and emission processes with individual branching ratios of η_i. States $|1a\rangle$ and $|1b\rangle$ are different Stark components of level $|1\rangle$. Finally a long-lived level is reached in which cooperative upconversion can occur spontaneously without further absorption of photons from the pump field. The remnant excited-state population can be recycled to level $|3\rangle$ and additional photons may be emitted, thereby enhancing quantum efficiency. The radiative transition $|2\rangle \rightarrow |1b\rangle$ is the focus of quantum-efficiency considerations.

Fig. 2 that excited-state population can be recycled through the emission channel if spontaneous upconversion occurs.

To quantify this concept and to show that quantum efficiency of optical emission can be enhanced by the presence of cooperative dynamics, we assume that the cooperative upconversion process can repeat itself n times. The number of sites at which upconversion occurs is taken to be small compared with the number of excited atoms. This ensures that the reservoir of state $|1\rangle$ ions surrounding upconversion sites remains undepleted through many upconversion cycles because of rapid energy migration within the reservoir. Ground-state A atoms at upconversion sites are continually reexcited to state $|1\rangle$ by means of resonant energy transfer from the reservoir, restoring the initial condition shown in Fig. 1 without requiring the absorption of additional photons. For very large n the effective quantum efficiency then becomes

$$\begin{aligned}\eta_{\text{eff}} &= \eta_0\eta_1\eta_2[1 + \eta_3\eta_{\text{up}}P^{(1)}\eta_1\eta_2 \\ &\quad + \eta_3\eta_{\text{up}}P^{(1)}\eta_1\eta_2\eta_3\eta_{\text{up}}P^{(2)}\eta_1\eta_2 + \cdots] \\ &= \sum_{n=0}^{\infty}\eta_0\eta_1\eta_2(\eta_3\eta_{\text{up}}\eta_1\eta_2)^n = \frac{\eta_0\eta_1\eta_2}{1 - \eta_1\eta_2\eta_3\eta_{\text{up}}}. \quad (1)\end{aligned}$$

Here factors $P^{(n)}$ are introduced to account explicitly for the probability of A's being reexcited by energy migration during the nth cycle. Both atoms A and B must be in state $|1\rangle$ for upconversion to occur with branching ratio η_{up}. However, $P^{(n)}$ may be set equal to unity without a significant loss of generality [$P^{(1)} = P^{(2)} = \ldots P^{(n)} = 1$]. For a fixed initial number of excited atoms, $P^{(n)}$ decreases as the reservoir depletes, but it is an excellent approximation to assume that $P^{(n)}$ is independent of n when the density of upconversion sites is low compared with the density of excited atoms, and steady-state illumination is assumed. We can compare the effective efficiency η_{eff} with that expected without population recycling by defining an enhancement factor M, given by

$$M = \eta_{\text{eff}}/\eta_0\eta_1\eta_2 = (1 - \eta_1\eta_2\eta_3\eta_{\text{up}})^{-1}. \quad (2)$$

It is immediately apparent from Eq. (2) that quantum efficiencies exceeding unity are possible. To see this, one can ignore decay from the upconversion state $|1a\rangle$ by setting $\eta_4 = 0$ and the value $\eta_{\text{up}} = (1/m) - \eta_4 = 1/m$ into Eq. (2). m is the number of atoms participating in the upconversion process itself. Then, for example, a quantum efficiency of 2 is expected when branching ratios for decay and emission in the system equal unity, and η_{up} is taken to be 0.5, the maximum value appropriate for pair upconversion. This is of great significance because population recycling also yields an enhanced energy conversion efficiency given by

$$\eta_E^* = \eta_{\text{eff}} \times \lambda_{\text{in}}/\lambda_{\text{out}}. \quad (3)$$

From Eq. (3) it is clear that, for rates of cooperative upconversion greatly exceeding the natural decay rate of state 2, energy efficiency ceases to depend sensitively on the actual value of the upconversion rate itself or on the upconversion branching ratio and attains an enhanced value.

This result exhibits a universality that holds irrespective of the pumping method. Two examples are instructive. First, if all excitation above level $|1\rangle$ is furnished by m-fold upconversion, one might expect the maximum energy efficiency to be [illegible] because with $\eta_{\text{up}} = 1/m$ only [illegible] reaches the emitting level. However, [illegible] recycling the maximum upconversion [illegible] is found from Eqs. (1) and (3) to [illegible] value $\eta_E^* = [1/(m-1)]\lambda_{\text{in}}/\lambda_{\text{out}}$. [illegible] be as short as $\lambda_{\text{in}}/(m-1)$ in this case, giving $\lambda_{\text{in}}/\lambda_{\text{out}} \leq (m-1)$, the energy efficiency can approach unity.

Second, when a short input wavelength is used to pump upper level $|3\rangle$ optically, as in a conventional laser-pumping scheme, cooperative enhancement of quantum

efficiency can still occur, provided that $\lambda_{in}/\lambda_{out} \leq (m-1)/m$, constraining downward and upward transitions to conserve energy in the cooperative process. We again find that the maximum conversion efficiency $(\eta_E{}^*)_{max} = \{m\lambda_{in}/[(m-1)\lambda_{out}]\}_{max} = 1$ exceeds the limiting value set by $(\eta_E)_{max} = (\lambda_{in}/\lambda_{out})_{max} = (m-1)/m$ for the same emission process in the absence of recycling. Energy conversion efficiency $\eta_E{}^*$ never exceeds unity because of the restrictions on $\lambda_{in}/\lambda_{out}$ necessary for energy transfer to occur between excited states.

B. Population Pulsations

Modifications of cooperative dynamics are to be expected in optical cavities. This may happen, for example, if stimulated emission follows cooperative upconversion. For a stimulated emission process that repopulates coupled levels while depleting the gain, a sudden increase in the cooperative upconversion rate follows gain quenching. The abruptly increased rate of upconversion tends to restore inversion, and a relaxation oscillation can take place.

Rate equation calculations indicate that steady relaxation oscillations cannot be sustained by cooperative dynamics, a result considered in more detail in Subsection 2.C. However, transient oscillations can appear during the buildup or the decay of light in the cavity. We may show this by solving the rate equations for populations N_i in each state $(i = 0, 1, \ldots, 3)$ together with the equation for cavity photon density Q:

$$\frac{dN_0}{dt} = \gamma_{30}N_3 + \gamma_{20}N_2 + \gamma_{10}N_1 + \alpha N_1{}^2 - B_{01}I(N_0 - N_1), \tag{4}$$

$$\frac{dN_1}{dt} = \gamma_{31}N_3 + \gamma_{21}N_2 - \gamma_{10}N_1 - 2\alpha N_1{}^2 + B_{01}I(N_0 - N_1) + B_{12}Q(N_2 - N_1), \tag{5}$$

$$\frac{dN_2}{dt} = \gamma_{32}N_3 - \gamma_2 N_2 - B_{12}Q(N_2 - N_1), \tag{6}$$

$$\frac{dN_3}{dt} = -\gamma_3 N_3 + \alpha N_1{}^2, \tag{7}$$

$$\frac{dQ}{dt} = B_{12}Q(N_2 - N_1) - \frac{Q}{\tau_c}. \tag{8}$$

In these expressions γ_{ij} is the decay constant between levels i and j, γ_i is the total decay rate for level i, B_{ij} is the Einstein coefficient for induced absorption on the $i \rightarrow j$ transition, and α is the upconversion coefficient, which has dimensions of volume. I is the intensity of incident light, and τ_c is the cavity lifetime.

To simulate the dynamics in a cavity after illumination stops, the stationary-state populations reached in levels $|0\rangle$ to $|3\rangle$ during constant pumping were obtained. Then we solved the undriven equations for times after pumping ceased by utilizing the stationary-state parameters $Q(0)$ and $N_i(0)$ as initial conditions. The resulting level $|2\rangle$ population dynamics are shown in Fig. 3.

Two aspects of the dynamics calculated with this rate equation approach are interesting. First, for times shorter than the lower-state lifetime but greatly in excess of the cavity lifetime, it is possible for a population inversion to persist between levels $|2\rangle$ and $|1\rangle$ after pumping has stopped. When the net rate of pumping into state $|1\rangle$ drops to zero, the rate of cooperative upconversion that feeds the upper laser level remains nearly constant initially, so the inversion improves for a short time. Second, the optical feedback in a cavity introduces transient atom–field interactions that cannot otherwise take place (see Subsection 2.C). Oscillations, reflecting population pulsations in the upconversion medium, are predicted in the rate equation limit and should be evident in light emitted from the cavity.

In the absence of inversion or a cavity, such population pulsations are possible only in spatially coherent cooperative interactions. To verify this, the role of delocalization in excited states must be examined carefully with a

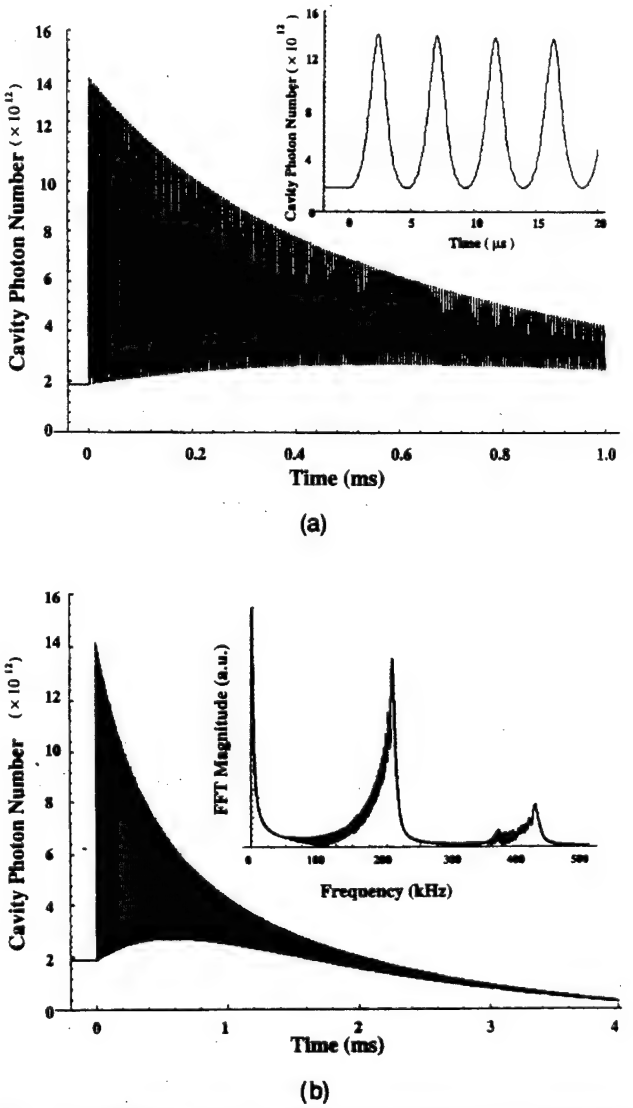

Fig. 3. Numerical rate equation calculation of pulsations in the inversion of the pair-pumped laser after termination of steady-state excitation. There are no free parameters: intensity $I = 153\ \mathrm{W/cm^2}$ (1.7 times threshold) in a cavity ($\tau_c = 1.5$ ns) of dopant density $5.7 \times 10^{20}\ \mathrm{cm^{-3}}$ with $\gamma_2 = 0.0714\ \mathrm{ms^{-1}}$, $\gamma_3 = 0.179\ \mathrm{ms^{-1}}$, $\gamma_{31} = 0.0769\ \mathrm{ms^{-1}}$, $\gamma_{32} = 0.103\ \mathrm{ms^{-1}}$, $\gamma_4 = 143\ \mathrm{ms^{-1}}$, $B_{01} = 6.9 \times 10^{-2}\ \mathrm{cm^2/J}$, $B_{12} = 2.4 \times 10^{-10}\ \mathrm{cm^3/s}$,[15] and $\alpha = 3.2 \times 10^{-17}\ \mathrm{cm^3/s}$.[16] (a) The initial part of postexcitation decay (inset, magnified trace with temporal resolution on the microsecond time scale showing quasi-periodicity). (b) Postexcitation decay at coarse temporal resolution [inset, fast-Fourier-transform (FFT) spectrum].

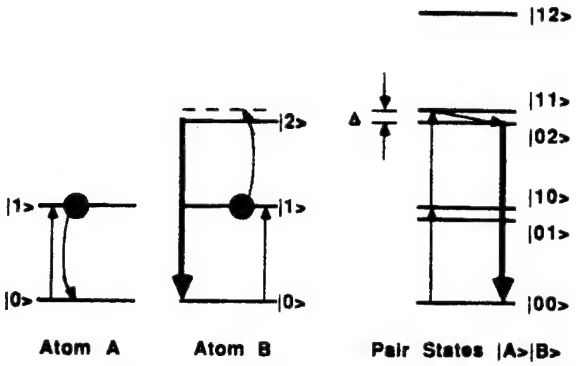

Fig. 4. Energy-level diagram of a model pair system. Left, individual atoms A and B may be pictured as each absorbing one pump photon (thin vertical arrow) to reach the interaction level indicated by the filled circles. Pair upconversion then leads to upconversion fluorescence after accommodation of the energy mismatch Δ, as indicated by the thick vertical arrow. Right, an alternative representation shows the coupled pair system as a ladder of product states |A⟩|B⟩. Absorption of two pump photons is required for promotion of the pair system to state |11⟩. Direct excitation to state |02⟩ by two-photon absorption of a single atom is off resonant because of the energy defect Δ. Emission from state |02⟩ occurs after spontaneous pair upconversion, which may be viewed as an internal relaxation from state |11⟩ to |02⟩ accompanied by emission of phonons for energy conservation.

different formalism. Although energy transfer is widely treated with rate equations as a one-way, incoherent process between a donor and an acceptor,[3] a density-matrix treatment can be used to incorporate the possibility of coherent back transfer.[17] Following this approach, we investigated the combined consequences of optical and spatial coherences in upconversion within the interacting pair system shown schematically in Fig. 4. Analytic results showed that sustained pulsations are expected in the populations of excited states in the intermediate to strongly coupled regime as the result of coherent cooperative upconversion.

Cooperative upconversion results from the excited-state atom–atom interaction between (unsymmetrized) product states |02⟩ and |11⟩ in the pair manifold shown in Fig. 4. Interactions between other excited pair states such as |01⟩ and |10⟩ are prevalent in rare-earth systems too but give rise only to companion phenomena such as rapid energy migration between sites. Such processes do not contribute to upconversion and are neglected here. Also, we considered the system at first to be undriven. Incident light prepares the system at time $t = 0$ in the doubly excited pair state |11⟩ but has zero intensity thereafter. Modifications of energy-transfer processes in the presence of radiation are considered in Subsection 2.D.

Excited-state dynamics may be calculated from the Liouville equation for the density matrix ρ, augmented by relaxation terms:

$$i\hbar \frac{d\rho}{dt} = [H, \rho] - i\hbar\gamma\rho. \tag{9}$$

The Hamiltonian is taken to be $H = H_0 + H_{int}$, where H_0 is the isolated ion Hamiltonian and H_{int} is the interaction between two coupled atoms. Typically, H_{int} arises from multipole–multipole or exchange interactions between electrons on adjacent atoms,[18] but its detailed form is not of concern from the point of view of basic dynamics. Relaxation terms represented globally by γ include population decay of each level i at the rate γ_i and dephasing of polarization on the ij transition at the rate $\gamma_{ij} = (\gamma_i + \gamma_j)/2$. Off-diagonal elements of H are written as state-specific coupling parameters multiplied by Planck's constant. This permits the strength of the ion–ion interaction, for instance, to be given as a characteristic frequency $i\hbar L = \langle 02|H_{int}|11\rangle$, thus avoiding the need to specify multipole–multipole interactions or accompanying phonon processes explicitly. When the energies of the initially uncoupled states |11⟩ and |02⟩ are degenerate, one finds their eigenvalues in the presence of interaction by diagonalizing the subdeterminant of matrix elements of H. For example, with the pair basis shown in Fig. 4, the eigenvalues of submatrix

$$H = \begin{bmatrix} E & -i\hbar L^* \\ i\hbar L & E \end{bmatrix} \tag{10}$$

are readily found in the subspace of states |11⟩ and |02⟩ to be

$$E_{1,2}' = E \pm \hbar(LL^*)^{1/2}, \tag{11}$$

revealing an energy splitting of the doubly excited eigenstates equal to $2\hbar(LL^*)^{1/2}$. This is the well-known Davydov splitting. The corresponding eigenstates of the interacting pair are

$$\Psi_1 = \frac{|11\rangle - |02\rangle}{\sqrt{2}}, \qquad \Psi_2 = \frac{|11\rangle + |02\rangle}{\sqrt{2}}. \tag{12}$$

We examined the temporal development of superposition states rather than stationary states. States such as |00⟩, |11⟩, and |02⟩ are spatially localized, and their dynamics directly reveal the spatial flow of energy within the system. This feature is extremely useful for understanding and predicting the energetics of the system. Because these states furnish a complete, alternative basis for describing pair dynamics in which intuitive ideas are easily incorporated, all the calculations were performed with them.

Introducing the convenient notation |00⟩ = |0⟩, |11⟩ = |1⟩, and |02⟩ = |2⟩, one can immediately write equations of motion for the pair superposition states in the absence of driving fields as follows. Assuming the Davydov splitting is energetically negligible, one finds that

$$\frac{d\rho_{11}}{dt} = L\rho_{21} + L^*\rho_{12} - \gamma_1\rho_{11}, \tag{13}$$

$$\frac{d\rho_{22}}{dt} = (L\rho_{21} + L^*\rho_{12}) - \gamma_2\rho_{22}, \tag{14}$$

$$\frac{d\rho_{12}}{dt} = L(\rho_{22} - \rho_{11}) - \gamma_{12}\rho_{12}. \tag{15}$$

The analytic, steady-state solutions are

$$\rho_{11}(t) = \exp(-\gamma_{12}t)\left(\frac{2LL^*}{\omega_0^2} - \frac{\Delta^2 - \omega_0^2}{2\omega_0^2}\cos\omega_0 t - \frac{\Delta}{\omega_0}\sin\omega_0 t\right) \tag{16}$$

$$\rho_{22}(t) = \exp(-\gamma_{12}t)\left(\frac{2LL^*}{\omega_0^2}\right)(1 - \cos\omega_0 t), \tag{17}$$

$$\rho_{12}(t) = \exp(-\gamma_{12}t)\left(\frac{2LL^*}{\omega_0^2}\right)[\Delta(1 - \cos\omega_0 t) - \omega_0 \sin\omega_0 t]. \tag{18}$$

In these expressions we have used the following definitions:

$$\Delta = (\gamma_1 - \gamma_2)/2, \tag{19}$$

$$\omega_0 = (4LL^* - \Delta^2)^{1/2}, \tag{20}$$

$$\rho_{12}'(t) = L\rho_{21} + L^*\rho_{12}. \tag{21}$$

Figure 5 shows the general behavior of these solutions for assumed initial conditions $\rho_{11} = 1$, $\rho_{22} = 0$, and $\rho_{12}' = 0$. The values of key parameters approximate those of Tm^{3+} in the crystal host $YAlO_3$, for which relevant relaxation rates are available in the literature.[19] Two values of the unknown coupling strength L were considered. For $L = 3$ kHz (three times the assumed dephasing rate), pulsations in the populations of pair superposition states $|1\rangle$ and $|2\rangle$ appeared as sinusoidal variations of ρ_{11} and ρ_{22} versus time. For $L = 1$ kHz (equal to the dephasing rate), no oscillations in population were predicted.

The population pulsations shown in Fig. 5(a) arise from periodic reversal of the cooperative upconversion process, a manifestation of (spatially coherent) partial delocalization of the excitation. Theoretically, the oscillation frequency provides a direct measure of the coupling strength L through the relation for ω_0 given in Eq. (20). At present this parameter may be estimated only roughly from measured pair cross-relaxation rates. However, this procedure does yield a value $L = 1$ kHz, which coincides with the experimental dephasing rate of level $|1\rangle$ (corresponding to the $^3F_4$ level of Tm^{3+}) in Tm:$YAlO_3$.[19] Because the coupling and decay rates are the same, this estimate suggests that, experimentally, L may be at the critical value separating regimes of localized from coherently delocalized dynamics. In Tm:$YAlO_3$ or other rare-earth crystals effects of delocalization may therefore be observable without optical cavities. Weakly delocalized dynamics may even seed unstable behavior in the presence of gain, an idea explored in more detail in Subsection 2.C.

C. Instabilities in Cooperative Dynamics

Because upconversion is inherently a nonlinear process, it can in principle exhibit unstable behavior.[29] Instabilities in excited-state populations or chaos might therefore be expected to arise from interatomic coupling of atoms[21] in at least two ways. First, one can imagine cooperative upconversion initiating population relaxation oscillations of the type indicated in Fig. 3, which might be amplified or sustained in the steady state by a driving field in a cavity. In this case oscillations would arise from cavity–atom interactions accompanied by stimulated emission. Second, the delocalization discussed in Subsection 2.B could initiate population pulsations and might be strong enough to mediate an instability even without a cavity. In this case unstable behavior would arise purely from atom–atom interactions driven by an optical field, without stimulated emission. In this subsection we find the surprising result that coherent delocalization is necessary to sustain steady-state oscillation with or without a cavity.

As an initial step, unstable solutions of the rate equations (4)–(8) were sought. Three-level lasers with linear driving terms respond universally to departures from steady-state intensity by exponential decay back to the original steady state.[22] However, upconversion is a nonlinear process, and a reexamination of this result in a multilevel pair system is warranted.

A linear stability analysis of Eqs. (4)–(8) was performed to investigate cooperative upconversion in a cavity in the limit of weak interatomic coupling. The steady-state population $(\rho_{ii})_{ss}$ for each excited state $|i\rangle$ was found for fixed intensity. Then linear departures from steady-state values were substituted into the dynamical equations through the replacement $\rho_{ii} \rightarrow (\rho_{ii})_{ss} + \Delta\rho_{ii}$. Eigenvalues of the equations of motion of $\Delta\rho_{ii}$ were then examined to determine whether deviations from steady-state values grew or decayed with time. This analysis (see Appendix A) revealed that populations always relax back to their steady-state values, with or without a cavity, for arbitrary values of incident intensity and decay constants. That is, rate equation analysis leads to the conclusion that pair-pumped upconversion lasers are universally stable.

In the intermediate-to-strong coupling regime a similar stability analysis of upconversion dynamics requires a density-matrix calculation. This begins with augmentation of the unperturbed Hamiltonian by the field Hamiltonian. In the basis of uncoupled pair states $|0\rangle$, $|1\rangle$, and $|2\rangle$ this yields

$$\hat{H}_0 = E|1\rangle\langle 1| + E|2\rangle\langle 2| + |\alpha|^2\hbar\omega|\alpha\rangle\langle\alpha|. \tag{22}$$

Here $|\alpha\rangle$ is a coherent state of the radiation field, chosen to represent the atomic interaction with a laser field,

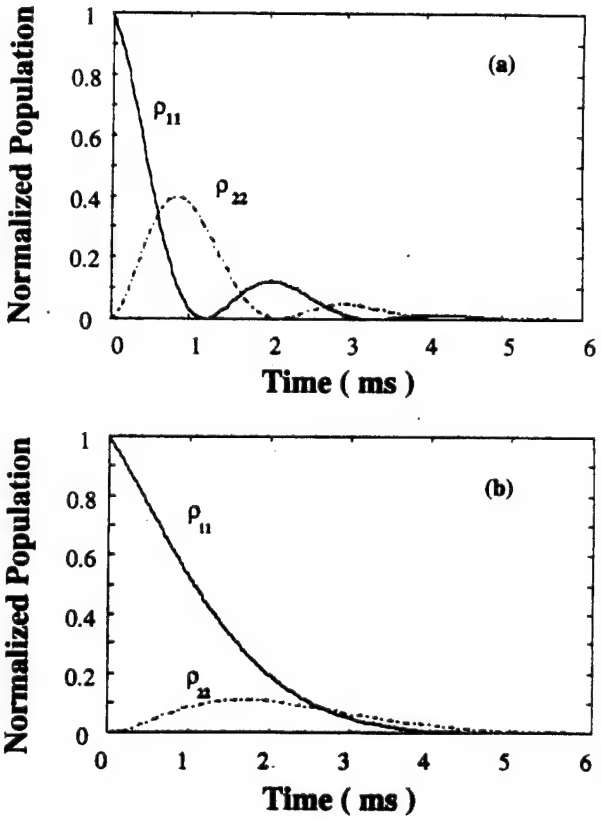

Fig. 5. Density-matrix calculation of excited pair state populations versus time in the presence of delocalization. The initial state is characterized by $\rho_{11} = 1$, $\rho_{22} = 0$, $\gamma_1 = \gamma_2 = 1$ kHz, and two values of interatomic coupling are considered, namely, (a) $L = 3$ kHz and (b) $L = 1$ kHz. Population pulsations are evident for the larger value of coupling.

and $|\alpha|^2 = \langle\alpha|a^\dagger a|\alpha\rangle$ is the expectation value of the number operator.[23] The energy contribution from vacuum fluctuations has been dropped. The ion–ion interaction Hamiltonian in this subspace is augmented by field-induced dipole transitions between the ground state $|0\rangle$ and the doubly excited pair state $|1\rangle$ (not state $|2\rangle$):

$$\hat{H}_{\text{int}} = i\hbar L|1\rangle\langle 2| + \text{h.c.} + \frac{\hbar f_A f_B^*|\alpha|^2}{\Delta\omega}|1\rangle\langle 0| + \text{h.c.} \quad (23)$$

In this expression $\Delta\omega$ is the $|00\rangle \rightarrow |01\rangle$ transition frequency, and h.c. denotes the Hermitian conjugate. The parameter f is the dipole moment on the $|0\rangle \rightarrow |1\rangle$ transition, defined by $f\alpha = \langle\mu \cdot E\rangle/\hbar$. Only the double-atom-excitation terms of interest have been retained from the second-order Hamiltonian $\langle 11|(\mu_A + \mu_B)\cdot E|01\rangle\langle 01|(\mu_A + \mu_B)\cdot E|00\rangle/\hbar\Delta\omega$. The subscripts A and B refer to atoms A and B of a coupled pair. Two-photon excitations of individual atoms have been specifically excluded from Eq. (23).

The populations of the pair system in the interaction representation are

$$\frac{d\rho_{00}}{dt} = \rho_3 + \gamma_1\rho_{11} + \gamma_2\rho_{22}, \quad (24)$$

$$\frac{d\rho_{11}}{dt} = \rho_3 + \rho_4 - \gamma_1\rho_{11}, \quad (25)$$

$$\frac{d\rho_{22}}{dt} = -\rho_4 - \gamma_2\rho_{22}. \quad (26)$$

The equations for optical and spatial coherences in the system are given by

$$\frac{d\rho_3}{dt} = I^2(\rho_{11} - \rho_{00}) - \gamma_{01}\rho_3, \quad (27)$$

$$\frac{d\rho_4}{dt} = 2\beta(\rho_{22} - \rho_{11}) - \gamma_{12}\rho_4, \quad (28)$$

respectively. Here γ_{01} and γ_{12} are the optical- and the spatial-coherence dephasing rates, and we have used the following definitions:

$$\rho_3 = (f\alpha)^2\rho_{10} + (f^*\alpha^*)^2\rho_{01}, \quad (29)$$

$$\rho_4 = -L(\rho_{12} + \rho_{21}), \quad (30)$$

$$I = 2|f|^2|\alpha|^2, \quad (31)$$

$$\beta = |L|^2. \quad (32)$$

We emphasize the role of incident light by replacing the expectation value of the number operator $\langle\alpha|n|\alpha\rangle = |\alpha|^2$ by a quantity I proportional to (but not identical with) intensity, as defined in Eq. (31).

In these equations the coherence term ρ_{02}, which is second order in the field, has been neglected. This at first appears unjustified because the coherence term ρ_{01}, which is similarly second order in the pumping field, has been retained. However, it can easily happen that sequential or simultaneous two-photon absorption processes fail to populate doubly excited states while cooperative upconversion takes place. If phonons accommodate the energy defect Δ, upconversion can occur rapidly and may generate weak spatial coherence or the delocalization described by ρ_{01}. At the same time, if energy levels are not in exact coincidence with the incident frequency, two-photon optical coherence does not develop ($\rho_{02} = 0$).

In a closed three-level pair system, population is conserved. Hence we can eliminate ground-state variables, using the relation $\rho_{00} + \rho_{11} + \rho_{22} = 1$. Making the substitutions $\rho_{11} \rightarrow \rho_1$ and $\rho_{22} \rightarrow \rho_2$ for convenience, we find that the equations of motion in matrix form become

$$\begin{bmatrix}\dot{\rho}_1\\ \dot{\rho}_2\\ \dot{\rho}_3\\ \dot{\rho}_4\end{bmatrix} = \begin{bmatrix}-\gamma_1 & 0 & 1 & -1\\ 0 & -\gamma_2 & 0 & -1\\ 2I^2 & I^2 & -\gamma_{01} & 0\\ -2\beta & 2\beta & 0 & -\gamma_{12}\end{bmatrix}\begin{bmatrix}\rho_1\\ \rho_2\\ \rho_3\\ \rho_4\end{bmatrix} + \begin{bmatrix}0\\ 0\\ I^2\\ 0\end{bmatrix}. \quad (33)$$

The overdots indicate differentiation with respect to time. The secular equation, of the general form $\lambda^4 + a_3\lambda^3 + a_2\lambda^2 + a_1\lambda + a_0 = 0$, has particularly simple coefficients if level $|1\rangle$ is assumed to be metastable ($\gamma_1 = 0$). Then the secular determinant factors into a trivial solution with zero eigenvalue and a cubic equation that can be solved analytically. Here we are interested only in identifying a condition that renders the real part of any eigenvalue positive because then the system will oscillate continuously. The Routh–Hurwitz criterion[24] for such an instability is that the system determinant $D = a_1a_2a_3 - a_{12} - a_0a_{32} = \beta\gamma_2^2(16\beta + 3\gamma_2^2 - 3I)/2$ must be zero or negative. This condition occurs when the intensity I exceeds the critical value

$$I_c = \left(\frac{16\beta + 3\gamma_2^2}{3}\right)^{1/2}. \quad (34)$$

From this result it may be concluded that spatial coherence can generate population oscillations in the steady state without optical feedback. This feature of coherent cooperative upconversion has not, to our knowledge, been previously discussed and may be a useful new signature of delocalization in upconversion. A numerical calculation of the growth of this instability is shown in Fig. 6.

D. Enhanced Upconversion and Energy Transfer

We now show that the energy-transfer rate between atoms is frequency dependent when modulated, incoherent light is used to excite pair upconversion. A resonant condition for enhanced upconversion emerges from this analysis.

The dynamical equations that we consider are identical to Eqs. (13)–(15), except that an incoherent driving term is added to the right-hand side of Eq. (14). The modified equation is

$$\frac{d\rho_{22}}{dt} = -(L\rho_{21} + L^*\rho_{12}) - \gamma_2\rho_{22} + \lambda_p. \quad (35)$$

The optical pumping rate λ_p depends on incident intensity, the Einstein B coefficient, and the population difference between levels $|0\rangle$ and $|1\rangle$. In the low-depletion limit $\rho_{00} - \rho_{11} \approx 1$, and λ_p is implicitly independent of the density-matrix elements. Writing the equations of motion in terms of ρ_{12}' defined in Eq. (20), we find that

$$\begin{bmatrix}\dot{\rho}_{11}\\ \dot{\rho}_{22}\\ \dot{\rho}_{12}'\end{bmatrix} = \begin{bmatrix}-\gamma_1 & 0 & 1\\ 0 & -\gamma_2 & -1\\ -2\beta & 2\beta & -\gamma_{12}\end{bmatrix}\begin{bmatrix}\rho_{11}\\ \rho_{22}\\ \rho_{12}'\end{bmatrix} + \begin{bmatrix}0\\ \lambda_p(t)\\ 0\end{bmatrix}. \quad (36)$$

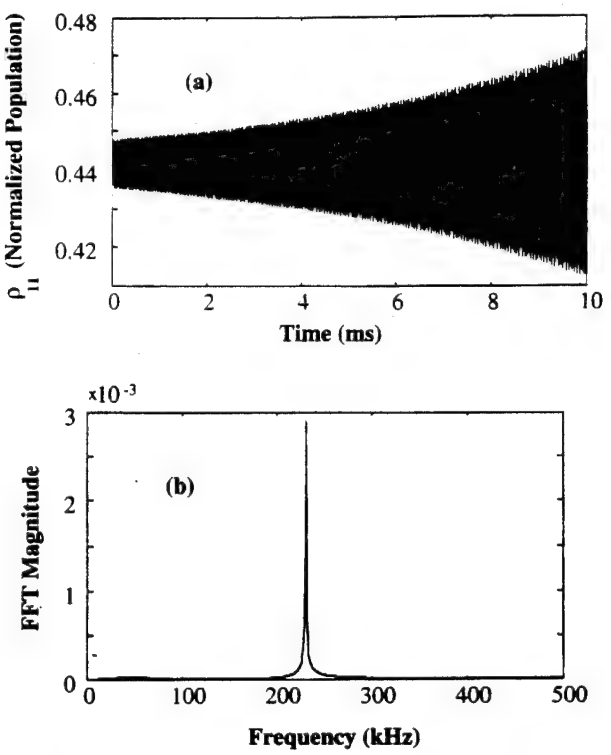

Fig. 6. Growth of quasi-periodic output from a constant steady-state condition of a pair-pumped laser (density-matrix calculation). (a) $l^2 = 2.6 \times 10^4$ kHz^2, $\beta = 900$ kHz^2, and $\gamma_2 = 100$ cm^{-1}, $\gamma_1 = 0$. (b) Fourier spectrum of (a).

If the incident field is modulated at a frequency ω according to $\lambda_p(t) = \lambda_p(0)\exp(i\omega t)$, then harmonic solutions exist of the form

$$\begin{bmatrix} \rho_{11}(t) \\ \rho_{22}(t) \\ \rho_{12}'(t) \end{bmatrix} = \begin{bmatrix} \rho_{11}(0) \\ \rho_{22}(0) \\ \rho_{12}'(0) \end{bmatrix} \exp(i\omega t), \tag{37}$$

and substitution into Eq. (36) yields the solutions given by

$$\rho_{11}(0) = \frac{(\gamma_2 + i\omega)(\gamma_{12} i\omega) + 2\beta}{(\gamma_{12} + i\omega)[(\gamma_{12} + i\omega)^2 + \omega_0^2]} \lambda_p(0), \tag{38}$$

$$\rho_{22}(0) = \frac{2\beta}{(\gamma_{12} + i\omega)[(\gamma_{12} + i\omega)^2 + \omega_0^2]} \lambda_p(0), \tag{39}$$

$$\rho_{12}'(0) = \frac{-2\beta(\gamma_2 + i\omega)}{(\gamma_{12} + i\omega)[(\gamma_{12} + i\omega)^2 + \omega_0^2]} \lambda_p(0). \tag{40}$$

In these expressions a resonant frequency ω_0 appears, defined by

$$\omega_0 = \left[4\beta - \left(\frac{\gamma_1 - \gamma_2}{2} \right)^2 \right]^{1/2}. \tag{41}$$

The physical meaning of Eqs. (38)–(40) can best be appreciated by comparison of the fluorescence intensity at a particular frequency with that at zero frequency ($\omega = 0$), with a response function defined by

$$R(\omega) = \left| \frac{\rho_{22}(0)}{\rho_{22}(0)|_{\omega=0}} \right| = \frac{\gamma_{12}(\gamma_{12}^2 + \omega_0^2)}{\{(\omega_0^2 + \gamma_{12}^2)[(\omega_0^2 - \omega^2 + \gamma_{12}^2)^2 + 4\omega^2\gamma_{12}^2]\}^{1/2}}. \tag{42}$$

$R(\omega)$ is proportional to emission intensity, which is dependent on energy transfer, and is plotted in Fig. 7 for two values of the interatomic coupling strength L, again with the use of decay parameters typical of Tm:$YAlO_3$. For weak coupling ($L = 0.5$ kHz), the energy-transfer response function falls off rapidly as the frequency of modulation is increased from zero. However, for stronger coupling ($L = 5$ kHz) it exhibits a resonant peak near the coupling frequency. The precise frequency at which the peak occurs is given by

$$\omega_{max}^2 = \frac{3\omega_0^2 - 4\gamma_{12}^2 + (\omega_0^2 - 32\omega_0^2\gamma_{12}^2)^{1/2}}{4}. \tag{43}$$

When the dephasing rate of spatial coherence is much less than the coupling frequency, the energy-transfer resonance is well defined. When the dephasing rate exceeds the coupling frequency, the peak broadens and becomes less pronounced, eventually disappearing.

3. EXPERIMENTAL PROCEDURES

To investigate some of these predictions, experiments were performed in single crystals of 5% Er:CaF_2 and 5% Er:$LiYF_4$. Two sample disks of 3-mm thickness were prepared as monolithic, hemispherical optical cavities, and a third sample of the same thickness was polished plane parallel. The monolithic crystals were cut and were polished identically for laser experiments, with one flat surface and one convex surface of radius 2.5 cm. Both surfaces were antireflection coated in the range 1.4–1.6 μm. Most observations were made in the first

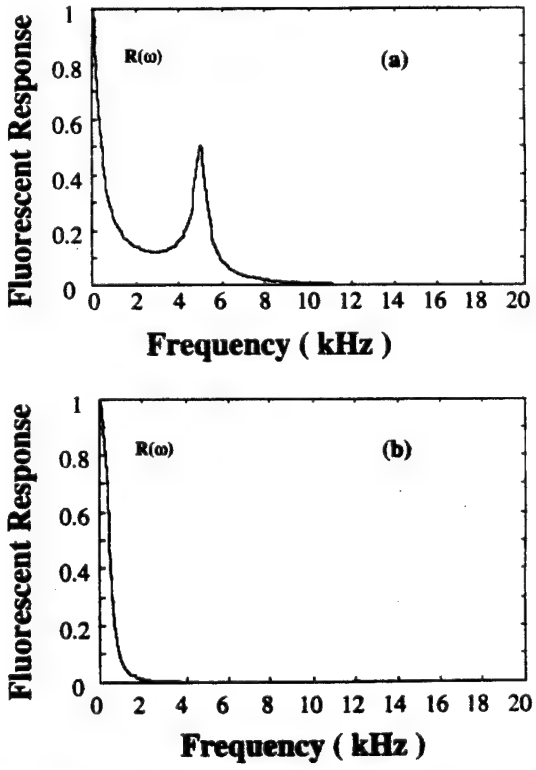

Fig. 7. Response function for enhanced energy transfer resulting from modulation of the optical driving field for two values of the interatomic coupling strength L. (a) $L = 5$ kHz, (b) $L = 0.5$ kHz. Other parameters used are $\gamma_1 = 0.43$ kHz (twice the measured[19] decay rate), $\gamma_2 = 1.6$ kHz, and $\gamma_{12} = 1.02$ kHz.

crystal, in which the curved surface coating gave total reflection between 2.7 and 2.9 μm and the flat served as a 2% output coupler. The other monolithic sample was coated for output at 854 nm. The third sample was used in an astigmatically compensated, three-mirror cavity designed for operation at 702 nm. Collectively these samples furnished light sources in which emission was sustained by pair, trio, and quartet upconversion processes, respectively.

Each sample was pumped longitudinally with a cw NaCl color-center laser, absorbing approximately 75% of incident radiation at 1.51 μm. Laser action at 2.8 μm was achieved at room temperature, as described previously.[14] The lasers with output wavelengths at 855 (Ref. 25) and 702 nm (Ref. 26) required cooling to liquid-nitrogen and liquid-helium temperatures, respectively. Cw laser emission was observed in each sample with output powers in the milliwatt range, sufficient for a variety of experiments related to cooperative dynamics. Laser output of the first crystal was monitored through a notch filter at 2.8 μm (FWHM 10 nm) with a fast InAs photodiode (rise time ~5 ns). Dynamics at 854 and 702 nm were monitored with fast photomultipliers and were recorded on a 1-GHz digital oscilloscope. Thermopile detection was used for power measurements.

Two main types of time-resolved measurement pertinent to a comparison with the theoretical concept outlined in Section 2 were made. The first consisted of observations of 2.8-μm laser output transients at the leading and trailing edges of square pump pulses generated by acousto-optic techniques. We made single-shot digital recordings with 100-ns temporal resolution (analog bandwidth), using a 1-MHz sampling rate over 8,000 points. Second, output intensity was digitally recorded versus time in the instability regime, with constant pumping.

4. RESULTS AND DISCUSSION

A. Enhanced Quantum Efficiency

The most efficient upconversion laser in our experiments was the unoptimized trio laser, which operated at 855 μm. Measurements yielded a slope efficiency of 28% and an overall energy efficiency of 26% for this laser. The latter value is to be compared with the maximum theoretical limits with and without recycling, which give $\eta_E^* = [1/(m-1)]\lambda_{in}/\lambda_{out} = 88\%$ and $\eta_E = (1/m)\lambda_{in}/\lambda_{out} = 59\%$, respectively. Although the cw trio laser worked remarkably well on a self-terminating transition, the actual laser efficiency gave no indication of quantum-efficiency enhancement.

Figure 8 shows representative data for upconversion laser emission on the $^2H_{9/2}$–$^4I_{11/2}$ transition at 701.5 nm, excited by 1.5-μm radiation and originating from a state at nearly four times the incident photon energy. The mere operation of this fourfold upconversion laser is surprising and immediately raises questions as to what fundamental limits may exist for cw laser action involving high degrees of upconversion and whether enhancement mechanisms are operative in such devices. However, the fourfold upconversion laser was also less efficient than either the maximum value $\eta_E^* = 71\%$ or $\eta_E = 53\%$. Consequently it was not possible to conclude directly from these laser measurements whether cooperative enhancement affected performance.

Nevertheless, other recent observations support the concept of cooperatively enhanced quantum efficiency outlined in Subsection 2.A. Output power measurements of a 2.8-μm laser pumped by conventional means at 980 nm in concentrated Er:$LiYF_4$ recently revealed performance marginally in excess of the theoretical efficiency limit set by $\eta_E = \lambda_{in}/\lambda_{out} \cong 35\%$.[27] This result was ascribed to pair upconversion dynamics, furnishing the first example of a laser with output enhanced by cooperative dynamics. Enhancement should extend to cooperative upconversion lasers as well, however. Although our own measurements do not reveal enhancement of upconversion laser output, we do furnish direct evidence of recycling dynamics in Subsection 4.B.

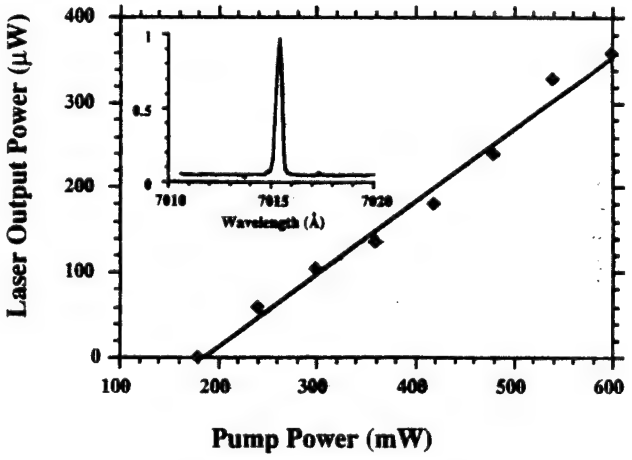

(a)

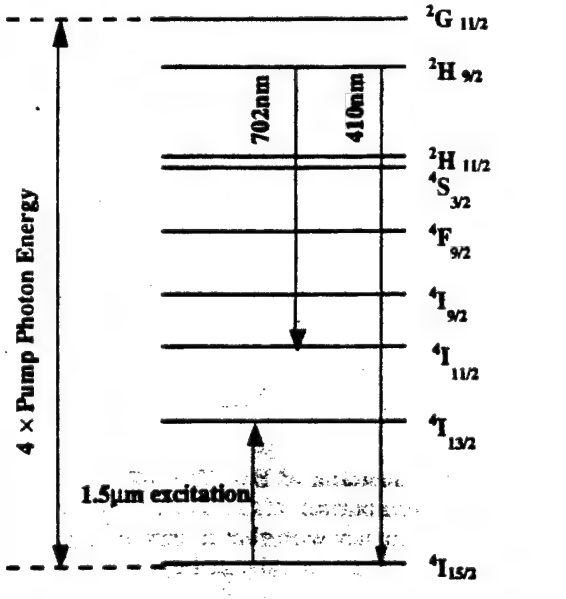

(b)

Fig. 8. Output versus input power for the fourfold cw upconversion laser operating at 701.5 nm ($\lambda_{ex} = 1.5$ μm). Inset, laser emission spectrum. (b) Energy diagram identifying the Er^{3+} levels involved in the pumping and the emission processes of the fourfold upconversion laser.

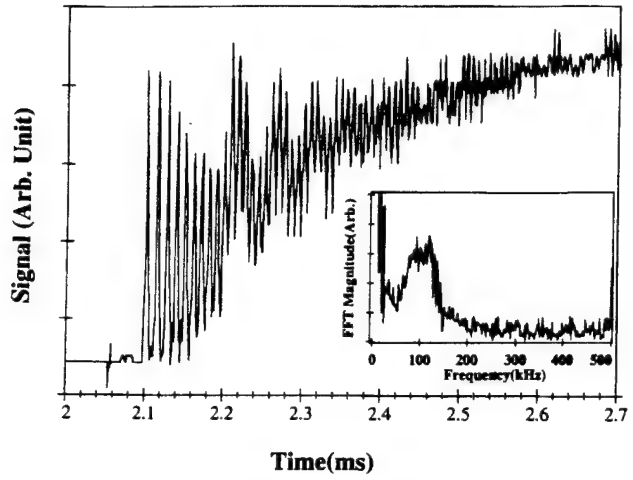

(a)

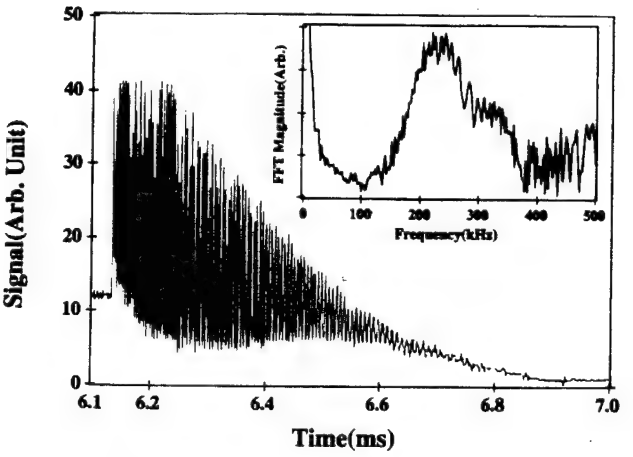

(b)

Fig. 9. Oscillations in output power observed at (a) the leading and (b) the trailing edges of a 2.8-μm Er:$LiYF_4$ laser pulse excited by a square pulse at $\lambda_{ex} = 1.5$ μm of 10-ms duration. Excitation was gated acousto-optically from the output of a cw NaCl laser. The rise and fall times of the pump pulses were less than 50 ns. Insets, Fourier transforms showing dominant frequency components.

B. Population Pulsations

When cw operation of the 2.8-μm pair-pumped laser was terminated, a transient increase in output power was observed. This result is in accord with the simple rate equation treatment presented in Subsection 2.B. In addition, for excitation at $\lambda_{ex} = 1.5$ μm, unexpected rapid oscillations occurred under the envelope of this transient peak, as shown in Fig. 9. Relaxation oscillations were observed at the leading edge of pump pulses also [Fig. 9(a)] but are not discussed here because of the analytic complication of including a driving field in the dynamics. Conclusions may be drawn more straightforwardly from an examination of trailing-edge transients.

An enlargement of postexcitation pulsations is shown in Fig. 9(b), together with their Fourier spectrum, revealing a chirped frequency spectrum centered near 210 kHz. This frequency is very near the measured inverse lifetime $(1/\pi\tau) = 210$ kHz of the $^4I_{9/2}$ level of Er^{3+}:$LiYF_4$. From Fig. 9(b) it is clear that pulsations of the stimulated emission continued long after external excitation of the system ceased. This clearly indicates that they originate from the interaction of the residual atomic inversion, the optical cavity, and the cavity photon density. Moreover, these pulsations are in excellent quantitative agreement with the rate equation calculation given in Fig. 3, with no adjustable parameters.

The origin of these transient pulsations can be pictured in the following way. Once external excitation ceases, inversion can recur only through pair upconversion to the $^4I_{9/2}$ level (analogous to level $|3\rangle$ in Fig. 2) of Er^{3+}. This process[14] is followed by nonradiative relaxation to the $^4I_{11/2}$ upper laser level ($|2\rangle$ in Fig. 2). While the upconversion rate is very high, the limiting rate at which inversion can be reestablished following depletion of the gain is set by the inverse $^4I_{9/2}$ lifetime. As long as the $^4I_{13/2}$ level ($|1\rangle$ in Fig. 2) responsible for pair upconversion remains well populated, cooperative upconversion efficiently replenishes the upper-state population in this way. Inversion density builds until the threshold is reached, whereupon stimulated emission depletes the accumulated gain. Quite distinct from conventional relaxation oscillations, these population pulsations are a direct manifestation of population recycling by cooperative dynamics, amplified by the feedback within an optical cavity.

C. Instabilities in Driven Systems

Whereas true cw operation of the pair-pumped 2.8-μm laser was achieved at low pumping intensity, instabilities became evident at intensities well above the threshold for cw lasing. These results are shown in Figs. 10–12.

For an excitation wavelength of $\lambda_{ex} = 1.5$ μm, inversion at 2.8 μm is sustained purely by cooperative dynamics.[14]

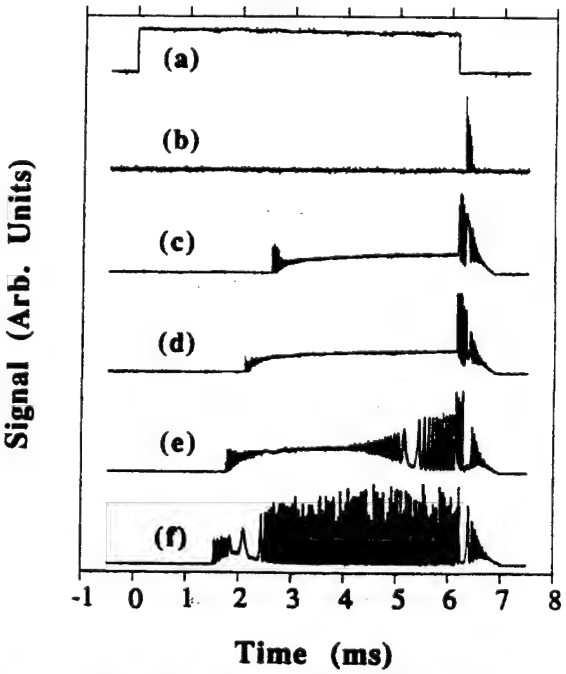

Fig. 10. Traces of pair-pumped Er:CaF_2 laser output at 2.8 μm at various pumping intensities. (a) The pump pulse. (b) Threshold operation. (c) True cw operation with leading- and trailing-edge transients (1.1 times threshold). (d) Cw operation at higher power (1.5 times threshold). (e) The growth of sustained oscillation from noise (two times threshold). (f) Unstable, quasi-periodic output (three times threshold).

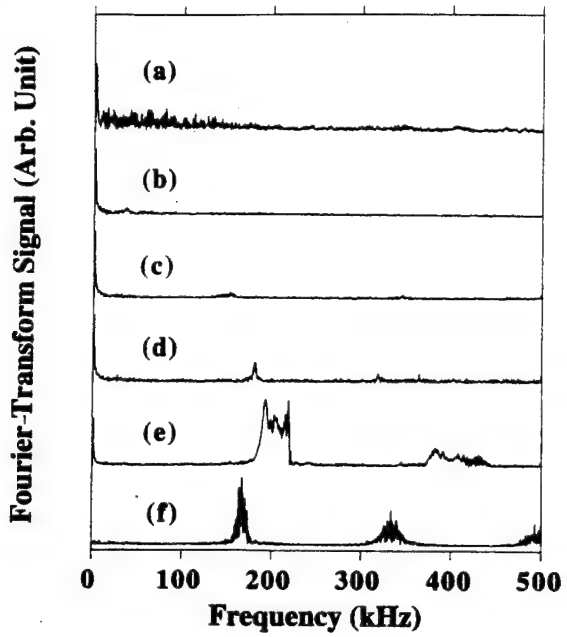

Fig. 11. Fourier transforms of the Fig. 10 time series, showing the presence of several modulation frequencies at high pumping intensity but no subharmonics. Leading- and trailing-edge transients were excluded from the analysis.

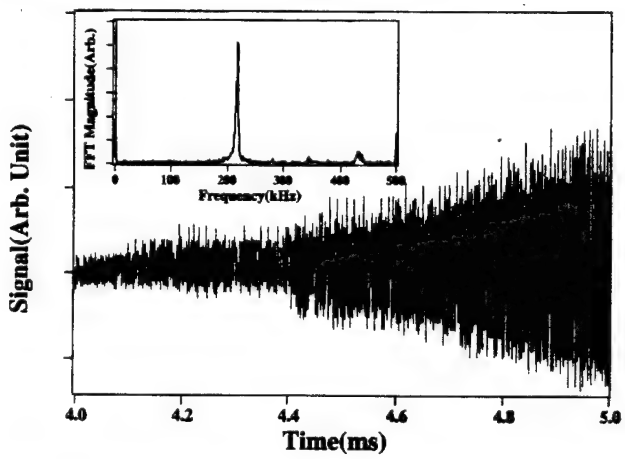

Fig. 12. Experimental trace of the growth of the instability shown in Fig. 10(e) with high temporal resolution. Inset, Fourier-transform spectrum.

At other excitation wavelengths the cooperative process occurs at a much reduced rate because the steady-state $^4I_{13/2}$ population from which pair upconversion originates is greatly reduced. The main result of this section is that instabilities are observed only when the excitation wavelength is chosen to maximize the cooperative dynamic contribution to laser inversion ($\lambda_{ex} = 1.5\ \mu m$).

The experimental observation of spontaneous growth of an instability from noise above a distinct threshold intensity is shown in Fig. 10. The associated Fourier spectrum is presented in Fig. 11, and a second recording is shown in Fig. 12, with higher temporal resolution. These experimental results are in excellent agreement with the density-matrix prediction given in Fig. 6. At this pumping intensity laser output experiences a hard loss of stability characteristic of a subcritical Hopf bifurcation,[28] suddenly developing a deep, periodic modulation above the instability threshold. Oscillations grow progressively more complex as pumping is increased, possibly because of a secondary Hopf bifurcation on a torus.

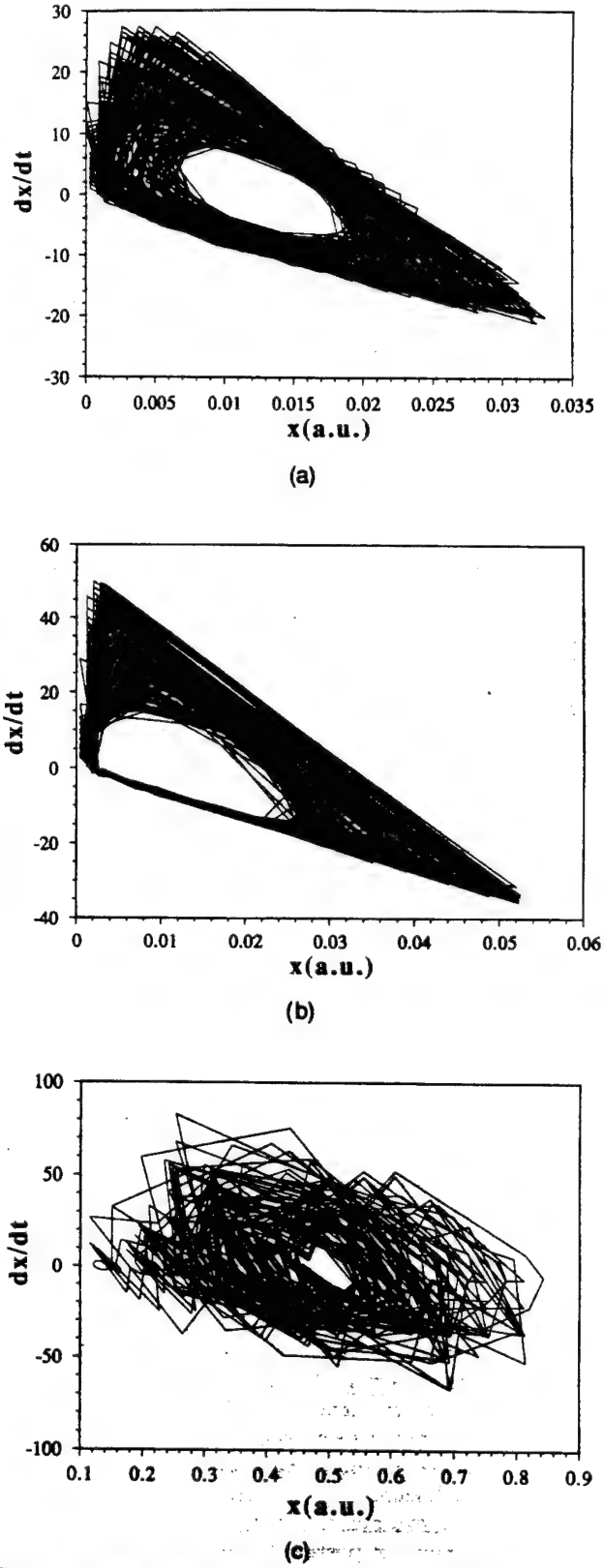

Fig. 13. Phase space plots of unstable output from the 2.8-μm pair-pumped laser: (a) dx/dt versus t for the $x(t)$ time sequence in the 3–6-ms interval shown in Fig. 10(e) at two times laser threshold (Er:CaF_2), (b) dx/dt versus t at three times laser threshold (Er:CaF_2), (c) dx/dt versus t at five times laser threshold (Er:$LiYF_4$).

This progression is reflected in the attractor plots shown in Fig. 13.

Although the 2.8-μm laser is renowned for being noisier than most other solid-state lasers under free-running conditions, to our knowledge no sustained oscillations like those reported here have been observed for excitation at pump wavelengths other than 1.5 μm. In our experiments, in addition to using $\lambda_{ex} = 1.5$ μm to pump 2.8-μm Er:CaF_2 and Er:$LiYF_4$ lasers, we tried alternative wavelengths of $\lambda_{ex} = 651-657$ nm and $\lambda_{ex} = 800$ nm. As indicated in Fig. 14, the output observed from the 2.8-μm Er:CaF_2 laser pumped three times over threshold at $\lambda_{ex} = 652$ nm showed no spiking behavior during continuous operation. After termination of pumping at $\lambda_{ex} = 652$ nm this laser showed transient enhancement of laser output (an afterpulse), but population pulsations beneath the afterpulse envelope were notably absent. Similarly, for $\lambda_{ex} = 800$ nm, no sustained oscillations were observed at equivalent levels above threshold, and no postexcitation pulsations occurred.

At pump wavelengths other than 1.5 μm, cooperative dynamics evidently served to overcome the self-terminating nature of the 2.8-μm emission but contributed only weakly to upper-laser-level population. Oscillations in 2.8-μm laser emission did not occur under these circumstances. Unstable operating conditions were reached only when excitation was provided at 1.5 μm, for only then did nonlinear cooperative dynamics dominate the inversion mechanism. We take these results, in combination with the theoretical considerations of Subsections 2.B and 2.C, to be strong evidence that the observed instabilities of the pair-pumped laser are completely attributable to cooperative nonlinear dynamics. Additionally, one may infer that noisy operation of the 2.8-μm Er laser pumped at wavelengths other than 1.5 μm originates from a subthreshold instability of the cooperative upconversion contribution to gain in the laser medium. Improved operation of this laser might therefore be attainable with feedback control of the type recently applied to stabilize chaotic laser output.[29]

5. SUMMARY

Cooperative nonlinear dynamics in highly doped media have important implications for upconversion and conventional solid-state lasers alike. In this paper we have introduced the concepts of population recycling in cooperative upconversion and enhancement of quantum efficiency. These concepts are relevant to an understanding of the theoretical efficiency limits of cw upconversion lasers and to potential improvements of conventional lasers in dense media.

Cooperative dynamics give rise to population pulsations and instabilities that can be observed in optical cavities. We have established that pulsations during afterpulses and sustained oscillations of the cw pair-pumped Er laser operating at 2.8 μm are due to the nonlinear dynamics of cooperative upconversion and can be reproduced by a density-matrix theory of cooperative upconversion that incorporates spatial coherence. Rate equations successfully describe transient upconversion behavior but fail to reproduce the observed steady-state instabilities, thereby indicating the importance of spatial coherence in pair dynamics of rare-earth ions in upconversion lasers. Coherent cooperative upconversion can in principle mediate population pulsations in rare-earth systems without cavities and admits a measure of control over energy transfer. These interesting prospects warrant further investigation.

APPENDIX A

To analyze the stability of the pair-pumped upconversion laser, the system response to small perturbations in Eqs. (4)–(8) must be examined. Solutions of the excited-state populations that grow with time are sought after one writes the time-dependent population $N_i(t)$ of level $|i\rangle$ as a sum of its steady-state value N_{is} and its fluctuation n_i, according to $N(t) = N_{is} + n_i$. Similarly, $Q(t) = Q_s + q$, and it is assumed that $n_i/N_{is} \ll 1$ and $q/Q_s \ll 1$.

Using $n_0 + n_1 + n_2 + n_3 = 0$, one obtains the following reduced set of dynamical equations for the fluctuations themselves:

$$\begin{bmatrix} \dot{n}_0 \\ \dot{n}_1 \\ \dot{n}_2 \\ \dot{q} \end{bmatrix} = \begin{bmatrix} -B_{01}I - \gamma_{30} & B_{01}I + 2\alpha N_{1s}\gamma_1 - \gamma_{30} & \gamma_{20} - \gamma_{30} & 0 \\ B_{01}I - \gamma_{31} & -B_{01}I - B_{12}Q_s - 4\alpha N_{1s} - \gamma_1 - \gamma_{31} & [B_{12}Q_s + \gamma_{21} - \gamma_{31}] & B_{12}(N_{2s} - N_{1s}) \\ -\gamma_{32} & B_{12}Q_s - \gamma_{32} & -B_{12}Q_s - \gamma_2 - \gamma_{32} & -B_{12}(N_{2s} - N_{1s}) \\ 0 & -B_{12}Q_s & B_{12}Q_s & 0 \end{bmatrix} \begin{bmatrix} n_0 \\ n_1 \\ n_2 \\ q \end{bmatrix}. \quad \text{(A1)}$$

Solutions of Eq. (A1) exist of the form

$$\begin{bmatrix} n_0(t) \\ n_1(t) \\ n_2(t) \\ q(t) \end{bmatrix} = \begin{bmatrix} n_0(t) \\ n_1(t) \\ n_2(t) \\ q(t) \end{bmatrix} \exp(\lambda t), \quad \text{(A2)}$$

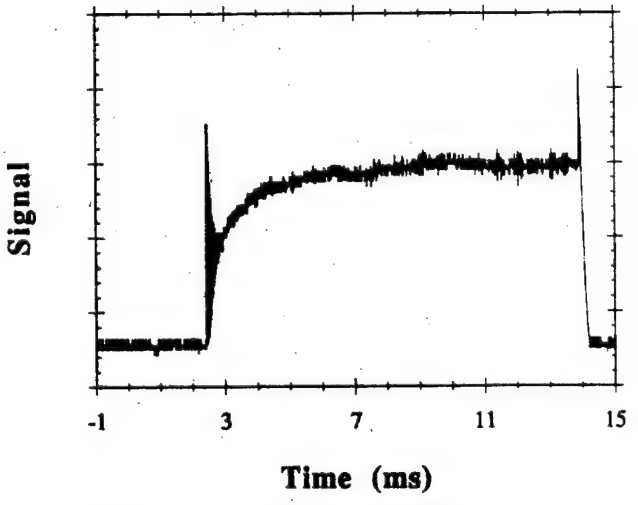

Fig. 14. Output trace of the 2.8-μm Er:CaF_2 laser pumped by a long square pulse in the red spectral region ($\lambda_{ex} = 652$ nm). At this pump wavelength output is continuous even at three times above threshold, and the trailing-edge spike has no rapid underlying oscillations.

where λ is an eigenvalue of the matrix $\mathbf{A}$ of coefficients in Eq. (A1). Eigenvalues are determined by setting $\mathrm{Det}[\mathbf{A} - \lambda U] = 0$, where U is the unit tensor, and this secular equation can be written in the form $a_4\lambda^4 + a_3\lambda^3 + a_2\lambda^2 + a_1\lambda + a_0 = 0$. The coefficients a_i are determined by explicit evaluation of the secular determinant. The system becomes unstable if any root is positive, for then the small initial perturbation will grow exponentially in time according to Eq. (A2).

The Routh–Hurwitz criterion[24] for stability requires an examination of the following determinants:

$$D_1 = a_1, \qquad D_2 = \begin{vmatrix} a_1 & a_0 \\ a_3 & a_2 \end{vmatrix}, \qquad D_3 = \begin{vmatrix} a_1 & a_0 & 0 \\ a_3 & a_2 & a_1 \\ 0 & a_4 & a_3 \end{vmatrix},$$

$$D_4 = \begin{vmatrix} a_1 & a_0 & 0 & 0 \\ a_3 & a_2 & a_1 & 0 \\ 0 & a_4 & a_3 & a_2 \\ 0 & 0 & 0 & a_4 \end{vmatrix}. \tag{A3}$$

The coefficients are

$$\begin{aligned} a_0 &= abcd + \gamma_3[3abd + bcd + bd(\gamma_{10} + \gamma_{20})] + bcd\gamma_{30}, \\ a_1 &= abc + 3abd + 2bcd + bd(2\gamma_3 + \gamma_{20} + \gamma_{10}) \\ &\quad + 3ab\gamma_3 + ac(\gamma_2 + \gamma_{32}) + bc(\gamma_3 + \gamma_{30}) + 2a\gamma_2\gamma_3 \\ &\quad + b\gamma_3(\gamma_{10} + \gamma_{20}) + c(\gamma_2\gamma_{30} + \gamma_2\gamma_3 + \gamma_{20}\gamma_{32}) \\ &\quad + \gamma_{10}\gamma_2\gamma_3, \\ a_2 &= ac + 3ab + 2bc + 2bd + 2a(\gamma_2 + \gamma_3) \\ &\quad + b(\gamma_{10} + \gamma_{20} + 2\gamma_3) + c(2\gamma_2 - 2\gamma_{30} + \gamma_{31} + 2\gamma_{32}) \\ &\quad + [\gamma_{10}(\gamma_2 + \gamma_3) + \gamma_2\gamma_3], \\ a_3 &= 2(a + b + c) + \gamma_1 + \gamma_2 + \gamma_3, \\ a_4 &= 1. \end{aligned} \tag{A4}$$

Here we have used the definitions $a = B_{01}l$, $b = B_{12}Q_s$, $c = 2aN_{1s}$, and $d = B_{12}(N_{2s} - N_{1s}) = t_c^{-1}$, and we note that all these quantities and the coefficients given above are positive above laser threshold. The system will become unstable if any determinant $D_i (i = 1, 2, 3, 4)$ is less than zero.

Because $a_4 = 1$ we note that $D_4 = D_3$, so the number of determinants that must be considered is reduced to three:

$$D_1 = a_1, \tag{A5}$$

$$D_2 = a_1a_2 - a_3a_0, \tag{A6}$$

$$D_3 = a_3D_2 - a_4a_1^2. \tag{A7}$$

From Eqs. (A4) it is evident that $a_i > 0$ for all i. Hence, for an instability to develop, it is necessary that either $D_2 < 0$ or $D_3 < 0$. However, one can easily verify, by expanding Eqs. (A6) and (A7) directly and by canceling all negative terms, that D_2 and D_3 are always positive for positive inversion (N_{2s}–N_{1s}). Consequently the rate equations describing pair-pumped laser operation are universally stable.

ACKNOWLEDGMENTS

The authors gratefully acknowledge research support by the U.S. Air Force Office of Scientific Research (H. Schlossberg) and thank S. Rai and J. Rai for useful discussions.

*Present address, Los Alamos National Laboratory, CLS-6 Group/MS E535, Los Alamos, New Mexico 87545.

REFERENCES AND NOTES

1. F. Auzel, Proc. IEEE **61,** 758 (1973).
2. S. Hufner, *Optical Spectra of Transparent Rare Earth Compounds* (Academic, New York, 1978), Chap. 5.
3. O. K. Alimov, M. Kh. Ashurov, T. T. Basiev, E. O. Kirpichenkova, and V. B. Murav'ev, in *Selective Laser Spectroscopy of Activated Crystals and Glasses,* V. V. Osiko, ed. (Nova Science, New York, 1988), Chap. 2.
4. J. Chivian, W. Case, and D. Eden, Appl. Phys. Lett. **35,** 124 (1979).
5. H. Ni and S. C. Rand, Opt. Lett. **16,** 1424 (1991).
6. A comprehensive review of upconversion processes is given by J. C. Wright, "Up-conversion and excited state energy transfer in rare-earth doped materials," in *Topics in Applied Physics,* F. K. Fong, ed. (Springer, New York, 1976), Vol. 15, p. 239.
7. R. M. Macfarlane, F. Tong, A. J. Silversmith, and W. Lenth, Appl. Phys. Lett. **52,** 1300 (1988).
8. R. J. Thrash and L. F. Johnson, J. Opt. Soc. Am. B **11,** 881 (1994).
9. J. Y. Allain, M. Monerie, and H. Poignant, Electron. Lett. **26,** 261 (1990).
10. R. G. Smart, D. C. Hanna, A. C. Tropper, S. T. Davey, S. F. Carter, D. Szebesta, Electron. Lett. **27,** 1307 (1991).
11. S. G. Grubb, K. W. Bennett, R. S. Cannon, and W. F. Humer, in *Conference on Lasers and Electro-Optics,* Vol. 12 of 1992 OSA Technical Digest Series (Optical Society of America, Washington, D.C., 1992), pp. 669–670.
12. D. S. Funk, S. B. Stevens, and J. G. Eden, IEEE Photon. Technol. Lett. **5,** 154 (1993).
13. P. Xie and S. C. Rand, Opt. Lett. **17,** 1116, 1822 (1992).
14. P. Xie and S. C. Rand, Opt. Lett. **15,** 848 (1990).
15. P. Xie, "Continuous-wave cooperative upconversion lasers," Ph.D. dissertation (University of Michigan, Ann Arbor, Mich., 1992).
16. H. Chou, "Upconversion processes and Cr-sensitization of Er- and Er, Ho-activated solid state laser materials," Ph.D. dissertation (Massachusetts Institute of Technology, Cambridge, Mass., 1989).
17. A. S. Davydov and A. A. Serikov, Phys. Status Solidi **51,** 57 (1972).
18. R. B. Barthem, R. Buisson, J. C. Vial, and H. Harmand, J. Lumin. **34,** 295 (1986).
19. L. M. Hobrock, "Spectra of thulium in yttrium orthoaluminate crystals and its four-level laser operation in the mid-infrared," Ph.D. dissertation (University of Southern California, Los Angeles, Calif., 1972). In the present paper we follow recent practice by exchanging the labels of the $^3H_4$ and the $^3F_4$ states of Tm with respect to Hobrock, designating $^3F_4$ as the first excited state. See, e.g., A. Brenier, J. Rubin, R. Moncorge, and C. Pedrini, J. Phys. (Paris) **50,** 1463 (1989).
20. See, e.g., R. Seydel, *From Equilibrium to Chaos* (Elsevier, New York, 1988).
21. J. Rai and C. M. Bowden, in *International Conference on Quantum Electronics,* Vol. 8 of 1990 OSA Technical Digest Series (Optical Society of America, Washington, D.C., 1990), paper QTuN3.
22. D. M. Sinnett, J. Appl. Phys. **33,** 1578 (1962).
23. R. Loudon, *The Quantum Theory of Light,* 2nd ed. (Clarendon, Oxford, 1983), pp. 146–152.
24. See, e.g., *Handbook of Mathematics,* I. N. Bronshtein and K. A. Semendyayev, eds. (Van Nostrand Reinhold, New York, 1985), p. 419.
25. P. Xie and S. C. Rand, Opt. Lett. **17,** 1198 (1992); **17,** 1822 (1992).
26. P. Xie and S. C. Rand, Appl. Phys. Lett. **63,** 3125 (1993).
27. R. C. Stoneman and L. Esterowitz, Opt. Lett. **17,** 816 (1992).
28. See, e.g., Ref. 20, p. 73.
29. Z. Gills, C. Iwata, R. Roy, I. B. Schwartz, and I. Triandaf, Phys. Rev. Lett. **69,** 3169 (1992).

Continuous-wave, fourfold upconversion laser

P. Xie and S. C. Rand
Division of Applied Physics, 1049 Randall Laboratory, University of Michigan, Ann Arbor, Michigan 48109-1120

(Received 1 July 1993; accepted for publication 23 September 1993)

We report a new Er^{3+}:$LiYF_4$ cryogenic upconversion laser pumped by a fourfold upconversion process. Excitation at 1.5 μm results in laser emission at 701.5 nm on a transition with an upper state at nearly four times the pump photon energy. Mechanisms and the concept of cooperative upconversion enhancement are examined.

Recent demonstrations[1-5] of room-temperature upconversion lasers have stirred interest in their potential as practical sources of short wavelength radiation for display and data storage applications, as well as for communications and ultrashort pulse generation at visible and ultraviolet wavelengths.[6] To date however, little consideration has been given to the relative merits of various fundamental mechanisms for achieving upconversion, basic limits to achievable degrees of upconversion (ratio of upper laser level energy to incident photon energy), or to questions of stability of the highly nonlinear pumping processes involved in these devices. In this article we discuss two of these topics in the context of new results demonstrating a continuous-wave, fourfold upconversion laser. The important third issue of stability of solid state lasers in which nonlinear cooperative dynamics play an important role has been considered by Xie[7] and will be published separately.[8]

Upconversion fluorescence observed in Er:$LiYF_4$ due to irradiation with a continuous-wave (cw) NaCl laser at 1.5 μm at liquid-helium temperature is shown in Fig. 1(a). The upconversion mechanisms responsible for fluorescent emissions near 850 and 550 nm have been studied in past work and arise from cooperative (multi-atom) energy transfer processes[9] when cw excitation is restricted to 1.5 μm.

Emissions near 410, 650, 702 nm from higher lying states have not yet been studied as thoroughly, but are sufficiently intense to draw attention as potential laser candidates. The two near-ultraviolet lines at 407 and 413 nm arise from transitions with upper levels at roughly four times the incident photon energy, as indicated in Fig. 1(b). The fluorescent emission at 702 nm arises from Stark components of the $^2H_{9/2} \rightarrow {}^4I_{11/2}$ transition.

Laser experiments were performed in a three-mirror, astigmatically compensated[9] cavity consisting of two 5 cm radius total reflectors and an output mirror with 97% reflectively at 702 nm. A 3-mm-thick crystal of 5% Er:$LiYF_4$ inserted at Brewster's angle within the focusing arm of the laser served as the gain medium. Its optic axis was oriented parallel to the crystal surface in the plane of incidence of horizontally polarized pump radiation and the crystal was suspended on a cold finger in vacuum. The laser emission spectrum at 701.5 nm, assigned to the $^2H_{9/2}(1) \rightarrow {}^4I_{11/2}(3)$ transition,[10] and the variation of output power with input are shown in Fig. 2. The overall efficiency was 0.06% and observed slope efficiency was 0.09%.

The excitation spectrum of laser emission revealed a one-to-one correspondence with erbium absorption wavelengths in the 1.5 μm region. This result is shown in Fig. 3 and is similar to earlier findings for pair[9] and trio[11] lasers, but contrasts the restrictive wavelength dependence expected for multiphoton upconversion processes. It therefore has important implications for the inversion mechanism of the fourfold laser.[12]

For multiphoton absorption to be effective, several ground and excited state absorption (ESA) frequencies must overlap sharply. Hence, excited state resonances should appear in the excitation spectrum when this mechanism is operative.[13] For cooperative upconversion, only a single pump transition is relevant, terminating anywhere within the metastable manifold in which cooperative inter-

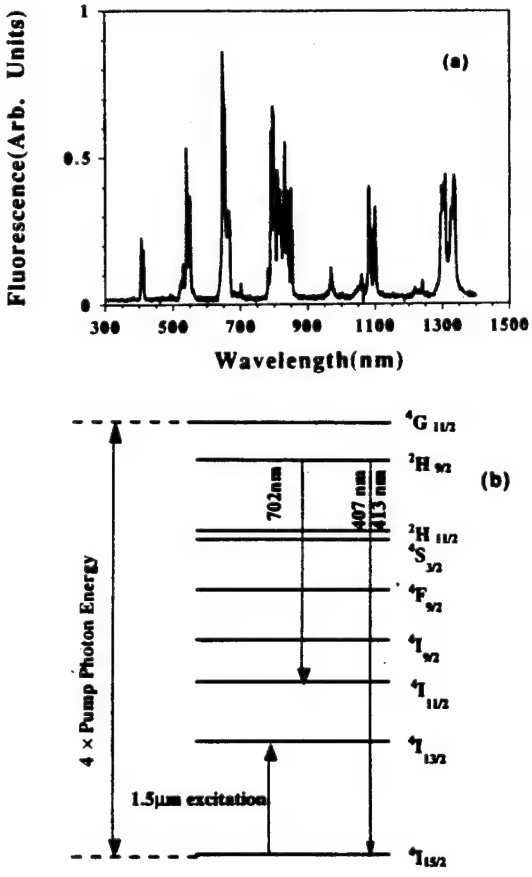

FIG. 1. (a) Upconversion fluorescence spectrum observed in Er^{3+}:$LiYF_4$ with excitation at $\lambda_{ex}=1.5$ μm ($T=10$ K), uncorrected for instrumental response. (b) Schematic diagram of Er^{3+} energy levels, showing emission at 410 and 701.5 nm from $^2H_{9/2}$ at nearly four times the incident photon energy.

 0003-6951/93/63(23)/3125/3/$6.00

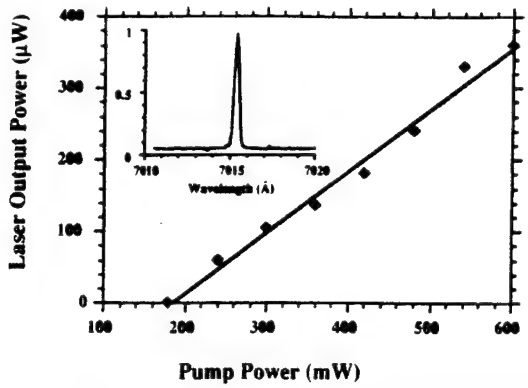

FIG. 2. Output vs input power of the cw fourfold upconversion laser operating at 701.5 nm ($T=10$ K). Inset: Laser emission spectrum.

actions occur. In this case only ground state absorption resonances should appear in the excitation spectrum. The results in Fig. 3 therefore provide ample evidence that absorption of light by excited ions does not occur and that the present fourfold laser operates by cooperative means.

This argument also rules out mechanisms combining cooperative and ESA processes. For example, ESA of 1.5 μm light from $^4S_{3/2}$ or $^2H_{11/2}$ states populated by trio upconversion[11] could in principle reach the high lying $^2H_{9/2}$ state responsible for laser action in this work, but such transitions are off resonant by over 218 cm^{-1} in $LiYF_4$ for all Stark levels[10] and are not present in the excitation spectrum. ESA transitions from $^4S_{3/2}$ to $^4G_{11/2}$ are still farther off resonance. On the other hand, quartet upconversion can provide very nearly *resonant* excitation of the $^4G_{11/2}$ state lying immediately above the upper laser level [generating the fluorescence at 380 nm in Fig. 1(a)]. The calculated energy defects on the quartet transitions $^4I_{13/2}(3,3,3,4)\rightarrow{}^4G_{11/2}(1)$ and $^4I_{13/2}(4,4,4,3)\rightarrow{}^4G_{11/2}(4)$, for example, are only 4 and 7 cm^{-1} in $LiYF_4$, respectively. The bracketed arguments of the initial state indicate Stark levels of the four interacting atoms, and the single argument of the final state gives the Stark level of the acceptor. Taken together with the close match between the excitation spectrum and ground state absorption (Fig. 3), this argues strongly against any contributions by ESA processes to $^2H_{9/2}$ population when 1.5 μm pumping is used.

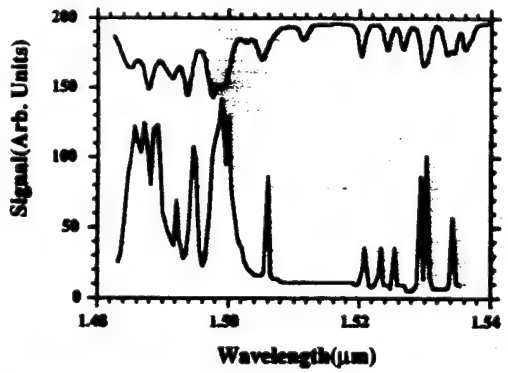

FIG. 3. Infrared excitation spectrum of fourfold upconversion laser emission at 701.5 nm ($T=10$ K, lower trace) and, for comparison, the Er^{3+} absorption spectrum ($T=9$ K, inverted).

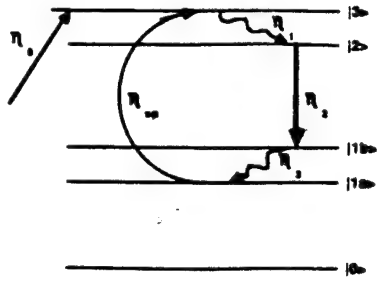

FIG. 4. Mechanism for enhanced quantum efficiency in cooperative upconversion systems. Following an initial excitation step (by direct pumping or upconversion), a cascade from higher to lower excited states occurs with branching ratios of η_i at each step. Wiggly arrows indicate nonradiative decay. A given atom can emit more than one photon per η_0 excitation if the upconversion rate exceeds the spontaneous decay rate of the lowest excited state (and detailed balance is satisfied).

The implication that laser operation may be sustained by a cooperative quartet process raises fundamental questions as to just how effective higher order *cooperative* upconversion processes can be in general. In this regard, we wish to point out that an enhancement mechanism exists for cooperative upconversion processes which can significantly extend their usefulness compared to multiphoton absorption. For emission terminating on or near levels in which strong cooperative interactions occur, no efficiency "penalty" is incurred for m-fold upconversion, where the integer m may be arbitrarily large. When upconversion emission terminates on an energy level which can renew cooperative upconversion, excited atoms are *recycled without external pumping* to enhance quantum efficiency by a factor of $(1-\eta_1\eta_2\eta_3\eta_{up})^{-1}$, where η_{up} is the m-fold cooperative upconversion efficiency. η_1, η_2, and η_3 are branching ratios for the decay processes indicated in Fig. 4. Energy conversion between input wavelength λ_{in} and output at λ_{out} can be much higher than the maximum value $\eta_{max}=\lambda_{in}/\lambda_{out}(100/m)\%$ based on a picture in which only one of m atoms is upconverted following the absorption of m pump photons. Ignoring decay to the ground state, the energy efficiency takes on the enhanced value

$$\eta_E^*=(\lambda_{in}/\lambda_{out})\eta_0\eta_1(1-\eta_1\eta_2\eta_3\eta_{up})^{-1} \quad (1)$$

and $\eta_E^*>\eta_{max}$ when upconverted atoms reside long enough in their lowest excited state to participate repeatedly in upconversion. With recycling, energy efficiency can approach 100% [for $\eta_i=1$ $(i=0,1...3)$ with a negligible energy defect such that $\lambda_{out}=\lambda_{in}/(1-\eta_{up})$].

In practice, theoretical enhancement of quantum efficiency by cooperative dynamics must be mitigated by losses due to an increasing number of intervening (radiative) levels on real atoms with increasing m. Branching ratios are typically less than unity. Also a statistical decrease is to be expected in the number of m-atom "clusters" with appropriate interatomic spacings, less than a nominal critical radius. However, the main conclusion is that a recycling mechanism exists whereby cooperative dynamics can mediate unexpectedly efficient upconversion emission for arbitrarily high degrees (m) of upconversion.

This has important implications not only for upconversion lasers, but also for other lasers in which cooperative nonlinear dynamics occur due to heavy rare-earth doping. One example is the 2.8 μm Er laser reported by Stoneman and Esterowitz.[14] These authors obtained an efficiency in practice which was marginally greater than the maximum theoretical quantum efficiency (ignoring cooperative dynamics). A calculation of enhanced quantum efficiency using the formula above, ignoring spontaneous radiative losses for simplicity, shows that for 980 nm pumping, complete recycling of terminal level population through pair upconversion results in a "renormalized" quantum efficiency of 2 (instead of 1) and a maximum energy efficiency of 70% (instead of 35%). Similar but less dramatic improvements due to cooperative enhancement of quantum efficiency are expected for 2.8 μm lasers pumped by other wavelengths.[8] Cooperative enhancement probably also accounts for the remarkable efficiency of the "self-terminating" Er trio laser at 855 nm.[11]

In the present experiment, we note that the 701.5 nm upconversion laser line terminates on the $^4I_{11/2}$ level of trivalent erbium. This level is known[15] to be effective in pair upconversion to the $^4F_{7/2}$ level, but is not the cooperative pumping level responsible for our inversion. The $^4I_{13/2}$ level, not the $^4I_{11/2}$ level, is responsible for cooperative pumping when excitation is tuned to 1.5 μm.[9,11] This situation therefore resembles, though it is not identical to, the general enhancement scheme of Fig. 4, and we suggest that enhanced upconversion efficiency through cooperative recycling may help account for successful operation of this laser, with its unprecedented (fourfold) degree of upconversion.

In summary, we have demonstrated operation of an upconversion laser in which population inversion is sustained in an upper laser level at nearly four times the incident photon energy,[16] through a fourfold upconversion process. The upconversion mechanism is thought to be exclusively cooperative in nature, arising from an atomic "quartet" interaction quite distinct from sequential energy transfer[13] or multiphoton absorption. The general notion of recycling of excited state population has been introduced and discussed as a possible mechanism for enhancing mth order upconversion processes and accounting for successful operation of the present fourfold upconversion laser. Extension of this result to fourfold laser operation at 410 nm, 555 nm, and other wavelengths appears feasible. In the case of the 555 nm transition, the terminal level would be in the $^4I_{13/2}$ manifold, and especially strong cooperative enhancement of the efficiency may be possible.

The authors gratefully acknowledge research support by the Air Force Office of Scientific Research (H. Schlossberg). P. Xie wishes to express gratitude to the CUSPEA program for graduate travel support.

[1] R. J. Thrash and L. F. Johnson, in *Technical Digest of the Conference on Compact Blue-Green Lasers* (Optical Society of America, Washington, DC, 1992), paper ThB3.
[2] J. Y. Allain, M. Monerie, and H. Poignant, Electron. Lett. **26**, 261 (1990).
[3] R. G. Smart, D. C. Hanna, A. C. Tropper, S. T. Davey, S. F. Carter, and D. Szebesta, Electron. Lett. **27**, 1307 (1991).
[4] S. G. Grubb, K. W. Bennett, R. S. Cannon, and W. F. Humer, in *Digest of the Conference on Lasers and Electro-Optics* (Optical Society of America, Anaheim, CA 1992), paper CPD18.
[5] D. S. Funk, S. B. Stevens, and J. G. Eden, IEEE Photon. Technol. Lett. **5**, 154 (1993).
[6] P. Xie and S. C. Rand, Opt. Lett. **17**, 1116 (1992); Opt. Lett. **17**, 1822 (1992).
[7] P. Xie, Ph.D. dissertation, University of Michigan, 1992.
[8] P. Xie and S. C. Rand, J. Opt. Soc. Am. B (in press).
[9] P. Xie and S. C. Rand, Opt. Lett. **17**, 1198 (1992).
[10] M. R. Brown, K. G. Roots, and W. A. Shand, J. Phys. C Solid State Phys. **2**, 593 (1969); S. M. Kulpa, J. Phys. Chem. Solids **36**, 1317 (1975).
[11] P. Xie and S. C. Rand, Appl. Phys. Lett. **60**, 3084 (1992).
[12] In our earlier publications, unsaturated $^4S_{3/2}$ emission intensity was shown to depend on the cube, not the fourth power, of incident intensity, thereby contradicting a sequential energy transfer model for visible upconversion with $\lambda_{ex}=1.5$ μm in erbium requiring four transfers. Sequential pair processes and sequential multiphoton absorption processes are ruled out not only by our previous work on time dependence of upconversion fluorescence, but also by the excitation spectra which are not convolutions of ground and excited state resonances.
[13] F. Auzel, J. Lumin. **45**, 341 (1990).
[14] R. C. Stoneman and L. Esterowitz, Opt. Lett. **17**, 816 (1992).
[15] H. Chou, Ph.D. dissertation, Massachusetts Institute of Technology, Tech. Rep. **26**, February 1989.
[16] A preliminary report of these results was first presented by S. C. R. at the Annual Meeting of the Optical Society of America, Albuquerque, New Mexico, Sept. 20–25 (1992), invited paper MJ2. Results at different output wavelengths have been reported by R. M. Macfarlane, E. A. Whittaker, and W. Lenth, Electron. Lett. **28**, 2136 (1992).

Cooperative Bistability in Dense, Excited Atomic Systems

M. P. Hehlen, H. U. Güdel
Institut für Anorganische Chemie
Universität Bern, Freiestrasse 3,
CH-3000 Bern 9, Switzerland
and
Q. Shu, J. Rai[†], S. Rai[††] and S. C. Rand
Division of Applied Physics
1049 Randall Laboratory
University of Michigan, Ann Arbor, MI 48109-1120

ABSTRACT

We report a new mechanism of intrinsic bistability, operative in excited atomic systems with substantial atom-atom coupling. Predictions and observations of bistable luminescence from Yb^{3+} pairs in crystalline $Cs_3Y_2Br_9$: Yb^{3+} are in good agreement and have interesting implications for local field effects in solids and dense, ultracold gases.

† Dept. of Physics, Indian Inst. of Tech., Kanpur 208016 India
†† Dept. of Physics, Indian Inst. of Tech., New Delhi, India

PACS Numbers: 42.65.Pc, 42.50.Fx, 78.55.Hx, 33.50.Hv

As first reported by Gibbs [1] many years ago, the transmission of nonlinear optical systems can sometimes exhibit two stable values for a single input intensity, a phenomenon known as bistability. Because of potential applications in all-optical switching for communications and optical computing, many different mechanisms of bistability have been studied. Mirrorless or intrinsic bistability in *dense media* was first considered by Bowden and Sung [2] and elaborated by subsequent authors [3-6] who found that ground state, near dipole-dipole (NDD) interactions responsible for making the local or Lorentz field different from the incident field could cause optical switching. To our knowledge however there have been no experimental reports of all-optical switching mediated by NDD interactions nor any theoretical treatments considering resonant contributions from cooperative excited state dynamics. Here we extend the two-level density matrix model to incorporate new contributions expected from strong, dipolar interactions among *excited states* [7] pertinent to a variety of systems, including quasi-resonant energy exchange collisions in gases [8], avalanche upconversion [9] and cooperative upconversion [10] in solids. Intrinsic bistability dependent on a combination of ground and excited state couplings is predicted and this phenomenon observed in cooperative pair luminescence of the dimeric compound $Cs_3Y_2Br_9:Yb^{3+}$ for the first time.

Pairs of atoms in dense systems, whether gases or solids, can relax through energy transfer mediated by exchange or multipolar electromagnetic interactions at close range, as depicted in Figures 1(a) and 1(b). In dense Cesium vapor for example, an atom prepared in the 6d $^2D_{3/2}$ level can relax non-radiatively to the 6p $^2P_{3/2}$ or $^2P_{1/2}$ level through a collision with a ground state atom which undergoes a simultaneous,

energy-conserving dipole transition upward to 6p [8]. Such a process corresponds to Fig. 1(a). As a second example, in crystals doped with Tm^{3+} impurities, ions prepared in the $^3H_4$ state may decay non-radiatively to $^3F_4$ if a neighbor makes a simultaneous transition to $^3F_4$ in a condensed matter process [11] referred to as cross relaxation. In either example, excitation energy is partitioned between the excited atom and a ground state "collision" partner at a rate which is bilinear in their respective densities, and therefore *nonlinear* with respect to occupation probabilities. Somewhat surprisingly, under selected initial conditions, nonlinear dynamics of this kind can dominate collisional relaxation in gases [12] or lead to cross relaxation avalanches in solids [11]. The reverse process, sketched in Fig. 1(b) and called cooperative upconversion, can also be efficient and is the process responsible for the observations reported here.

Our upconversion experiments were performed in single crystals of $Cs_3Y_2Br_9$:10%Yb^{3+}, one of a family of compounds $Cs_3M_2X_9$ ($M=Ho^{3+}...Lu^{3+}$, Y^{3+} when $X=Cl^-$; $M=Sm^{3+}...Lu^{3+}$, Y^{3+} when $X=Br^-$) crystallizing with space group $R\bar{3}c$ such that rare earth dimer units $[M_2X_9]^{3-}$ form with trigonal axes coinciding with the trigonal crystal axis. A key feature of these dimer or pair-forming materials is that the M-M distance between lanthanide ions is much shorter than in most compounds [13], including the phosphate crystal in which Yb^{3+} cooperative luminescence was observed originally [14]. Since the coupling between lanthanides depends strongly on inter-ion separation, materials of this type exhibit intense cooperative upconversion emission, and give other indications of strong ground and excited state interactions. Neutron scattering measurements of the Yb^{3+}

ground state electronic splitting in $Cs_3Yb_2Br_9$ [15] for example yield the value 3.0 cm^{-1}, which is exceptionally large for rare earth ions. A low power, continuous-wave Ti:Al_2O_3 laser tuned to various Stark components of the $^2F_{7/2} \rightarrow {}^2F_{5/2}$ transition of Yb^{3+} was adequate to excite green pair luminescence at a wavelength of 500 nm in samples cooled to liquid helium temperatures. The intensity of the emission was carefully recorded as temperature and incident intensity were slowly varied.

The dynamics of interest (Fig. 1(b)) can be treated with a two-level pair model of cooperative processes (Fig. 2). This model incorporates ground state dipolar interactions which produce local field corrections in the optical polarization, following previous work [5, 16]. However, excited state interactions are also included. Of the three states shown in Fig. 1, we note that one participates merely as an intermediate state. Its role as a virtual state can nevertheless be preserved in a two-level model, as illustrated in Fig. 2(a) and 2(b), by the incorporation of relaxation terms in the equations of motion with density-dependent rates. For example in Fig. 2(b), cooperative upconversion mediates decay of state $|2\rangle$ population ρ_{22} at a rate of $2\alpha\rho_{22}^2$, where α is the pair upconversion rate constant and the factor of 2 refers to the two excited atoms which decay for each cooperative event. This contributes a term $-\alpha(\sigma_3-\sigma_{30})^2$ to decay of the inversion $\sigma_3 \equiv \rho_{22}-\rho_{11}$ with respect to its equilibrium value σ_{30} in the absence of fields, provided there is negligible thermal occupation of the excited state ($\sigma_{30}=-1$). From the Schrodinger equation of motion for the density matrix, the dynamic equations for the off-diagonal coherence σ_{21} and the inversion σ_3 are therefore:

$$\dot{\sigma}_{21} = -i\,(\Delta + \varepsilon\sigma_3)\,\sigma_{21} - \frac{1}{2}\,i\Omega\sigma_3 - \Gamma\sigma_{21} \qquad (1)$$

$$\dot{\sigma}_3 = -i\,\Omega\,(\sigma_{21} - \sigma_{21}^*) - \gamma(\sigma_3 - \sigma_{30}) - \alpha(\sigma_3 - \sigma_{30})^2 \qquad (2)$$

Here $\varepsilon = n\mu^2/(s\hbar\varepsilon_0)$ is the local field correction term, which has units of frequency, just like α. n is the number density, μ is the dipole transition moment, s is a factor (equal to 3 in cubic solids) determined by a lattice sum [17], ε_0 is the permittivity of vacuum, γ is the excited state decay rate and Γ the dephasing rate. The detuning of light from the resonance frequency at ω_0 is $\Delta = \omega_0 - \omega$, and $\Omega = \mu E/\hbar$ is the Rabi frequency. $\sigma_{21} = -i\tilde{\rho}_{21}$ is a convenient, slowly-varying amplitude of the off-diagonal density matrix element $\rho_{21} = \tilde{\rho}_{21}\exp[-i(\omega t - k.r)]$. Overdots indicate time derivatives.

From (1) and (2) the population inversion σ_3 and the slowly-varying envelope of the optical polarization $P = 2ni\mu_{12}\sigma_{21}$ may be calculated. Since cooperative upconversion and cross relaxation are inverse processes, they are both described by very similar dynamical equations and conclusions drawn below also pertain to avalanche upconversion processes (Figs. 1(a), 2(a)). In steady-state conditions the time derivatives in (1) and (2) equal zero. This yields

$$\sigma_{21} = \frac{\frac{1}{2}\,i\,\Omega\sigma_3[\Gamma - i\,(\Delta + \varepsilon\sigma_3)]}{\Gamma^2 + (\Delta + \varepsilon\sigma_3)^2} \qquad (3)$$

By substituting (3) into (2) and simplifying, we find

$$a\sigma_3^4 + b\sigma_3^3 + c\sigma_3^2 + d\sigma_3 + e = 0 \qquad (4)$$

where the coefficients are given by

$a = \alpha\varepsilon^2$, $b = -2\alpha\sigma_{30}\varepsilon^2+\gamma\varepsilon^2+2\alpha\Delta\varepsilon$, $c = -\gamma\sigma_{30}\varepsilon^2+2\gamma\Delta\varepsilon+\alpha\sigma_{30}^2\varepsilon^2+\alpha\Gamma^2-4\alpha\sigma_{30}\Delta\varepsilon+\alpha\Delta^2$,
$d = -2\gamma\sigma_{30}\Delta\varepsilon+\Omega^2\Gamma+\gamma\Gamma^2+2\alpha\sigma_{30}^2\Delta\varepsilon-2\alpha\sigma_{30}\Gamma^2+\gamma\Delta^2-2\alpha\sigma_{30}\Delta^2$, and
$e = \alpha\sigma_{30}^2\Gamma^2-\gamma\sigma_{30}\Gamma^2-\gamma\sigma_{30}\Delta^2+\alpha\sigma_{30}^2\Delta^2$.

The quartic equation in (4) has solutions which are multi-valued and describe the full features of bistability to be expected in the inversion of cooperative dynamic systems. When the upconversion rate α is zero, the coefficient of the quartic term $\alpha\varepsilon^2$ vanishes and we recover the results of Refs. [2-6,16]. However when both α and ε are not zero, the fourth order coefficient becomes finite and leads to changes in the nonlinear dynamics which are the *joint* result of ground and excited state NDD interactions.

In Fig. 3, the solution of (4) for the steady state inversion σ_3 is used to plot $(\sigma_3-\sigma_{30})^2$, a quantity proportional to the pair luminescence intensity, as a function of incident intensity Ω^2. Without upconversion, the leftmost curve shows that weak bistability is predicted when the local field factor ε exceeds excited state relaxation frequencies γ and Γ. The solutions in the central portion of this plot between the turning points (dashed) are demonstrably unstable, causing hysteresis in the inversion versus incident intensity. As intensity is increased from zero, the predicted pair luminescence intensity at first follows the lower branch of the curve, but reaches a point at which the only stable solution available at higher powers lies on the upper branch of the curve. Here, switching to the upper branch occurs and switch-down only occurs subsequently if the incident intensity falls below the point at which only a lower branch solution exists.

As the upconversion rate α is increased from zero to a value comparable to ε (curve farthest to the right in Fig. 3), two significant

effects occur. First, a higher input power is required to reach bistability. Second, an immense magnification of the area of the hysteresis loop occurs with only minor changes in the relative shape of the curve. This is evidence that excited state dipole-dipole interactions influence nonlinear dynamics in much the same way ground state interactions do, in keeping with the fact that both enter the coefficient of the quartic term on a similar footing as the product $\alpha\varepsilon^2$. However, for reasons not yet completely understood but possibly related to the resonant nature of excited state interactions considered here, the effect of α is much greater than that of ε.

In Fig. 4, experimental results are shown which confirm basic predictions of the model. In Fig. 4(a) upconversion emission abruptly increases at a well-defined intensity as the incident power increases. Sample emission maintains an almost constant value as the incident intensity is increased further and switches down only when the power is decreased well below the original switching point. As the atom-atom coupling increases toward lower temperatures, the hysteresis loops enlarge and move to higher excitation energies as expected. However the step height enlarges, in a trend which is not understood at present. This may result from neglect of resonant energy migration in the excited state, which cannot be included using single atom basis states in a 2-level model although it would undoubtedly enhance the importance of cooperative interactions. In Fig. 4(b), similar hysteresis is apparent when the incident intensity is held fixed and temperature is varied. In this case the effective inter-atom coupling changes, because the overlap integral and competing decay processes are temperature dependent. Hence this is roughly equivalent to varying α at a fixed intensity in our model, in which

case the theory predicts very similar bistability results. Both sets of observations clearly show that cooperative emission exhibits hysteresis without feedback (mirrors).

Broad inferences may be drawn from the present work by adopting the following perspective. In both gases and solids, cooperative interactions like cross relaxation or upconversion may be pictured as "collisional" processes which occur on timescales comparable to or shorter than the average collision time. In gases, collision times are typically very short, and collisional interactions brief. On the other hand, near-neighbor rare earth impurities in solids, separated by short distances as if in a "frozen" collision, interact in excited states on timescales limited by lifetimes of the energy levels, which can be as long as ten milliseconds. This analogy with gaseous collisions is in fact more apt than generally recognized, since collisional depolarization ratios of rare gases for example can be calculated from elasto-optic coefficients of rare gas solids [18]. Hence when long interaction times are encountered, such as in rare earth solids or for nearly stationary atoms in optical traps, the concept of *slow collisions* can be invoked to unify the seemingly distinct domains of coupled dopants in solids and colliding ultracold atoms in vacuum. The model presented here, in which atoms are assumed to be effectively at rest, is expected to encompass both physical situations.

Although not explicitly reported here, optical absorption in this and other coupled systems is also expected to undergo switching, since it is proportional to σ_3. That is, absorption by coupled atoms in dense excited systems with transition energy coincidences should exhibit hysteresis. This implies that many related effects may be observable in dense vapors

and gases. For example, the absorption behavior of ultracold colliding atoms which happen to have nearly identical ground and excited state transition energies should exhibit hysteresis on selected transitions. At microkelvin temperatures and below, atoms are essentially at rest on the time scale of excited state relaxation processes. Consequently, we expect behavior related to that calculated and observed here for stationary atoms in a concentrated rare earth solid to apply to ultracold dense gases too.

In summary, we have shown that pair emission of Yb^{3+} ions in $Cs_3Y_2Br_9:Yb^{3+}$ exhibits intrinsic bistability as a function of incident intensity and temperature. A model in which contributions to the nonlinear polarization from ground and excited state interactions between Yb^{3+} ions are treated on an equal footing gives good agreement with experiments. Furthermore, the mere fact that the first example of bistability due to atom-atom interactions has emerged from a cooperative upconversion system supports the general conclusion that resonant excited state interactions amplify nonlinear response associated with the Lorentz field, rendering bistability much easier to observe. It confirms experimentally that cooperative nonlinearities can induce hysteretic behavior in crystals without a cavity. Bistability from this mechanism can be expected to occur also in avalanche systems which decay by run-away cross relaxation. Furthermore, while our results are most pertinent to stationary atoms in solids, we have argued that they have broader implications for selected transitions in vapors which induce quasi-resonant collisional interactions. Similar effects may occur in high density optical traps below the Doppler cooling limit when internuclear separation does not change appreciably during an excited state lifetime.

Finally, these results suggest new extensions of theories of the local field [17] in dense atomic systems.

We are indebted to C.M. Bowden for reading the manuscript and to N. Furer for assistance with crystal growth. Several authors (J.R., S.R. and S.C.R.) gratefully acknowledge research support by the U.S. Air Force Office of Scientific Research (H. Schlossberg) and the University of Michigan Program for Nonlinear Studies. Two of us (M.P.H. and H.U.G.) wish to thank the Swiss National Science Foundation for financial support.

References:

1. H. M. Gibbs, S. L. McCall and T. N. C. Venkatesan, Phys. Rev. Lett. 36, 1135(1976).

2. C. M. Bowden and C. C. Sung, Phys. Rev. A19, 2392(1979).

3. F. A. Hopf, C. M. Bowden and W. Louisell, Phys. Rev. A29, 2591(1984).

4. F. A. Hopf and C. M. Bowden, Phys. Rev. A32, 268(1985).

5. Y. Ben-Aryeh, C. M. Bowden and J. C. Englund, Phys. Rev. A34, 3917(1986).

6. M. E. Crenshaw, M. Scalora and C. M. Bowden, Phys. Rev. Lett. 68, 911(1992).

7. S. C. Rand, "Cooperative Optical Nonlinearities", Quant. Elect. and Laser Spectr. Conf. (QELS'91), Baltimore, Maryland, May12-17, 1991, invited paper QThK1.

8. A. C. Tam, T. Yabuzaki, S. M. Curry, M. Hou, and W. Happer, Phys. Rev A17, 1862(1978); M. Allegrini, C. Gabbanini and L. Moi, J. de Phys. (Fr.) 46, C1-61(1985).

9. J. S. Chivian, W. E. Case and D. D. Eden, Appl. Phys. Lett. 35, 124(1979).

10. P. Xie and S. C. Rand, Opt. Lett. 17, 1198(1992).

11. H. Ni and S. C. Rand, Opt. Lett. 16, 1424(1991).

12. S. C. Rand, A. Lenef and D. Kreysar, "Atomic Collisional Avalanche", Proc. of Eleventh Int. Conf. on Laser Spectroscopy (Elicols'93), Hot Springs, Virginia, June 13-18, 1993, paper MP-3.

13. M. P. Hehlen and H. U. Güdel, J. Chem. Phys. 98, 1768(1993).

14. E. Nakazawa and S. Shionoya, Phys. Rev. Lett. 25, 1710(1970).

15. H. U. Güdel, A. Furrer, and H. Blank, Inorg. Chem. 29, 4081(1990).

16. C. M. Bowden and J. P. Dowling, Phys. Rev. A47, 1247(1993).

17. J. Van Kranendonk and J. E. Sipe, in Progress in Optics XV, edited by E. Wolf (North-Holland, Amsterdam, 1977), p. 245; F. Hynne and R.K. Bullough, Philos. Trans., R. Soc. London, Ser. A 312, 251(1984); 321, 305(1987); 330, 253(1990).

18. J. E. Sipe, Can. J. Phys. 56, 199(1978).

FIGURE CAPTIONS

Figure 1. Cooperative dynamics involving two 3-level atoms, giving rise to (a) cross relaxation, and (b) pair upconversion. Wiggly arrows indicate photons. Curved arrows indicate (non-radiative) coupled atom (cooperative) dynamics.

Figure 2. Two-level theoretical models of the cooperative dynamics depicted in Fig. 1 in which the third (intermediate) states are treated as virtual states. Wiggly arrows indicate photons. Curved arrows indicate (non-radiative) cooperative relaxation processes.

Figure 3. Calculated pair luminescence intensity (proportional to $(\sigma_3-\sigma_{30})^2$) in a system undergoing pair emission, plotted as a function of incident intensity (Ω^2) on resonance ($\Delta=0$). The solid (dashed) curves indicate stable (unstable) solutions. From left to right, the five plotted curves correspond to values of inter-atomic coupling of $\alpha=0$, 2, 4, 6, 8 respectively. All frequencies are referenced to $\gamma=\Gamma=1$ and the local field parameter has the fixed value $\varepsilon=10\ \varepsilon_{cr}$, where $\varepsilon_{cr}=3\sqrt{3}$ is a critical field needed for bistability when $\alpha=0$.

Figure 4. Upconversion emission intensity at $\lambda=$ 500 nm versus incident laser power from Yb^{3+}-Yb^{3+} pairs in $Cs_3Y_2Br_9$:10% Yb^{3+} at various fixed temperatures (top to bottom): 31K, 27K, 23K, 19K, 15K, 11K. (b) Upconversion emission intensity at $\lambda=$ 500 nm versus temperature in $Cs_3Y_2Br_9$:10% Yb^{3+} at various fixed incident intensities (top to bottom): 814 , 640, 539, 415 W/cm^2.

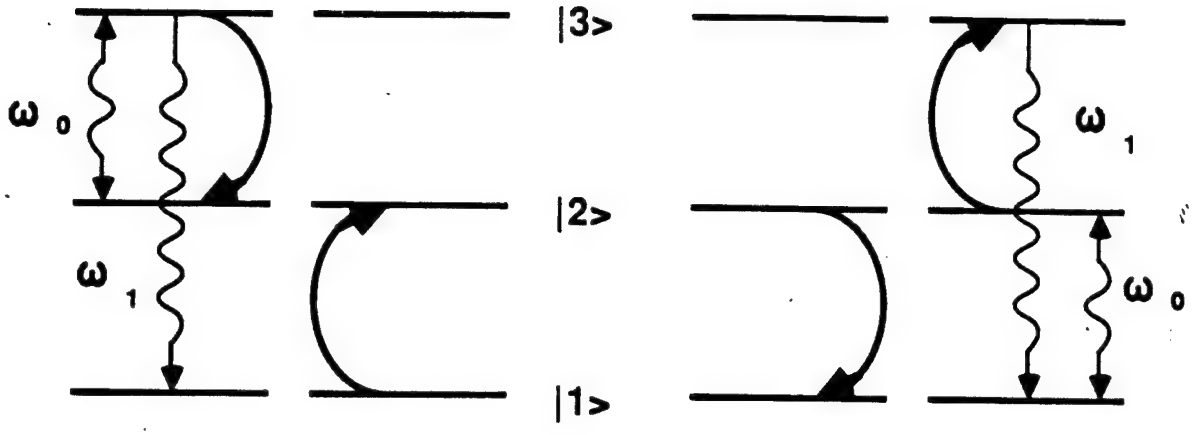

Figure 1.

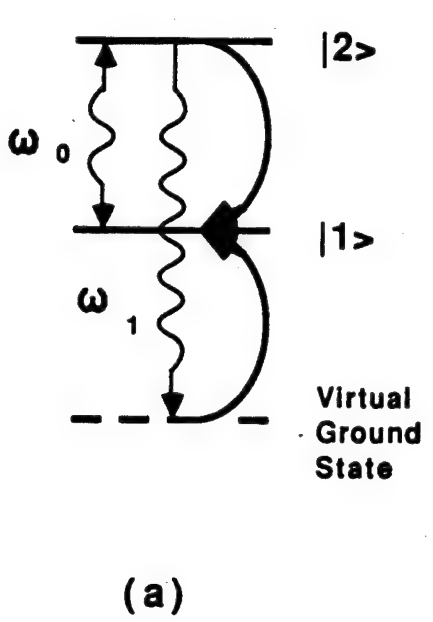

(a)

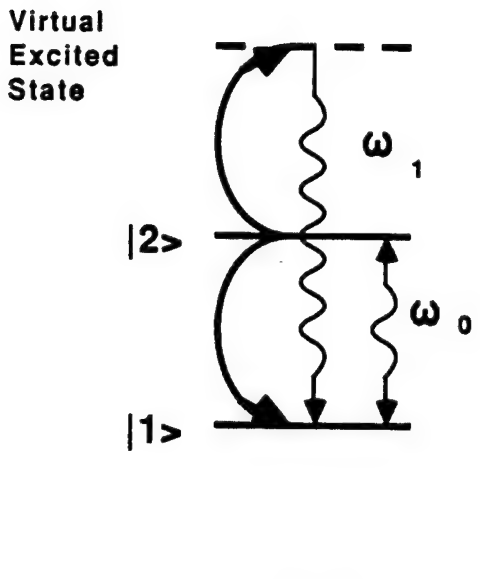

(b)

Figure 2.

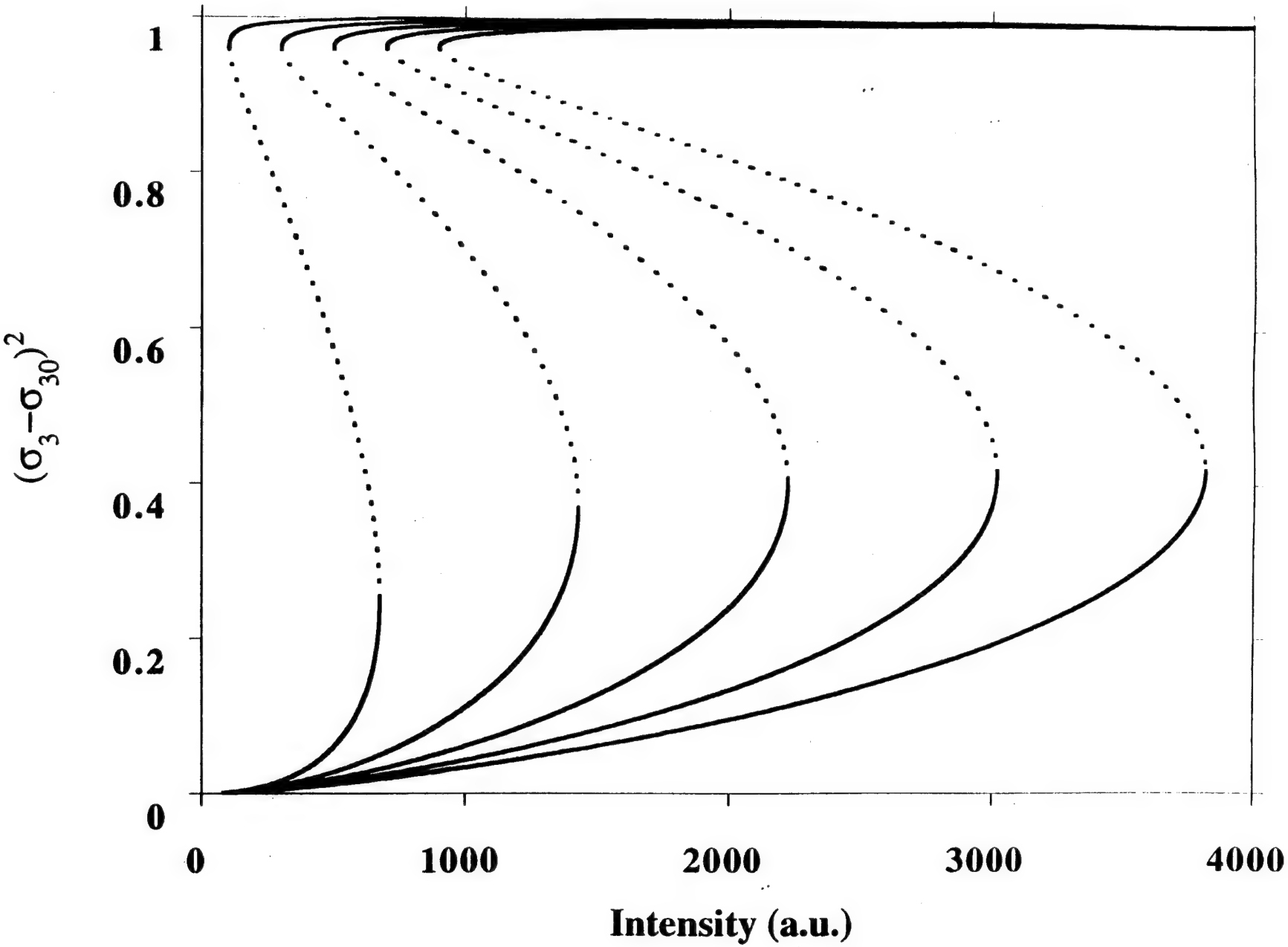
1
0.8
0.6
0.4
0.2
0
$(\sigma_3-\sigma_{30})^2$
0
1000
2000
3000
4000
Intensity (a.u.)

FIG. 3

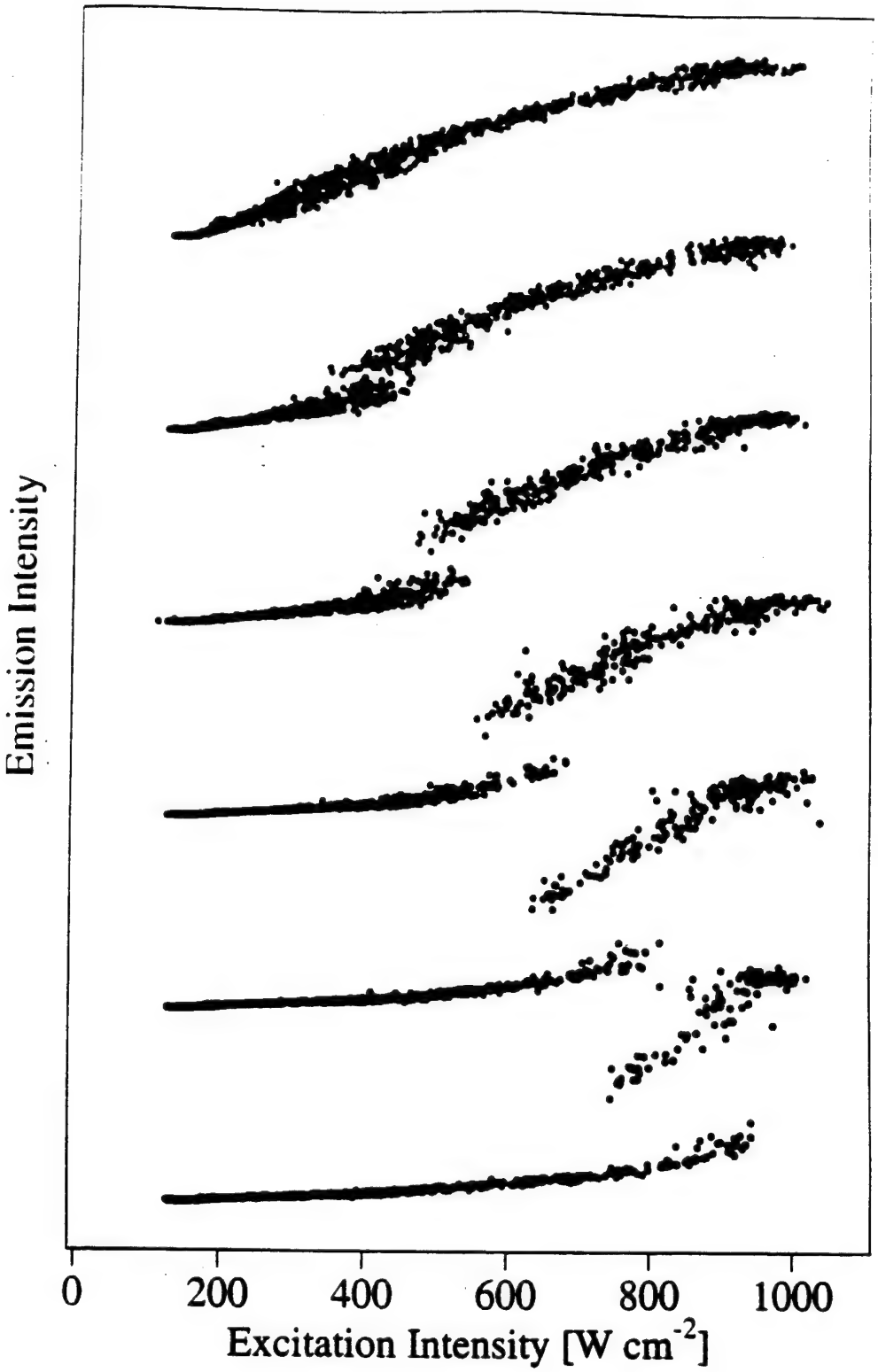
Emission Intensity
0
200
400
600
800
1000
Excitation Intensity [W cm^{-2}]

FIG. 4 (a)

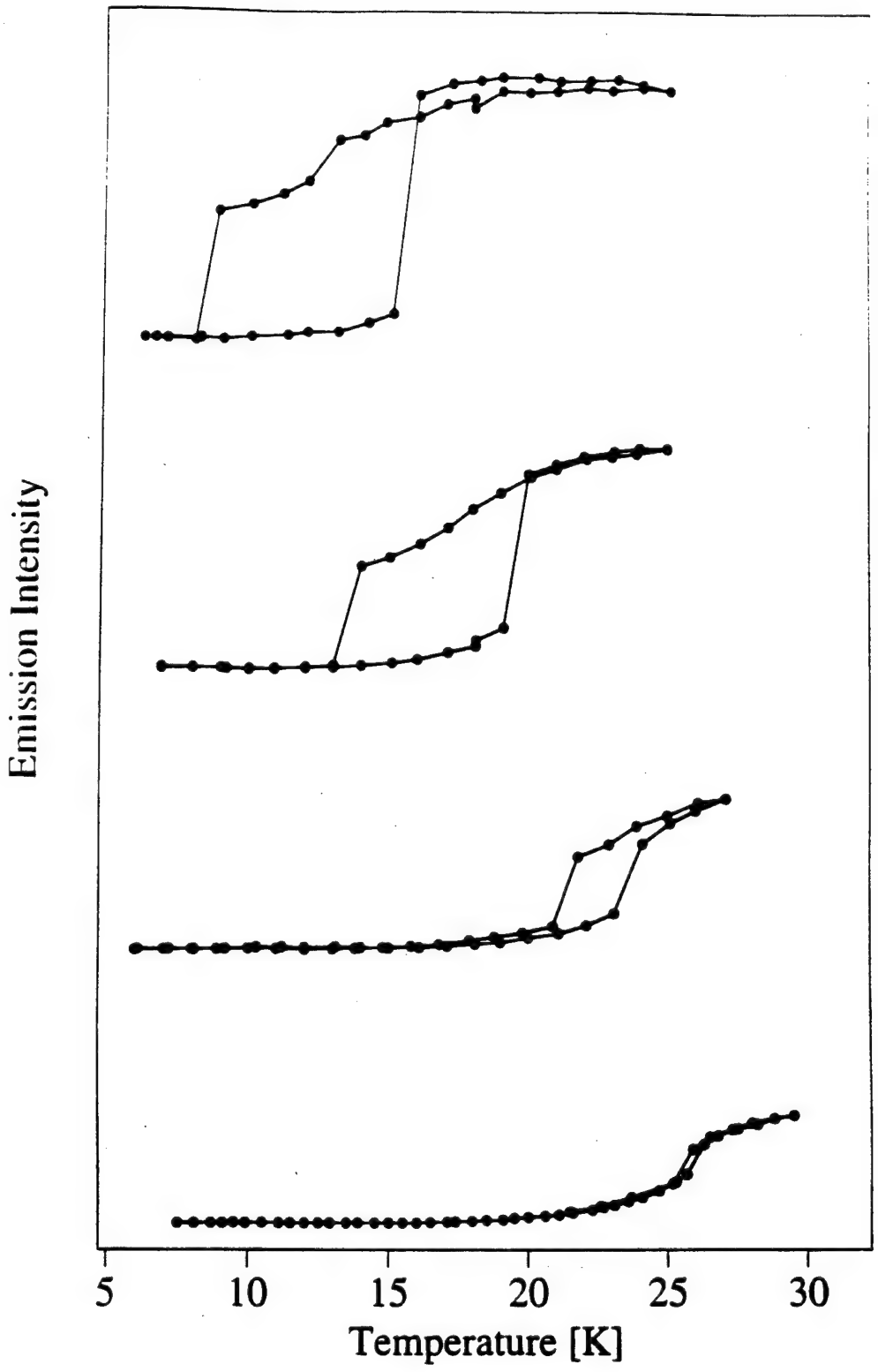

FIG 4(b)

PROPERTIES AND GROWTH OF Diamond

Edited by

GORDON DAVIES

King's College, London, UK

IEE

inspec

Published by: INSPEC, the Institution of Electrical Engineers,
London, United Kingdom

Institution of Electrical Engineers
Michael Faraday House,
Six Hills Way, Stevenage,
Herts. SG1 2AY, United Kingdom

British Library Cataloguing in Publication Data

A CIP catalogue record for this book
is available from the British Library

ISBN 0 85296 875 2

Printed in England by Short Run Press Ltd., Exeter

7.4 Diamond lasers

S.C. Rand

August 1992

A INTRODUCTION

Many of the properties which make diamond uniquely attractive for mechanical and electronic applications also lend interest to its potential for optical applications. In particular, its wide bandgap and the exceptional stability of various optical centres in this host make it attractive for generation of radiation throughout the visible spectral region. Furthermore, the high thermal conductivity, excellent hardness, and high damage threshold of diamond suit it well to high power laser operation. Here we present a review of progress and prospects in diamond laser development.

In Section B, a few radiation-induced defect centres which may be useful for the generation of laser radiation in diamond are compared with high gain laser centres of the alkali halides. In Sections C and D, progress on H3 laser development and prospects for other diamond centres are discussed.

B OPTICAL CENTRES FOR LASERS IN DIAMOND

Pure diamond is an indirect gap material like silicon. As a consequence, there is little hope of obtaining stimulated emission directly at the bandgap recombination wavelength of 227 nm [1]. However intrinsic point defects, impurities, and centres composed of both point defects and impurities provide potential candidates for laser action at longer wavelengths. Here, we tabulate spectroscopic parameters and theoretical laser gain for a few centres which combine impurities and vacancies and review their potential for laser applications. Procedures for the synthesis of centres and general characteristics of colour centre lasers may be found in [2] and [3] respectively.

From TABLE 1 two general conclusions may be drawn. First, diamond colour centres have exceptionally broad fluorescence linewidths $\Delta\nu$ compared to those of the commercially successful alkali halide lasers, exemplified by the F_2^+ laser. As a result, their potential tuning range is many times greater. Second, their gain coefficients are lower than that of F_2^+:KCl, but still very respectable considering the breadth of emission. The order of magnitude difference between F_2^+ and N-V gain coefficients may be overcome in principle by merely increasing the excited state density by a factor of ten.

TABLE 1 Comparison of diamond and F_2^+:KCl colour centre gain coefficients γ for constant inversion density $N = 10^{16}$ cm^{-3}.

Centre	n	T (K)	τ_{fl} (ns)	η	$\Delta\nu$ (10^{13} s^{-1})	λ_o (μm)	γ (cm^{-1})
F_2^+	1.4841 [3]	77	τ_{fl}/η = 80 [3]	τ_{fl}/η = 80 [3]	1.69 [3]	1.680 [3]	3.52
N-V	2.4065 [4]	295	13.3 [5]	0.99 [5,6]	6.53 [5]	0.697 [5]	0.366
H3	2.4262 [4]	295	16 [2]	0.95 [7]	5.27 [5]	0.531 [5]	0.201

C PROGRESS ON H3 LASERS

Since the discovery of the first diamond laser [8], two other experiments have demonstrated laser action in diamond using H3 colour centres. In this unpublished work, high densities of H3 centres in natural and synthetic diamonds were used, as described briefly below.

In 1988 at the Itami Research Laboratories of Sumitomo Electric in Japan, a flashlamp-pumped Coumarin dye laser with pulsewidth of 500 ns was used to side-pump a natural diamond crystal of dimensions 3 x 2 x 2 mm^3 at an excitation wavelength of 490 nm inside a 2-mirror resonant cavity. The end mirror was a total reflector with a radius of 40 cm and the output mirror had the same curvature and a reflectivity of 97%. Both mirrors were spherical and separated by approximately 35 cm. Laser action in the yellow spectral region was obtained at room temperature with a threshold of 3 MW/cm^2 without auxiliary cooling [9]. Laser output ceased when cavity mirrors were detuned or blocked, thus extending the original result by the use of an external cavity.

Continuous-wave laser action was demonstrated in the same year at the University of Strathclyde [10]. Optical excitation was performed with a continuous-wave argon ion laser operating at 488 nm. In this case a 3-mirror cavity was used to compensate for astigmatism introduced by tilting the sample to Brewster's angle for minimum reflective losses, and the crystal was cooled to 77 K. Output power is shown as a function of input power in FIGURE 1 for two synthetic diamond samples from De Beers. Although slope efficiency was very low (6.6 x 10^{-4}%), the tuning range of this laser was remarkably wide, comparable with the fluorescence spectrum shown in FIGURE 2. Its low efficiency may be related to residual N-V absorption in the laser emission region, or to transient losses associated with B or Ni impurities used to facilitate H3 formation during crystal growth. Sumitomo researchers have also synthesised H3 crystals [11] with very bright photoluminescence, but to date have not reported continuous lasing.

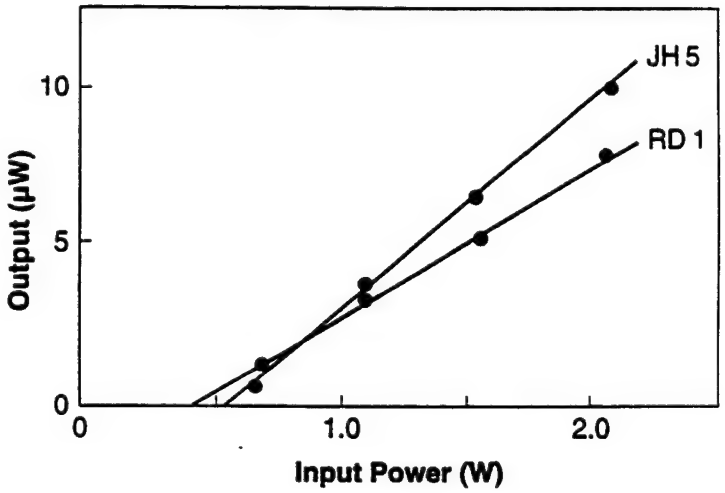

FIGURE 1 Continuous-wave laser output power as a function of input pump power at 488 nm in two synthetic diamond crystals (De Beers JH5, RD1) at T = 77 K. (With permission [10].)

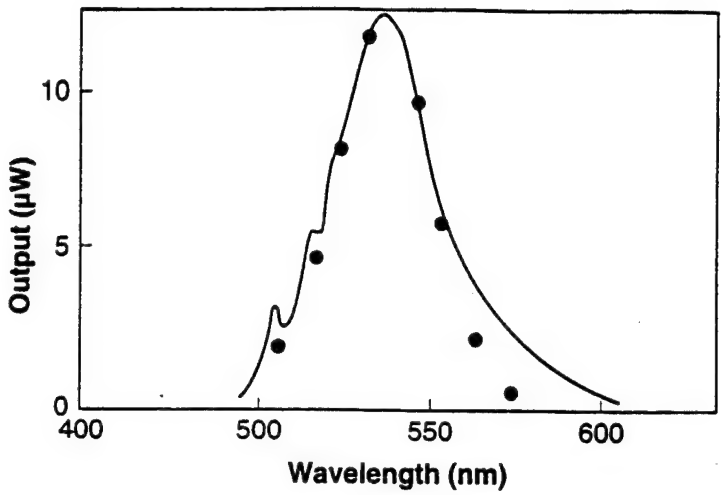

FIGURE 2 Comparison between tuning range of the CW diamond laser (solid circles) and the fluorescence spectrum (solid curve) of the laser active H3 centre, obtained by time resolved photoluminescence. (With permission [10].)

D PROSPECTS FOR NEW DIAMOND LASERS

The H3 laser described above is the only laser of any kind able to scan continuously through the wide visible range from 500 - 600 nm. This unique capability argues strongly for renewed research to improve crystal synthesis in an effort to minimise parasitic losses. Additionally however, other promising approaches for lasers at both shorter and longer wavelengths in diamond should be considered. Several of these are outlined below.

The theoretical gain coefficient for the N-V centre (TABLE 1) is nearly twice that of the H3 centre. Hence it is an excellent laser candidate, compatible with efficient diode laser pumping schemes. Of course, absorptive losses in the emission band must be kept very low for net positive gain to be realised experimentally. Encouragingly, the only centre with broadband absorption in the range 650 - 750 nm is the GR1 vacancy centre, which exhibits very low absorption (and emission) at room temperature and can be removed by appropriate annealing procedures. Also, the intrinsic quantum efficiency of the N-V centre is unity [6]. Although recent spectroscopic studies [12] confirmed the presence of a metastable level below the 638 nm fluorescent level of the N-V centre which acts as a sink for excited state population, its effect is negligible. Furthermore, high concentrations of this centre can be produced by a simple procedure, so its overall prospects for laser action remain good.

Other nitrogen-related centres may be viable laser candidates. Scant information is available on detailed models or stability of such centres, however, and few have strong broadband emission in the visible or near infrared (IR) spectral regions. Other approaches nevertheless offer promising new directions. For example, changing diamond into a direct gap material through the use of strained layer structures has been considered [13]. Additionally, radiation-induced and aggregate impurity centres in boron-doped diamond should be investigated. Boron is easily substituted into the diamond matrix and results in useful semiconductivity. By incorporating other impurities which fit reasonably well into the lattice (C^{+4} ionic radius = 0.16 Å), like nitrogen, sulphur, chlorine, phosphorus and silicon (ionic radii of 0.16 Å, 0.44 Å, 0.37 Å, 0.34 Å and 0.42 Å respectively), many new stable aggregate

centres can undoubtedly be created and pumped electrically, warranting further investigation. By combining such centres with radiation-induced vacancies using suitable annealing procedures, additional possibilities for stable centres may be realised.

Rare earth (RE) dopants, which are currently under investigation for lasers and display components in compound semiconductors [14], and constitute the laser active species in dozens of commercial solid state lasers, may also be useful for semiconductor diamond defect lasers. However, the ionic radii of trivalent rare earth ions all exceed 0.86 Å. Hence it seems unlikely that high enough concentrations of such impurities can be achieved in diamond to permit such applications. Transition metal ions tend to have smaller radii and may therefore be more promising candidates for laser research in this host. Boron itself absorbs strongly throughout the visible spectrum, so it is likely that in B-doped semiconducting diamond useful emission wavelengths of impurity metal laser ions (possibly associated with compensating, radiation-induced defects) will be restricted to the infrared. At very long wavelengths because of its renowned transparency in the far infrared (FIR), diamond might ultimately prove, however, to be the material of choice, indeed perhaps the only material compatible with solid-state FIR laser operation.

ACKNOWLEDGEMENT

The author wishes to thank S. Satoh, K. Tsuji, S. Yazu of Sumitomo Electric and B. Henderson and G. Taylor of the University of Strathclyde for sharing unpublished results. The author gratefully acknowledges partial support of this work by the Air Force Office of Scientific Research and the NSF STC Center for Ultrafast Optical Science (STC PHY 8920108).

REFERENCES

[1] C.D. Clark, P.J. Dean, P.V. Harris [*Proc. R. Soc. Lond. A (UK)* vol.277 (1964) p.312]

[2] S.C. Rand [*Synthetic Diamond for Color Center Lasers*, Springer Ser. in Opt. Sci., vol.52, Eds A. Budgor, L. Esterowitz, L.G. DeShazer (Springer-Verlag, New York, USA, 1986) p.276-80]

[3] L. Mollenauer [*Methods Exp. Phys. (USA)* vol.15B (1979) pt.6]

[4] F. Peter [*Z. Phys. (Germany)* vol.15 (1923) p.358]

[5] D. Redman, Q. Shu, A. Lenef, S.C. Rand [*Opt. Lett. (USA)* vol.17 (1992) p.175]

[6] Optical pumping losses from the lowest ^{3}E level (labelled 4) to both the ^{1}A state (3) and the second (spin-split) ground state level (2) estimated from unpublished transient hole-burning experiments together with results of [12,15]. Absolute changes in population of metastable levels were determined and compared with steady-state theoretical population ratios governed by simple decay ratios. Values determined in this way were $\gamma_{42} = 2.2 \times 10^4\ s^{-1}$ and $\gamma_{43} = 7.8 \times 10^4\ s^{-1}$. Since $\gamma_4 = (\pi \times 13.3 \times 10^{-9})^{-1}$ [5], we find intrinsic quantum efficiency $Q = \gamma_{41}/(\gamma_{41} + \gamma_{42} + \gamma_{43}) = 0.99$.

[7] G. Davies [*Diamond Res. (UK)* 15-24 (1977)]; M.D. Crossfield, G. Davies, A.T. Collins, E.C. Lightowlers [*J. Phys. C (UK)* vol.7 (1974) p.1909]

[8] S.C. Rand, L.G. DeShazer [*Opt. Lett. (USA)* vol.10 (1985) p.481]; S.C. Rand, L.G. DeShazer [US patent no.4, 638, 484 (1987)]

[9] S. Satoh, K. Tsuji, S. Yazu [private communication, 15 July 1988]

[10] G. Taylor [M.Sc. Thesis, University of Strathclyde, 1988 (unpublished)]

[11] S. Satoh [European patent no.88121859.8 (1988)]

[12] D. Redman, S. Brown, R.H. Sands, S.C. Rand [*Phys. Rev. Lett. (USA)* vol.67 (1991) p.3420]

[13] W.E. Pickett, M.J. Mehl [*Proc. SPIE (USA)* vol.877 (1988) p.64-9]

[14] K. Pressel et al [*Appl. Phys. Lett. (USA)* vol.61 (1992) p.560]; P. Galtier et al [*Appl. Phys. Lett. (USA)* vol.55 (1989) p.2105]

[15] D.A. Redman [Electronic Structure of the Nitrogen-Vacancy Center in Diamond, Ph.D. Dissertation, University of Michigan, Ann Arbor, Michigan, USA, 1991]

ELSEVIER

Journal of Luminescence 60&61 (1994) 739–741

JOURNAL OF LUMINESCENCE

Zeeman coherence and quantum beats in ultrafast photon echoes of N-V centers in diamond

S.C. Rand*, A. Lenef, S.W. Brown

Division of Applied Physics, 1049 Randall Laboratory, University of Michigan, Ann Arbor, MI 48109-1120, USA

Abstract

Ultrafast photon echo experiments reveal highly modulated quantum beats in nitrogen-vacancy centers in diamond, providing direct measurements of excited state splittings for the first time. We also confirm the existence of new peaks in echo excitation spectra and report novel polarization dependent interferences.

The establishment of definitive models of luminescent centers in solids, particularly in widegap semiconductors, is becoming increasingly important in the context of next generation flat panel displays. Here, we report the direct determination of excited state structure and dephasing dynamics of the nitrogen-vacancy (N-V) center in diamond from ultrafast photon echo observations. These results provide the basis for a detailed model of the center.

Previous results from isochronal annealing experiments and uniaxial stress measurements by Davies and Hamer [1] on the 638 nm zero phonon transition of the N-V center provided evidence for a trigonal center of C_{3v} symmetry consisting of a carbon vacancy adjacent to a nitrogen impurity. The ground and excited states were determined to be of A and E symmetry, respectively [1]. Electron paramagnetic resonance (EPR) measurements by Loubser and Van Wyk [2] confirmed the basic physical model of the center. Transient hole-burning experiments [3] and Curie-law dependence of the magnetic susceptibility from ground state EPR measurements at 2.88 GHz by Redman et al. [4] established the triplet character of the ground state. Persistent hole-burning measurements also revealed transitions at frequencies combining the ground state spin–spin splitting with other frequencies on the GHz scale, providing indirect evidence for ^3E excited state structure [5]. Optically detected microwave resonance (ODMR) measurements [6], in which the laser probe was tuned across the ZPL, also revealed a larger $40\,cm^{-1}$ splitting in the ODMR spectrum, suggesting that an even larger splitting existed in the excited state.

In the present work, ultrafast stimulated photon echo experiments were performed to investigate excited state structure directly. A dual jet, synchronously-pump DCM dye laser was employed, generating cavity-dumped subpicosecond pulses at a variable repetition rate near 100 KHz. The sample was a high-quality synthetic, nitrogen rich single crystal. This was irradiated with 1.7 MeV electrons and subsequently annealed to produce

* Corresponding author.

SSDI 0022-2313(93)E0263-W

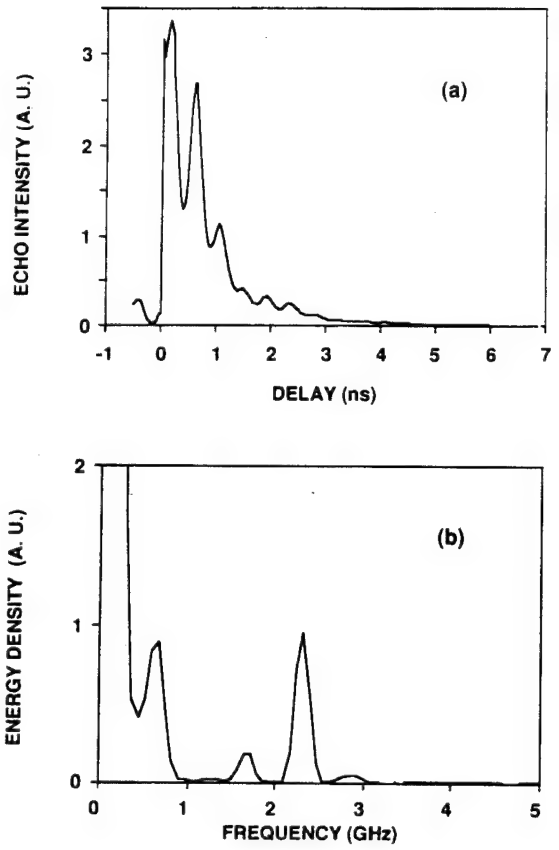

Fig. 1. (a) Stimulated photon echo decay data from diamond N–V centers, showing highly modulated quantum beats at 6 K, $\lambda = 638.2$ nm. Incident beams are all linearly polarized in the $\langle 0\,0\,1\rangle$ direction. (b) Power spectrum of echo data.

high concentrations of N-V centers. Three input beams were arranged in a phase conjugate geometry with counter-propagating pump waves and a probe wave incident at a small angle with respect to the forward pump. Pump waves were aligned parallel to the [1 0 0] direction. Spatially filtered, time-averaged echo signals were recorded using lock-in detection techniques with a photomultiplier. Signals were recorded as a function of probe delay, incident wavelength, and temperature, and they verified to be independent of repetition rate. For polarization-dependent studies, quarter-wave plates were inserted into all three incident beams, using an additional quarter-wave plate and polarizer combination to analyze the resulting echo.

The photon echo intensity is shown in Fig. 1(a) as a function of probe delay, revealing deep modulations in the photon echo decay. The wavelength was tuned to the red side of the ZPL ($\lambda = 638.2$ nm) with all incident beams polarized in the $\langle 0\,0\,1\rangle$ direction. Figure 1(b) shows the power spectrum of these data. The exponential decay in Fig. 1(a) was first divided from the data before Fourier transformation. We measured frequency components at $A = 2.87 \pm 0.01$ GHz, corresponding to the known ground state splitting, as well as components at $B = 0.61 \pm 0.02$ GHz, $C = 1.65 \pm 0.01$ GHz, and $D = 2.30 \pm 0.01$ GHz, related to excited state splittings. These observed frequencies agree with our persistent hole-burning observations [5], but in addition confirm that all modulations originate directly from splittings in the ^{3}E and ^{3}A states coupled by the light, rather than relaxed states, since the signal appears as a quantum beat from coherence established within the incident pulse duration.

The existence of two ^{3}E excited states with different dephasing behaviors was revealed directly by recording the excitation spectrum of the echo signals across the ZPL. The excitation spectrum shows two distinct peaks separated by a width of $42 \pm 2\,\mathrm{cm}^{-1}$; not resolvable in linear absorption measurements of these strongly inhomogeneously broadened centers. The dephasing rates versus temperature of these two states were measured with the laser tuned to the red (638.9 nm) and blue (636.5 nm) sides of the ZPL linear absorption peak. Dephasing times at 5.5 K for the red and blue peaks were 4.92 ± 0.24 ns and 56 ± 8 ps, respectively, corresponding to four times the measured decay times in the photon echo signals. Theoretical fits confirm that the upper of the two ^{3}E states decays rapidly by a direct process to the lower level as one might expect, while the lower state dephases more slowly through a virtual 2-phonon process. The dominant activation energy for the direct process was $67 \pm 25\,\mathrm{cm}^{-1}$, in reasonable correspondence with the measured splitting of the two ^{3}E states. For the lower level, an Orbach process dominates at low temperatures with an activation energy of $39 \pm 10\,\mathrm{cm}^{-1}$, also in good agreement with the measured excited state splitting.

Finally, a detailed investigation of the polarization dependence of the echo intensities with circu-

larly polarized beams revealed an interesting selection rule which caused signal intensities to drop by an order of magnitude when the pulse polarization sequence was $\sigma^+\sigma^-\sigma^+$ or $\sigma^-\sigma^+\sigma^-$. This effect arises from interferences in the echo signal due to a superposition of third-order interactions in the presence of ground state magnetic degeneracies. For fixed probe delay, ignoring quantum beat contributions and population relaxation, the ith component of the echo polarization $P_i^{(3)}$ has the form

$$P_i^{(3)} = 2\,\mathrm{Re}\left[\frac{1}{8}\sum_{\alpha}\sum_{jkl}\varepsilon_0\chi_{ijkl}^{(3)}(\alpha) \times\left(E_{1j}^{*}E_{2k}E_{3l} + E_{1j}^{*}E_{2l}E_{3k}\right)\right], \quad (1)$$

where $E_{\eta j}$ is the jth component of the applied electric field of the ηth pulse, and $\chi^{(3)ijkl}(\alpha)$ is a third-order susceptibility that includes the tensoral nature of the interaction. The summation over α in Eq. (1) is over the different defect orientations in the lattice.

If we consider the specific example of a $\sigma^+\sigma^-\sigma^+$ sequence for a specific orientation, the x component of the third-order polarization in Eq. (1) is

$$P_x = \varepsilon_0 E_0|E_0|^2\left[\left(\chi_{xxxx}^{(3)} - \chi_{xxyy}^{(3)} - \chi_{xyxy}^{(3)} - \chi_{xyyx}^{(3)}\right) - \mathrm{i}\left(\chi_{xyyy}^{(3)} - \chi_{xxxy}^{(3)} - \chi_{xxyx}^{(3)} - \chi_{xyxx}^{(3)}\right)\right], \quad (2)$$

where E_0 is the magnitude of the applied fields. In a center with cubic symmetry, the only nonzero terms in Eq. (2) are $\chi_{xxyy}^{(3)} = \chi_{xyxy}^{(3)} = \chi_{xyyx}^{(3)} = \frac{1}{3}\chi_{xxxx}^{(3)}$, in which case $P_x = 0$. For the more complicated case of the C_{3v} symmetry N-V center, P_x is still reduced significantly for the $\sigma^+\sigma^-\sigma^+$ case when all defect orientations are considered. Explicit group-theoretical calculations of $\chi^{(3)}$ for a transition between a doubly degenerate E symmetry state in the ground state manifold and a nondegenerate excited state in the N-V center predict relative echo intensities with ratios of 64:25:4 for $\sigma^+\sigma^+\sigma^-$, $\sigma^+\sigma^+\sigma^+$ or $\sigma^+\sigma^-\sigma^-$, and $\sigma^+\sigma^-\sigma^+$ polarization sequences (and equivalent sequences with reversed circular polarization), respectively. These results, which will be presented in detail in a later work, assume applied fields propagate in the [0 0 1] direction and are in good agreement with our observations.

In summary, we have presented quantum beat measurements of excited state splittings in the N-V center in diamond. The existence of a large splitting in the excited state manifold was revealed in echo excitation spectra. Temperature-dependent dephasing studies of these two states indicated that direct and virtual 2-phonon processes were the primary mechanisms responsible for dephasing from the upper and lower ^{3}E levels, respectively. Finally, we observed a polarization selection rule which can be explained as an interference effect due to Zeeman coherence within the center which is consistent with our model of the electronic structure.

Acknowledgements

This research was sponsored in part by the Air Force Office of Scientific Research and the National Science Foundation and Technology Center for Ultrafast Optical Science (STC PHY 8920108). A. Lenef gratefully acknowledges support from the Department of Education in the form of a DSO fellowship.

References

[1] G. Davies and M.F. Hamer, Proc. Roy. Soc. London A 348 (1970) 285.
[2] J.H.N. Loubser and J.A. Van Wyk, Diamond Research (Industrial Diamond Information Bureau, London, 1977) p. 11.
[3] N.R.S. Reddy, N.B. Manson and E.R. Krausz, J. Lumin. 38 (1987) 46.
[4] D.A. Redman, S.W. Brown, R.H. Sands and S.C. Rand, Phys. Rev. Lett. 67 (1991) 3420.
[5] D.A. Redman, S.W. Brown and S.C. Rand, J. Opt. Soc. Am. B 9 (1992) 768.
[6] E. van Oort, B. van der Kamp, R. Sitters and M. Glasbeek, J. Lumin. 48&49 (1991) 803.

ARTICLES

Tunneling dynamics of squeezed states in a potential well

A. Lenef and S. C. Rand
Division of Applied Physics, 1049 Randall Laboratory, University of Michigan, Ann Arbor, Michigan 48109-1120
(Received 6 August 1993)

WKB calculations have revealed that tunneling dynamics of localized wave packets in simple potential wells depend sensitively on the degree of squeezing of the wave function. Squeezed states are shown to tunnel more slowly in general than eigenstates of the well and states which are initially localized near the bottom of a well have much lower tunneling rates than states localized at the sides of the well. The dependence of tunneling time on energy also exhibits steps related to quasi-bound-state energies in a complex way. Additionally, modulations in the tunneling probability correlate with the motion of the squeezed wave packet in the well. These results have implications both for the dynamics of squeezed radiation fields and squeezed matter states, and examples of applications to controlled vibrational-state chemistry, ultralow-noise measurements of weak signals with Josephson junctions, and optical crystals are discussed.

PACS number(s): 03.65.Ge, 32.80.Pj, 42.50.Dv

I. INTRODUCTION

Theoretical work on the class of minimum-uncertainty states known as squeezed states was initiated as early as the 1920s [1], and revived in the context of quantum optics in the 1960s [2]. However, it as not until 1995 that experimental methods were developed to generate, propagate, and detect squeezed states of the radiation field [3]. This caused an immense increase of interest in the field. To date, schemes used to generate squeezed light have included four-wave mixing in atomic vapor, four-wave mixing in fibers, second-order parametric interactions in nonlinear crystals, and pump-noise-suppressed lasers [4–6]. It has been shown that squeezed states are important for sub-shot-noise-limited interferometry and spectroscopy with sensitivity below the shot-noise limit, and quantum nondemolition measurements. As a consequence of these applications and improved understanding of the uncertainty limits of quantum measurement, interest has grown recently in the possibility of creating squeezed states of matter which may similarly exhibit unusual and useful properties [7].

In this work, the effect of squeezing on tunneling from a simple potential well to a continuum of final states is investigated. The treatment is sufficiently general to apply to squeezed states of both radiation and matter fields. However, it is primarily motivated by an interest in modifications of tunneling phenomena due to localization of matter wave packets within potential wells. Several previous studies have analyzed tunneling of squeezed states in double well quantum oscillators [8,9], but have not been extended to describe transport. Here we analyze the evolution of squeezed states in a one-dimensional parabolic well with an infinite barrier on one side and a finite barrier on the other, explicitly incorporating the concept of transport. We show that squeezing of spatial coordinates can have a significant effect on tunneling probability and introduces structure in the dependence of tunneling time on energy of the wave packet which is related to the occurrence of quasibound states. Some of the implications of the sensitivity of tunneling probability to squeezing in the context of controlled vibrational-state chemistry, macroscopic quantum tunneling, and in optical crystals are discussed.

Calculations presented in the next section use a WKB procedure to obtain wave functions and the tunneling propagator for a parabolic well coupled to a continuum region of constant potential energy. Analytic expressions are obtained for wave functions and tunneling probabilities when the system is initially prepared in a squeezed state. Subsequently we examine the case of a cubic barrier, explain the relationship between localization, quasibound states, and tunneling probability, and discuss several applications.

II. TUNNELING BY A SQUEEZED STATE

A. Wave functions

The tunneling region considered in this paper is depicted in Fig. 1, where five distinct regions (I–V) are identified for convenience. A particle with average energy E is assumed to be initially localized in the potential well on the left and tunnels into the classically allowed region on the right which is terminated by a boundary at $x=L$. The maximum potential of the barrier is denoted by V_0. The points a, b, and c are the classical turning points. In the classically allowed region beyond the barrier, the potential falls to zero at $x=w$, and maintains a constant value $-\phi$ for $x>d$, where ϕ is assumed to be positive. The potential energy in the well region (region II of Fig. 1) is assumed to be harmonic:

$$V_{\parallel}(x)=\tfrac{1}{2}m\omega_0^2x^2 . \quad (1)$$

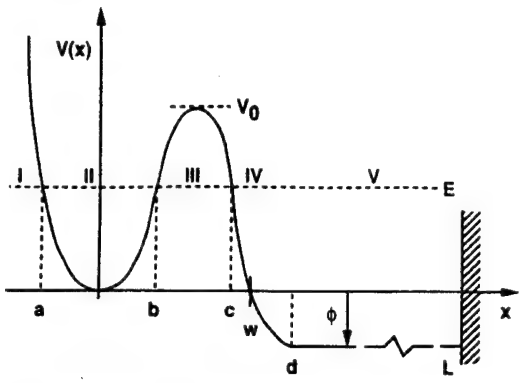

FIG. 1. Schematic of the potential well considered in this work, coupled to continuum of states at constant potential $-\phi$ and bounded by an infinite potential at $x=L$. Turning points for energy E are at $x=a$, b, and c.

Here, m is the particle mass, ω_0 is the frequency of oscillation, and x is the particle position. A characteristic length α^{-1} can be defined for the linear harmonic oscillator (LHO) wave functions corresponding to this potential well. This localization length gives the standard deviation of the particle position in the LHO ground state and is a useful quantity for discussing normalization and density of states:

$$\alpha=\sqrt{2m\omega_0/\hbar}\,. \tag{2}$$

The time evolution of a wave packet Ψ initially localized in the well is given by

$$\Psi(x,t)=\int_{-\infty}^{\infty} G(x',x;t)\Psi(x',0)dx'\,, \tag{3}$$

where $G(x',x;t)$ is the propagator which accounts for the evolution of the wave function from its initial value $\Psi(x',0)$ at time zero and position x' to its later value $\Psi(x,t)$ at time t and position x. The propagator $G(x',x;t)$ is given by

$$G(x',x;t)=\sum_k \psi_k^*(x')\psi_k(x)e^{-iE_k t/\hbar}\,. \tag{4}$$

Here, the sum is over wave vectors k in the continuum region, $x>d$, which are defined by

$$k=\sqrt{(2m/\hbar^2)(E_k+\phi)}\,. \tag{5}$$

The energies E_k of the eigenstates $\psi_k(x)$ for the potential $V(x)$ in Fig. 1 are a discrete set derived from the boundary conditions $\psi_k(L)=\psi_k(-\infty)=0$.

To obtain a simple analytic form for the propagator, we consider only states with energies which lie below the barrier peak V_0 and use a WKB approach. We neglect those states with energies close to V_0 for which the WKB approximation with linear turning points is not valid. For example, the WKB approximation breaks down for states within about $\hbar\omega_0$ of the barrier peak in a cubic potential containing roughly ten quasibound states. For moderate amounts of squeezing and energies limited to those below V_0, this condition restricts the average energy of the wave packet to within two or three $\hbar\omega_0$ below the top of the barrier.

Upon applying the appropriate connection formulas for linear turning points [10], the WKB eigenstates $\psi_k(x)$ with energies $0<E_k<V_0$ are of the form

$$\psi_k(x)=A_0U_k(x)\,, \tag{6}$$

where A_0 is a normalization constant. The unnormalized WKB solutions for the potential shown in Fig. 1 are given by

$$U_k^{\mathrm{I}}(x)=\frac{1}{\sqrt{Q}}\exp\left[-\int_x^a Q\,dx'\right],\quad x<a \tag{7}$$

$$U_k^{\mathrm{II}}(x)=\frac{2}{\sqrt{q}}\cos\left[\int_a^x q\,dx'-\frac{\pi}{4}\right],\quad a<x<b \tag{8}$$

$$U_k^{\mathrm{III}}(x)=\frac{1}{\sqrt{Q}}\sin\xi\exp\left[-\int_b^x Q\,dx'\right]+\frac{2}{\sqrt{Q}}\cos\xi\exp\left[\int_b^x Q\,dx'\right],\quad b<x<c \tag{9}$$

$$U_k^{\mathrm{IV}}(x)=\frac{\theta^{-1}}{\sqrt{q}}\sin\xi\cos\left[\int_c^x q\,dx'+\frac{\pi}{4}\right]+\frac{4\theta}{\sqrt{q}}\cos\xi\cos\left[\int_c^x q\,dx'-\frac{\pi}{4}\right],\quad c<x<d \tag{10}$$

In the continuum region we find

$$U_k^{\mathrm{V}}(x)=\frac{2}{\sqrt{k}}\left[4\theta^2\cos^2\xi+\frac{1}{4}\theta^{-2}\sin^2\xi\right]^{1/2}\times\cos\left[k(x-d)+\eta+\varphi-\frac{\pi}{4}\right],\quad x>d \tag{11}$$

where the phase factor φ is given by

$$\varphi=\tan^{-1}\left[\frac{\theta^{-2}}{4}\tan\xi\right]. \tag{12}$$

The wave vectors for the classically allowed and forbidden regions near the origin are

$$q(x)=\alpha\sqrt{[E_k-V(x)]/\hbar\omega_0},\quad x<d \tag{13}$$

and

$$Q(x)=\alpha\sqrt{[V(x)-E_k]/\hbar\omega_0},\quad x<d \tag{14}$$

respectively. In these expressions, we have made convenient use of a barrier parameter θ defined by

$$\theta=\exp\left[\int_b^c Q\,dx'\right]. \tag{15}$$

The inverse of θ^2 is the tunneling probability for an eigenstate with energy E_k. Phases accumulated between turning points in the classically allowed region have been designated by

$$\xi=\int_a^b q\,dx' \tag{16}$$

and

$$\eta=\int_c^d q\,dx'\,. \tag{17}$$

For a parabolic well, ξ has the particularly simple form

$$\xi=\frac{\pi E_k}{\hbar\omega_0}\equiv\frac{\pi\omega_k}{\omega_0}\ . \tag{18}$$

An examination of Eq. (11) reveals that the probability of the particle being found in the continuum region is close to zero for particular values of the phase parameter ξ, namely $\xi=(n+\frac{1}{2})\pi$, where n is an integer. Particles with these phases are strongly localized in the well in quasibound states which, according to Eq. (18), occur almost exactly at the LHO eigenenergies and are easily seen to have narrow energy widths on the order of $\hbar\omega_0\theta^{-2}$. For energies below the bottom of the well ($-\phi<E_k<0$), the WKB wave functions decay exponentially for $x<c$ and can be neglected in the propagator [Eq. (4)] for the case of wave packets initially localized in the well.

The normalization constant A_0 is easily determined from Eqs. (6) and (11) for wave-packet energies far from LHO eigenenergies when L is large. However, near quasi-bound-state resonances, the probability amplitude in the well region is very sensitive to energy if the condition

$$L\gg\alpha^{-1}\theta^2 \tag{19}$$

cannot be satisfied. For modest values of $\theta\approx10^4$, Eq. (19) implies that L must be on the order of centimeters if the localization of the wave packet within a well a few angstroms in size is to be meaningful. As a consequence, we consider off-resonant and near-resonant cases separately (Appendix A), finding

$$A_0=\begin{cases}\left[\dfrac{k}{2L}\right]^{1/2}\left[4\theta^2\cos^2\xi+\dfrac{1}{4}\theta^{-2}\sin^2\xi\right]^{-1/2}, & \xi\neq\pi(n+\frac{1}{2})\\ \left[4\pi\alpha^{-2}+\dfrac{2L}{k}\left[4\theta^2\cos^2\xi+\dfrac{1}{4}\theta^{-2}\sin^2\xi\right]\right]^{-1/2}, & \xi\approx\pi(n+\frac{1}{2})\ .\end{cases} \tag{20}$$

B. Density of states and the propagator

The determination of the density of states for evaluating the propagator requires similar considerations. Applying the boundary condition $\psi_k(L)=0$ to Eq. (11) implies $k(L-d)+\eta+\varphi-\pi/4=(n+\frac{1}{2})\pi$. The density of states is then given by the derivative of this quantization condition:

$$\frac{dn}{dk}=\frac{1}{\pi}\left[(L-d)+\frac{d\eta}{dk}+\frac{d\varphi}{dk}\right]\ . \tag{21}$$

Far from resonance, only the first term is significant in the limit of large L. However, as seen from Eq. (12), the phase φ also displays strong resonant behavior near the LHO eigenenergies. Including both of these terms for the general case gives the density of states

$$\frac{dn}{dk}=\frac{L}{\pi}+\frac{2k\alpha^{-2}}{4\theta^2\cos^2\xi+\frac{1}{4}\theta^{-2}\sin^2\xi}\ . \tag{22}$$

The propagator can now be evaluated by replacing the summation over k in Eq. (4) by an integral over the density of states. Applying the results of Eqs. (6), (20), and (22) yields the following expression for the propagator, valid both for on-resonance and off-resonance conditions:

$$G(x',x;t)=\frac{1}{2\pi}\int\frac{ke^{-iE_kt/\hbar}U_k^*(x')U_k(x)}{4\theta^2\cos^2\xi+\frac{1}{4}\theta^{-2}\sin^2\xi}dk,\quad x>d\ . \tag{23}$$

The denominator in the integrand of Eq. (23) becomes strongly resonant at quasi-bound-state energies. Only states $\psi_k(x)$ near these energies make important contributions to the integral. Moreover, since the initial wave functions are assumed to be strongly localized in the well, these states can be replaced by the LHO Hermite-Gaussian wave functions with appropriate normalization (Appendix A). With a change of variable from k to ω, the propagator becomes

$$G(x',x;t)=\frac{\alpha}{2\pi^{1/2}\omega_0}\sum_{n=0}^{N}(-1)^n\psi_n^{\mathrm{LHO}}(x')\int_{n\omega_0}^{(n+1)\omega_0}k^{-1/2}e^{-i\omega t}\left\{\frac{e^{i[k(x-d)+\eta-i\pi/4]}}{2\theta\cos\xi-(i/2)\theta^{-1}\sin\xi}+\text{c.c.}\right\}d\omega\ ,$$
$$x'<c,\quad x>d\ . \tag{24}$$

Here, the remaining summation is over the N quasibound states that lie below the barrier for which the WKB and parabolic approximations are valid.

The denominators in the integrand of Eq. (24) can be expanded about each resonance and are well approximated by simple poles. For $\xi\approx(n+\frac{1}{2})\pi$, the denominators can be written as

$$\frac{1}{2\theta\cos\xi\pm(i/2)\theta^{-1}\sin\xi}\cong(-1)^{n+1}\frac{\Gamma_n\theta_n}{[\omega-(n+\frac{1}{2})\omega_0]\pm i(\Gamma_n/2)}\ , \tag{25}$$

where

$$\Gamma_n = \frac{\omega_0}{2\pi\theta_n^2} . \tag{26}$$

In this approximation, we ignore frequency shifts on the order of $\omega_0\theta^{-4}$ and higher-order imaginary contributions which introduce corrections to these first-order quasibound-state decay rates. Note that we have also made explicit use of the parabolic well assumption.

To complete the evaluation of Eq. (24), we expand the phase η about frequency $\omega=(n+\frac{1}{2})\omega_0$. From Eq. (17), we find

$$\eta=\eta_n+\tau_n[\omega-(n+\tfrac{1}{2})\omega_0] , \tag{27}$$

where

$$\eta_n=\alpha\int_c^d\sqrt{(n+\tfrac{1}{2})-V(x')/\hbar\omega_0}\,dx' \tag{28}$$

and

$$\tau_n=\left[\frac{\alpha}{2\omega_0}\right]\int_c^d\frac{dx'}{\sqrt{(n+\frac{1}{2})-V(x')/\hbar\omega_0}} . \tag{29}$$

Here, η_n is the phase accumulated from traversing the classically allowed region between the barrier and the continuum; τ_n is the respective classical transit time across the same region.

Similarly, the wave vector k may be expanded about ω, yielding

$$k=k_n+\gamma_n[\omega-(n+\tfrac{1}{2})\omega_0] , \tag{30}$$

where

$$k_n=\alpha\left[n+\frac{1}{2}+\frac{\phi}{\hbar\omega_0}\right]^{1/2} \tag{31}$$

and

$$\gamma_n=\frac{\alpha^2}{2\omega_0 k_n} . \tag{32}$$

By extending the limits of integration in Eq. (24) to infinity and making use of these results, the integral can easily be evaluated by the method of residues. Retaining only the term representing a wave traveling to the right, and removing the slowly varying term $k^{-1/2}$ from the integral, the final expression for the propagator is

$$G(x',x;t)=\left[\frac{\alpha}{4\pi}\right]^{-1/2}\sum_{n=0}^{N}\left[n+\frac{1}{2}+\frac{\phi}{\hbar\omega_0}\right]^{-1/4}\theta_n^{-1}\psi_n^{\mathrm{LHO}}(x')e^{i[k_n(x-d)+\eta_n]}$$
$$\times e^{-i(n+\frac{1}{2})\omega_0 t}e^{-(\Gamma_n/2)[t-\tau_n-\gamma_n(x-d)]}\Theta[t-\tau_n-\gamma_n(x-d)] . \tag{33}$$

Here, $\Theta(x)$ is the Heaviside step function. The arbitrary exponential phase factor $\pi/4$ in Eq. (24) has been ignored.

The propagator in Eq. (33) consists of a superposition of exponentially decaying traveling waves which are delayed by corresponding classical transit times from the edge of the barrier to the continuum region. Each of the quasibound states decays with the usual WKB decay rate given by Eq. (26). The sharp turn-on of each quasibound state is related to the simple pole approximation used to evaluate the propagator. We point out that these results are also valid when the continuum lies above the bottom of the well ($\phi<0$) if the lower limit in the summation in Eq. (33) is replaced by the lowest LHO level which lies above the continuum energy. True LHO bound states in the well which lie below the continuum decay exponentially in the region $x>b$ in Fig. 1 and make negligible contributions to the probability beyond the barrier.

C. Tunneling probability

Application of Eqs. (3) and (33) to an arbitrary wave packet composed of LHO eigenstates with probability amplitudes c_n reveals that, beyond the barrier, $\Psi(x,t)$ in Eq. (33) is simply a superposition of tunneling components weighted by their appropriate c_n. The probability of escape for a wave packet initially localized in the well is defined to be

$$P(t)=\int_d^L|\Psi(x',t)|^2dx' . \tag{34}$$

Ignoring the rapid interference modulations between different quasibound states, this gives a tunneling probability of

$$P(t)=\frac{\sum_{n=0}^{N}|c_n|^2[1-e^{-\Gamma_n(t-\tau_n)}]\Theta(t-\tau_n)}{\sum_{n=0}^{N}|c_n|^2} , \tag{35}$$

when normalized to the probability of the initial wave packet lying below the barrier. This result is easily interpreted. The tunneling probability is simply the sum of the individual probabilities for each of the exponentially decaying quasibound states to tunnel through the barrier, weighted by the probability of the wave packet to be in that particular quasibound state. As $t\to\infty$, the probability in Eq. (35) approaches unity.

III. TUNNELING OF SQUEEZED STATES

A. Tunneling times

To investigate the significance of squeezing on tunneling times, we calculate the tunneling probability in Eq. (35) for the case in which the initial state $\Psi(x,0)$ is a squeezed state. To do this, we evaluate θ and η for the specific case of a cubic barrier coupled to a flat continu-

um (Fig. 1). The barrier is assumed to have a height $V_0 = 10\hbar\omega_0$, and we take the number of corresponding quasibound states to be $N = 10$. Details of the evaluation of barrier quantities are presented in Appendix B.

We consider only pure amplitude and phase-squeezed states. The initial squeezed wave packet can be represented as [11]

$$\Psi(x,0) = (2\pi)^{-1/4}(\alpha S)^{1/2} e^{-(\alpha S x/2-\beta)^2} . \quad (36)$$

The standard deviation Δx of wave-packet position within the parabolic well is $(\alpha S)^{-1}$, where S is related to a squeezing parameter R which is a linear measure of squeezing and defined by the relation $S = e^R$ [11]. If $S < 1$, the wave packet is phase squeezed and characterized by a Δx greater than the ground-state standard deviation. If $S > 1$, amplitude squeezing applies, and Δx is smaller than the ground-state standard deviation. The initial mean displacement in $2\beta(\alpha S)^{-1}$.

The initial squeezed state may easily be represented in terms of LHO states with probability amplitudes which can be calculated by various methods [11,12]. Tunneling escape times τ_t, arbitrarily defined by the condition

$$P(\tau_t) = 1 - e^{-1} , \quad (37)$$

may then be calculated by direct application of Eq. (35). This definition of escape time permits direct comparison with the purely exponential decay of LHO eigenstates. The tunneling escape times for various degrees of squeezing versus average energy are plotted in Fig. 2, together with tunneling times for eigenstates of the parabolic well. Figure 3 reveals that the tunneling times for squeezed states reach a minimum at $S \approx 1.5$ for an average energy $E = 4.5\hbar\omega_0$. Interestingly, this does not correspond to the case of a pure coherent state ($S = 1.0$). Instead, it corresponds closely to the value of S at which energy fluctuations reach a minimum, as indicated in Fig. 4 and discussed below.

To understand first how squeezing affects the energy distribution, we consider the relationship between squeezing and the energy variance $\langle (\Delta E)^2 \rangle$. This is given by

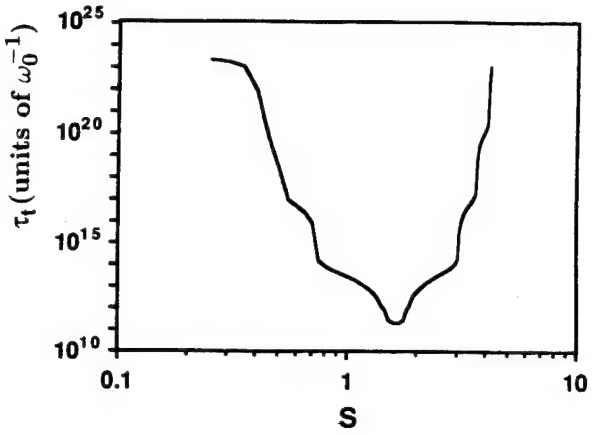

FIG. 3. Example of tunneling escape times versus squeezing parameter for an arbitrary fixed energy $E = 4.5\hbar\omega_0$.

the expression [12]

$$\langle (\Delta E)^2 \rangle = \tfrac{1}{8}(\hbar\omega_0)^2[(8\beta^2+1)S^{-4}+S^4-2] . \quad (38)$$

The energy of a squeezed state is given by a similar expression,

$$\langle E \rangle = \tfrac{1}{4}\hbar\omega_0[(4\beta^2+1)S^{-2}+S^2] . \quad (39)$$

The average energy in Eq. (39) depends both on the initial mean displacement of the squeezed state $2\beta(\alpha S)^{-1}$ as well as the position and momentum uncertainties, Δx and Δp. These in turn are proportional to S^{-1} and S, respectively. These uncertainties contribute additional kinetic and potential energy to the wave packet, increasing its energy above that of a pure coherent state with displacement β.

From Eq. (39), we see that for small displacements β the energy is dominated by uncertainties in position and momentum. For small energies ($2\beta S^{-1} \approx 0$), these uncertainties contribute equally to potential energy $(\Delta x)^2$ and kinetic energy $(\Delta p)^2$. Thus, for small energies, the total fluctuation in energy is minimized when potential and kinetic energy fluctuations are simultaneously minimized,

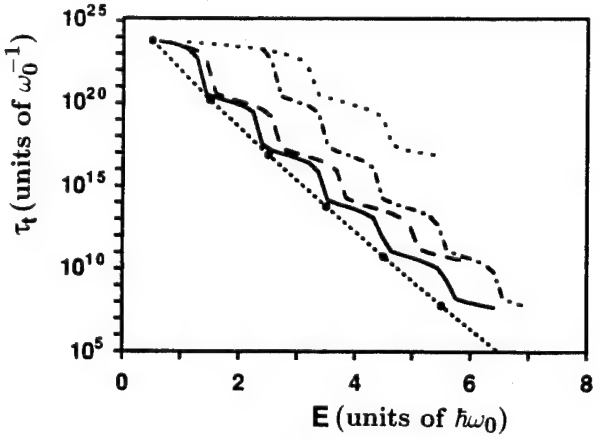

FIG. 2. Tunneling escape times versus energy for cubic barrier, plotted for various values of squeezing: $S = 0.5$ (solid), 1.0 (dashed), 1.5 (dotted), and 3.0 (chain). Barrier and continuum parameters are $V_0 = 10\hbar\omega_0$, $N = 10$, and $\phi = 2\hbar\omega_0$.

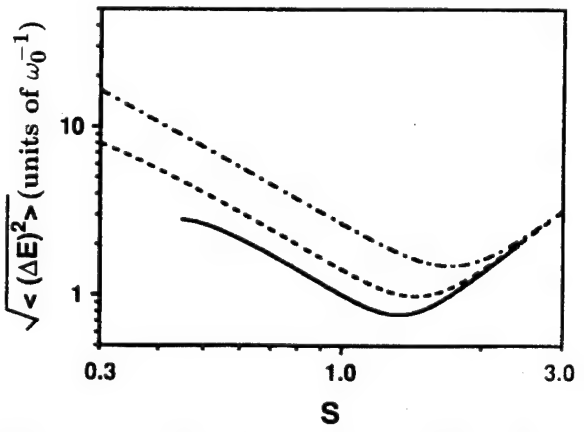

FIG. 4. Energy fluctuations of a squeezed state versus squeezing parameter S. The three curves correspond to different particle energies: $E = 2.0$ (solid), 5.0 (dashed), and 50 (dotted).

or S is close to one. On the other hand, for larger initial displacements ($2\beta S^{-1}>0$), the potential energy acquires contributions not only from position and momentum uncertainties, but from the mean displacement itself. Furthermore, large wave-packet displacements increase the *slope* of the potential energy curve, amplifying the contributions of positional fluctuations Δx. Thus, at large average energies ($2\eta S^{-1}\gg 0$), fluctuations of potential energy are weighted more heavily than fluctuations of kinetic energy. In this way, energy fluctuations can be expected to minimize for a value of S greater than one, in agreement with an algebraic minimization of Eq. (38) with respect to S which furnishes the result $S_{\min}=(1+8\beta^2)^{1/8}$.

The corresponding minimization of tunneling times occurs as a result of the LHO occupation probability distributions narrowing to a small number of LHO quasibound states as S approaches $S_{\min}$ (Fig. 5). Quasibound-state tunneling probabilities for neighboring levels vary by several orders of magnitude, so a wave packet composed of a wide distribution of LHO states requires many very long-lived quasibound states to decay before the tunneling probability becomes appreciable. However, for squeezed wave packets with $S\approx S_{\min}$, only a few short-lived, quasibound states need to decay before the wave packet has tunneled significantly. This also explains why LHO eigenstates have the shortest tunneling escape times for a given energy, as seen in Fig. 2.

In addition to the sensitivity of wave-packet escape times on squeezing, the tunneling escape times plotted in Fig. 2 also exhibit interesting steplike features near quasi-bound-state energies. These steps are related to the decomposition of the initial squeezed state into a superposition of discrete quasibound states. A squeezed state dominated by a single quasibound state exhibits tunneling behavior dominated by that level. If the average energy is increased by some fraction of $\hbar\omega_0$, then additional levels must be occupied significantly to account for this additional energy. Because of the very large differences in tunneling rates between neighboring LHO levels, significant changes in tunneling rates are to be expected as higher LHO levels become significantly occupied.

For large amounts of phase squeezing ($S=0.5$, Fig. 2) the steps in tunneling time become less prominent and do not occur at every LHO eigenenergy. Under these conditions, the broad energy distributions of phase-squeezed states cover more than one LHO level spacing so that the correspondence between particular quasibound states and individual steps is lost. The tunneling time also exhibits steplike features as a function of squeezing for fixed energies, as depicted in Fig. 3. These features similarly arise from changes in occupation of LHO discrete levels as the amount of squeezing is varied.

B. Coherences

Coherent effects become evident when the properties of the tunneled wave function can be resolved on time scales on the order of ω_0^{-1} and length scales on the order of α^{-1}. For example, the probability $|\psi(x,t)|^2$ for a pure coherent state develops deep modulations at the wave-packet oscillation frequency ω_0 as shown in Fig. 6. These modulations arise from interferences between adjacent quasibound states.

Wave-packet squeezing can emphasize higher harmonics of ω_0 and alter the shape of tunneling modulations. These effects are apparent in Figs. 7(a)–7(d), where $|\psi(x,t)|^2$ is plotted for $x=d$ with various degrees of squeezing at a fixed energy close to the LHO ground-state energy. Figure 7(a) depicts a pure coherent state with modulations at ω_0, consistent with the purely oscillatory motion of the wave-packet mean $\langle x(t)\rangle$ in the well. As the wave packet becomes amplitude squeezed, the wave-packet variance $\langle[\Delta x(t)]^2\rangle$ begins to oscillate at $2\omega_0$, so that second harmonic modulations begin to appear in the tunneling probability beyond the barrier [Fig. 7(b)]. Similarly, phase squeezing introduces second harmonics, but with the phase reversal evident in Fig. 7(c).

With maximum squeezing ($\beta=0$), wave packets localized in the well consist of superpositions of even harmonics only, with the result that breathing-type oscillations in $\langle[\Delta x(t)]^2\rangle$ occur purely at $2\omega_0$ as shown in Fig. 7(d). At higher energies, these coherent effects become less pro-

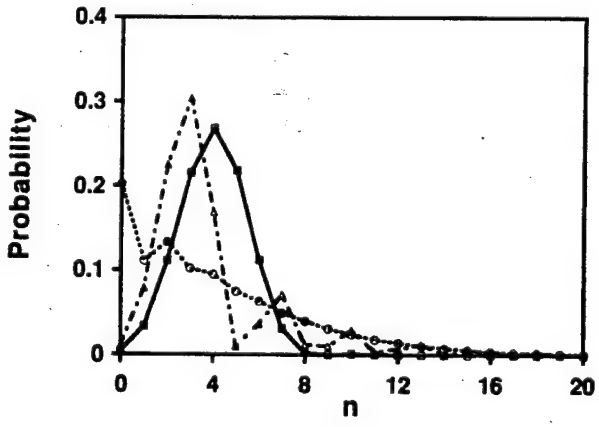

FIG. 5. Probability distribution $|c_n|^2$ for squeezed states versus occupation number n, plotted for various values of squeezing: $S=0.5$ (circles), 1.5 (squares), and 3.0 (triangles) with arbitrary fixed energy $E=4.5\hbar\omega_0$. The curves are to guide the eye.

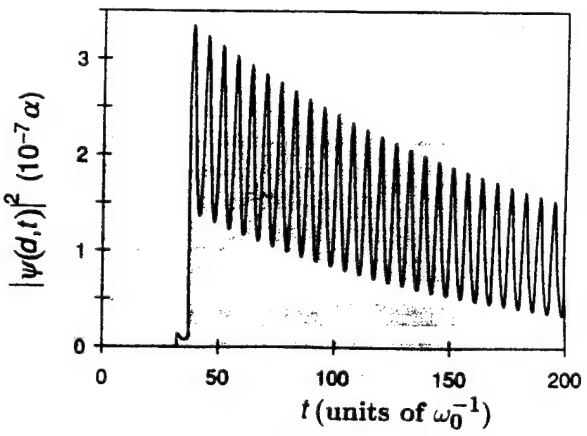

FIG. 6. Probability $|\psi(d,t)|^2$ of particle detection at point d beyond the barrier as a function of time for a coherent state with $S=1.0$ and energy $E=0.6\hbar\omega_0$. Barrier and continuum parameters are $V_0=4\hbar\omega_0$, $N=4$, and $\phi=2\hbar\omega_0$.

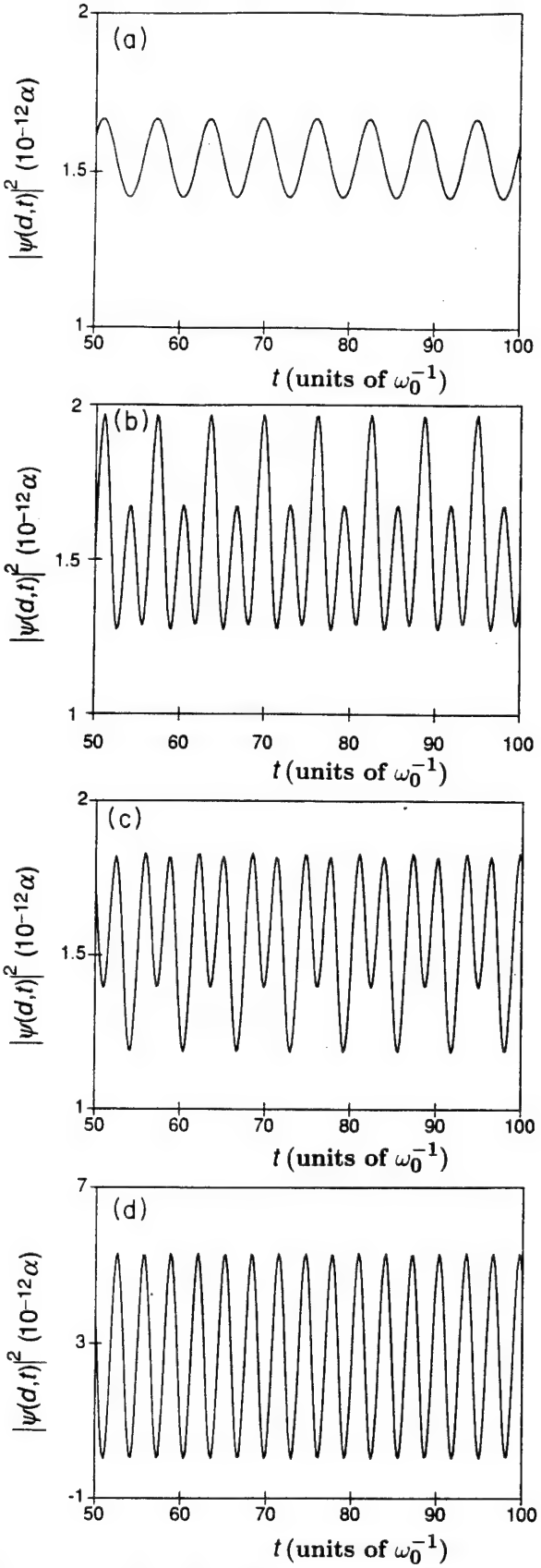

FIG. 7. Probability $|\psi(d,t)|^2$ for various degrees of squeezing and initial displacements β for particle energies exceeding the ground-state energy $E_g = 0.5\hbar\omega_0$ by only $\Delta E = 10^{-6}\hbar\omega_0$: (a) $S = 1.0000$, $\beta = 10^{-3}$; (b) $S = 1.0001$, $\beta = 9.95\times10^{-4}$; (c) $S = 0.9999$, $\beta = 9.95\times10^{-4}$; and (d) $S = 1.0010$, $\beta = 0$. Barrier and continuum parameters are $V_0 = 4\hbar\omega_0$, $N = 4$, and $\phi = 2\hbar\omega_0$.

nounced as excited quasibound states become progressively more populated. This occurs because θ_n^{-2} increases exponentially with energy level n and dominates the behavior of the tunneling probability contributions $\theta_n^{-2}|c_n|^2$ at higher energies, reducing modulation contrast. Modulations become large only when the probabilities $|c_n|^2$ decrease rapidly enough to counterbalance the θ_n^{-2} term in $\theta_n^{-2}|c_n|^2$. For squeezed states tunneling through a cubic barrier, this occurs at average particle energies approaching that of the ground state.

IV. DISCUSSION AND CONCLUSIONS

The results obtained in this paper have interesting implications for quantum control [13] of chemical systems with effective potentials of the general form shown in Fig. 1, where an energy barrier separates the initial from the final state. For example, simple molecules such as diatomic alkali metals occasionally have excited-state potentials with centrifugal barriers separating shallow quasibound regions from dissociative continua. The $^1\Pi_u$ state of Cs_2 accessed at 766.7 nm, for example, has a potential of this type [14]. In principle, for excited-state potential wells deep enough to contain several vibrational states, dissociative dynamics would then depend on the detailed nature of the initial wave packet.

Our results are most relevant, however, to cases of very deep potential wells with part or all of the well located above the dissociative asymptote. This situation is more typical of predissociative states of simple molecules like IBr (electronic predissociation [15]) and HgH (vibrational dissociation [16]). Examples among the diatomic alkali metals include the $C\,^1\Pi_u$ state of Cs_2 [17] and the $6\,^1\Sigma_g^+$ state of Na_2 [18] which form adiabats through avoided crossings with repulsive states similar to the model considered here. The influence of tunneling was specifically considered as early as the work of Farkas and Levy [19] on AlH. In such systems, our calculations indicate that initial-state preparation strongly affects the evolution of excited-state reactions. Both the amplitude and phase of individual quasibound states encompassed in the initial superposition state affect the rate of tunneling through the barrier. Reaction time scale and yield should therefore be amenable to manipulation using incident light pulses of durations less than a vibrational period with tailored amplitude, bandwidth, central frequency, and chirp to slow down or speed up chemical dynamics. In optically initiated unimolecular reactions, ultrafast dissipation of excitation to intramolecular vibrational reservoirs should be impeded by appropriate phase and chirp manipulation of incident pulses. This suggests useful extensions of the experimental techniques developed recently [20] for molecular wave-packet preparation, to exploit optical phasing in the creation of squeezed matter states analogous to squeezed states of the radiation field [11] with correspondingly modified, nonclassical dynamics.

The modification of tunneling dynamics by squeezing also has interesting consequences for dc-biased Josephson junctions and Josephson interferometers and is particularly germane to precision measurements of magnetic flux or voltage close to the shot-noise limit with these struc-

tures [21]. Here, the relevant variable is the Cooper pair center-of-mass phase difference δ in the BCS ground-state wave functions on either side of the Josephson barrier [22]. The dynamics of the phase difference δ arise from a quantum-mechanical "binding energy" $V(\delta)$ due to coupling of Cooper pairs on either side of the barrier by the tunneling interaction [23]. These dynamics have been studied extensively in both the classical regime [24] and more recently in the quantum regime at low temperatures where quantized energy levels observed in interactions with microwave radiation [25] and tunneling of the phase difference δ from potential minima in $V(\delta)$ have been observed [26].

The tunneling dynamics of the phase difference δ and corresponding junction voltage $V=(\hbar/2e)\dot{\delta}$ across a Josephson junction with capacitance C can be described by an effective quantum-mechanical Hamiltonian consisting of a potential energy

$$V(\delta)=-E_J(\cos\delta+\delta I/I_J) \tag{40}$$

and a kinetic charging energy $(2en)^2/2C$, where $2en$ is the amount of charge transferred across the junction, $I_J=2eE_J/\hbar$, and E_J is a constant related to the tunneling interaction matrix elements and density of states [23,27,28]. When the applied current I is less than I_J in Eq. (40), the potential $V(\delta)$ is locally well approximated by a cubic potential of the form shown in Fig. 1 with $\phi \gg \hbar\omega_0$. The preparation of squeezed states $\psi(\delta)$ should then be feasible by application of a constant bias current and a microwave current at $2\omega_0$ to modulate the resonant frequency of the "quantum well" [25] $\omega_0=(2\sqrt{2}eI_JC/\hbar)^{1/2}(1-I/I_J)^{1/4}$ together with seed currents at ω_0 to provide additional control of mean wave-packet displacement and phasing. This is closely analogous to optical [5] and microwave squeezing [29] by parametric interactions.

The results of this work indicate that large amounts of phase squeezing ($S \gg 1$) would strongly inhibit tunneling decay in a potential of the form given in Eq. (40), and permit improved ultralow-noise measurements of weak signals at low temperatures by squeezed states whose noise properties are well known to be highly affected by loss [30]. Furthermore, we expect these results to be important in fundamental dynamics of coupled junctions where wave-packet localization can be expected to enhance or inhibit tunneling in a fashion reminiscent of numerical simulations of forced double potential wells [31].

Optical crystals, formed by trapping laser-cooled atoms in periodic optical potential wells, constitute another system in which squeezing of atomic states could significantly affect tunneling. In this case, tunneling occurs as nonclassical motion of escaping atoms or those moving between minima of the optical field configuration. Recent results have demonstrated quantized motion of atoms trapped within optical potential wells, indicated by the presence of vibrational sidebands in resonance fluorescence spectra or in stimulated Raman spectra [32]. Just as for quasibound states of molecules, the induced vibrational manifolds of such atoms should be amenable to preparation of squeezed vibrational states [7]. The results of the present work indicate that squeezing of trapped atoms could strongly influence their tunneling rates into neighboring wells as well as their escape from the trap.

In summary, we have calculated tunneling times for squeezing states initially confined to a harmonic potential well coupled to a continuum. The fastest tunneling rates are observed for wave packets prepared with small amounts of amplitude squeezing, but their rates never exceed those of pure LHO eigenstates. On the other hand, tunneling is inhibited by large squeezing. We have also elucidated the relationship between the energy dispersion of wave packets and tunneling rates, as well as more subtle steplike behavior arising from the discrete nature of quasibound states in the well. Oscillatory behavior of the wave packet can give rise to modulations in the tunneling wave-function probability which are most visible when relative contributions to excited-state populations decrease exponentially with increasing vibrational quantum number. Finally, applications of squeezed matter wave packets have been identified for control of excited-state chemical reactions by appropriately tailored ultrafast light pulses, modification of macroscopic tunneling dynamics in Josephson junctions, and inhibition of tunneling of trapped atoms in optical crystals.

ACKNOWLEDGMENTS

The authors gratefully acknowledge E. Ben Jacob for suggesting this problem and for many helpful discussions. We would also like to thank K. T. Hecht for helpful conversations. Partial support of this research was provided by the Air Force Office of Scientific Research (H. Schlossberg).

APPENDIX A

The question of normalization of wave functions may be handled by first matching the WKB solutions $U_{k_n}(x)$ to the normalized LHO eigenstates in the semiclassical limit. By explicit integration, the WKB solution in Eq. (8) for a parabolic well yields

$$U_{k_n}^{\mathrm{II}}(z)=(2\alpha)^{1/2}\left[4\left[n+\frac{1}{2}\right]-z^2\right]^{-1/4} \times\cos\left[\frac{\pi}{4}-\frac{\pi}{2}\left[n+\frac{1}{2}\right]+\vartheta\right], \tag{A1}$$

where $z=\alpha x$. The phase ϑ is given by

$$\vartheta=-\frac{z}{4}\left[4\left[n+\frac{1}{2}\right]-z^2\right] + \left[n+\frac{1}{2}\right]\sin^{-1}\left[\frac{z}{2(n+\frac{1}{2})}\right]. \tag{A2}$$

In the limit of large quantum numbers, this result matches the asymptotic expansion for the parabolic cylinder functions $D_n(-z)$ to within a constant of pro-

portionality [33]. For integer values of n, the parabolic cylinder functions reduce to Hermite-Gaussian LHO solutions. Comparing the WKB solution in Eqs. (A1) and (A2) to the normalized asymptotic LHO solutions for integer n reveals

$$U_n(x)=2(-1)^n\pi^{1/2}\alpha^{-1}\psi_n^{\mathrm{LHO}}(x), \quad x<c \tag{A3}$$

where

$$\psi_n^{\mathrm{LHO}}(x)=2^{-n/2}(2\pi)^{-1/4}\alpha^{1/2}e^{-\alpha^2x^2/4}\mathrm{H}_n(\alpha x/\sqrt{2}) . \tag{A4}$$

Here, $\mathrm{H}_n(x)$ are Hermite polynomials of order n.

We can now calculate the normalization constant A_0 for the on-resonance and off-resonance cases by integrating $|\psi(x)|^2$ in Eq. (6) over all space. When the resonance condition $\xi=\pi(n+\frac{1}{2})$ is not met, only the wave-function amplitude in continuum region contributes significantly to the total wave-function probability. Integrating $|U_k^{\mathrm{V}}(x)|^2$ over the continuum region gives the off-resonant result in Eq. (20). However, close to quasi-bound-state resonances, the wave-function amplitude in the well region becomes appreciable. Replacing the WKB wave functions in the well region [Eqs. (7)–(9)] with the LHO wave functions normalized to the WKB solutions in Eq. (A3), we find A_0 is approximately

$$A_0=\left[4\pi\alpha^{-1}\int_{-\infty}^{d}|\psi_n^{\mathrm{LHO}}(x')|^2dx' + \int_d^L|U_{k_n}^{\mathrm{V}}(x')|^2dx'\right]^{-1/2}, \quad \xi\approx\pi(n+\tfrac{1}{2}) . \tag{A5}$$

The small contributions just beyond the barrier (region IV) have been neglected. Evaluating Eq. (A5) explicitly yields the result for the on-resonant case in Eq. (20).

APPENDIX B

In this appendix, we compute the barrier parameters for the specific case of a cubic potential. The cubic potential in Fig. 1 has the general form

$$V(x)=(27V_0/4)x^2(w-x)/w^2 . \tag{B1}$$

At the LHO eigenenergies $E=\hbar\omega_0(n+\frac{1}{2})$, the tunneling parameter [Eq. (15)] is

$$\theta_n=\exp\left[\alpha\int_b^c\sqrt{V(x)/\hbar\omega_0-(n+\tfrac{1}{2})}dx'\right] , \tag{B2}$$

where b and c are the barrier turning points. To obtain accurate results for intermediate energies, the integral in (B2) is evaluated exactly. This can be performed by factoring the cubic polynomial in the radical of the integrand in Eq. (B2). The zeros of the polynomial are simply the three turning points a, b, and c. The integral can be expressed in terms of the Gauss-hypergeometric function [34]. The resulting tunneling parameter becomes

$$\theta_n=\exp(I_n) , \tag{B3}$$

where I_n is

$$I_n=\left[\frac{\pi}{4}\right]B^2(y_2-y_1)^{1/2}(y_3-y_2)^2 \times{}_2F_1\left[-\frac{1}{2},\frac{3}{2};3;-\frac{y_3-y_2}{y_2-y_1}\right] . \tag{B4}$$

The parameters $y_3>y_2>y_1$ are the turning points in units of w and are roots of the cubic equation

$$B^2y^2(y-1)+(n+\tfrac{1}{2})=0 . \tag{B5}$$

The constant B is given by

$$B=\sqrt{27V_0/4\hbar\omega_0} . \tag{B6}$$

The phase parameter η_n and the classical delay time τ_n, given by Eqs. (28) and (29), are most easily evaluated by assuming the potential in region IV of Fig. 1 is linear. We simply state the results:

$$\eta_n=\left[\frac{4}{3B}\right]\left[\eta+\frac{1}{2}+\frac{\phi}{\hbar\omega_0}\right]^{3/2} \tag{B7}$$

and

$$\tau_n=2B\omega_0\left[n+\frac{1}{2}+\frac{\phi}{\hbar\omega_0}\right]^{3/4} . \tag{B8}$$

[1] E. H. Kennard, Z. Phys. **44**, 326 (1927).

[2] E. Takahashi, in *Advances in Communications Systems*, edited by V. Balakrishnan (Academic, New York, 1965), p. 227.

[3] R. E. Slusher, L. W. Hollberg, B. Yurke, J. C. Mertz, and J. F. Valley, Phys. Rev. Lett. **55**, 2409 (1985).

[4] R. M. Shelby, M. D. Levenson, S. H. Perlmutter, R. G. Devoe, and D. F. Walls, Phys. Rev. Lett. **57**, 691 (1986).

[5] L. A. Wu, H. J. Kimble, J. L. Hall, and H. Wu, Phys. Rev. Lett. **57**, 2520 (1986).

[6] Y. Yamamoto, S. Machida, and O. Nilsson, Phys. Rev. A **34**, 4025 (1986).

[7] J. I. Cirac, A. S. Parkins, R. Blatt, and P. Zoller, Phys. Rev. Lett. **70**, 556 (1993).

[8] H. Dekker, Phys. Lett. A **119**, 10 (1986).

[9] D. Mugnai, A. Ranfagni, M. Montagna, O. Pilla, and G. Viliani, Phys. Rev. A **40**, 3397 (1989).

[10] E. Merzbacher, *Quantum Mechanics* (Wiley, New York, 1970), p. 121.

[11] H. P. Yuen, Phys. Rev. A **13**, 2226 (1976).

[12] R. W. Henry and S. C. Glotzer, Am. J. Phys. **56**, 318 (1988).

[13] W. S. Warren, H. Rabitz, and M. Dahleh, Science **259**, 1581 (1993).

[14] P. Kusch and M. Hessel, J. Mol. Spectrosc. **32**, 181 (1969).

[15] M. B. Faist and R. B. Bernstein, J. Chem. Phys. **64**, 2971 (1976).

[16] G. Herzberg, *Spectra of Diatomic Molecules* (Van Nostrand Reinhold, Toronto, 1950), p. 427.

[17] G. Rodriguez and J. G. Eden, Chem. Phys. Lett. **205**, 371 (1993).

[18] C.-C. Tsai, J. T. Bahns, and W. C. Stwalley, J Chem.

Phys. (to be published); C.-C. Tsai, J. T. Bahns, T.-J. Whang, H. Wang, and W. C. Stwalley, Phys. Rev. Lett. (to be published).

[19] L. Farkas and S. Levy, Z. Phys. **84**, 195 (1933).

[20] T. J. Dunn, J. N. Sweester, I. A. Walmsley, and C. Radzewicz, Phys. Rev. Lett. **70**, 3388 (1993); M. Dantus, M. J. Rosker, and A. H. Zewall, J. Chem. Phys. **87**, 2395 (1987).

[21] S. T. Pavlov and A. V. Prokhorov, Fiz. Tverd. Tela (Leningrad) **33**, 2460 (1991) [Sov. Phys. Solid State **33**, 1384 (1991)]; **34**, 97 (1992) [**34**, 50 (1992)].

[22] R. P. Feynman, *Statistical Mechanics* (Benjamin, Reading, MA, 1972).

[23] D. J. Scalapino, in *Tunneling Phenomena in Solids*, edited by E. Burnstein and S. Lundqvist (Plenum, New York, 1969), Chap. 32.

[24] D. N. Langenberg, in *Tunneling Phenomena in Solids*, edited by E. Burnstein and S. Lundqvist (Plenum, New York, 1969), Chap. 33.

[25] M. H. Devoret, J. M. Martinis, D. Esteve, and J. Clarke, Helv. Phys. Acta **61**, 622 (1988).

[26] R. F. Voss and R. A. Webb, Phys. Rev. Lett. **47**, 265 (1981); D. Esteve, J. M. Martinis, C. Urbina, E. Turlot, M. Devoret, H. Grabert, and S. Linkwitz, Phys. Scr. **129**, 121 (1989).

[27] A. O. Caldeira and A. J. Leggett, Ann. Phys. (N.Y.) **149**, 374 (1983).

[28] E. Shimshoni and E. Ben-Jacob, Phys. Rev. B **43**, 2705 (1991).

[29] R. Movshovich, B. Yurke, P. G. Kaminsky, A. D. Smith, A. H. Silver, R. W. Simon, and M. V. Schneider, Phys. Rev. Lett. **17**, 1419 (1990).

[30] L. Wu, M. Xiao, and H. J. Kimble, J. Opt. Soc. Am. B **4**, 1465 (1987).

[31] W. A. Lin and L. E. Ballentine, Phys. Rev. Lett. **65**, 2927 (1990).

[32] P. S. Jessen, C. Gerz, P. D. Lett, W. D. Phillips, S. L. Rolston, R. J. C. Spreeuw, and C. I. Westbrook, Phys. Rev. Lett. **69**, 49 (1992); P. Verkerk, B. Lounis, C. Salomon, C. Cohen-Tannoudji, J. Courtois, and G. Grynberg, *ibid.* **68**, 3861 (1992); G. Grynberg, B. Lounis, P. Verkerk, J.-Y. Courtois, and C. Salomon, *ibid.* **70**, 2249 (1993).

[33] *Handbook of Mathematical Functions*, edited by M. Abramowitz and I. A. Stegun (Dover, New York, 1970), p. 690.

[34] I. S. Gradshteyn and I. M. Ryzhik, *Tables of Integrals, Series, and Products* (Academic, Orlando, 1980).

Mode-Locking Applications of Nonlinear Cooperative Interactions

S.C. Rand, H. Ni, Q. Shu, D. Kreysar and P. Xie
Division of Applied Physics, 1049 Randall Lab, University of Michigan
Ann Arbor, MI 48109-1120

and T. Morse
Division of Engineering, Brown University
Providence, RI 02912

ABSTRACT

We present results on the first application of upconversion dynamics for short pulse generation in visible solid state lasers. We also describe prospects for passive mode-locking mechanisms based on cooperative nonlinearities and instabilities.

I. INTRODUCTION

In recent years, Coulombic interactions between impurity atoms in concentrated laser media have attracted attention in the context of continuous-wave upconversion lasers and enhanced operation of conventional solid state lasers [1,2]. However, at least two aspects of cooperative dynamics of rare earth ions in concentrated solids have interesting implications for ultrashort pulse generation. In this paper, the unique ability of cooperative upconversion to furnish visible sources of mode-locked pulses in solids is first outlined. Then, the potential use of cooperative nonlinearities as a new mechanism for passive mode-locking of Nd and other solid state lasers is explored.

The development of continuous-wave and cw mode-locked sources at short wavelengths in solid state media is a challenging problem. Many factors contribute to this, but chief among them are losses associated with transient color center and band edge absorptions at pump and lasing wavelengths. This problem is compounded by the scarcity of pump sources at short wavelengths. One approach which overcomes such difficulties is the use of upconversion, shown in recent years to permit short wave laser operation sustained by long wave excitation. Cooperative upconversion in particular is considered here as a means of furnishing useful gain in the visible and ultraviolet regions for direct generation of short pulses by active mode-locking [3].

Additionally, we explore the potential of the nonlinear susceptibility generated by cooperative processes as a novel mechanism for passive mode-locking. Both the nonlinear response due to population dynamics and that due to delocalization of rare earth interactions are examined for prospects of new sources with self-starting, passively mode-locked operation achieved through cooperative dynamics.

EXPERIMENTS

Using apparatus described previously [4], cw mode-locked pulse generation in the green spectral region was demonstrated using cooperative upconversion of Erbium ions in 5% Er:$LiYF_4$ excited by infrared radiation at 1.5 μm. Infrared pumping was provided by a cw NaCl color center laser tuned with a grating to the first absorption resonance of trivalent Erbium. A 3 mm thick laser crystal was cooled to 9K inside a dewar which also contained all of the cavity optics except the output coupler in a standing wave geometry with astigmatism correction. A self-resonant, piezo-acoustic mode-locker fabricated from $LiNbO_3$ was inserted at Brewster's angle in the collimated arm of the cavity external to the dewar. Using active AM mode-locking at a repetition rate of 119 MHz, pulse trains were then generated continuously at 544 nm when the cavity length was adjusted to within 50 μm of the

synchronous length near 60 cm. Instrument-limited pulsewidths of 180 ps were observed in real time using a fast photodiode and a 20 GHz sampling oscilloscope.

In a second set of experiments, light from a cw Nd:YAG laser was focused into a single mode silica fiber doped with 2% Tm^{3+}. A maximum of 70 mW at 1.06 μm was coupled into the fiber. The fundamental Nd wavelength is not in resonance with any ground state absorption of Tm^{3+} but nevertheless caused strong excitation, visible to the naked eye. Blue upconversion emission from excited Thulium ions was monitored through interference filters at the exit of a 10 m fiber, and measurements made to determine the dependence of upconversion on input power. At the same time, evidence was sought for a measurable threshold in the upconversion emission, indicative of avalanche upconversion [5,6] rather than step-wise, multi-photon absorption among excited states [7].

RESULTS

Cooperative upconversion among Er ions in $LiYF_4$ was able to sustain continuous-wave, mode-locked operation of a solid state laser in the green spectral region at liquid helium temperatures. The output pulse train is shown in Fig. 1.

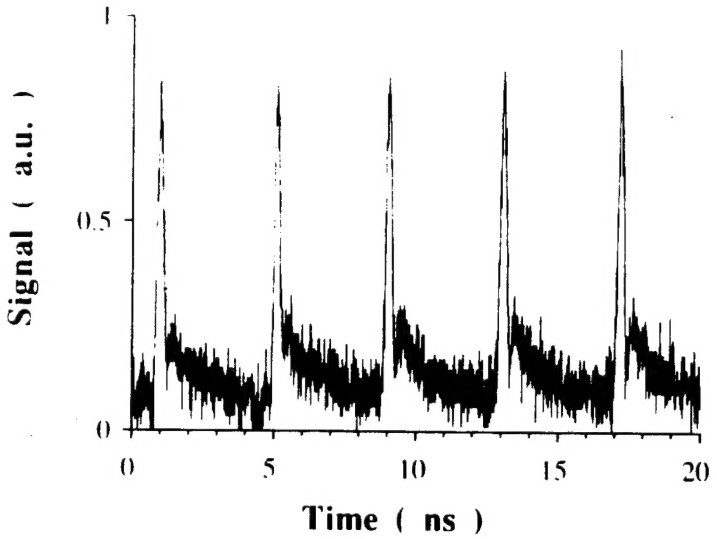

Figure 1. Mode-locked output versus time at 0.5440 μm for an infrared pump power at 1.5 μm of 500 mW power focused to a spot radius of 18 μm in the gain medium. T=9K.

The dependence of pulsewidth on output mirror position is shown in Fig. 2. An interesting result of restricting the inversion mechanism to cooperative processes was that the tendency of Er:$LiYF_4$ to undergo self Q-switching on the transition at 551 nm [8] when pumped by multi-photon absorption upconversion processes was avoided. Average output power was low, only 2 mW compared to 20 mW obtained in cw operation under identical conditions without the piezo-acoustic modulator. Evidently this was due to unexpectedly high losses in the mode-locker. Work in progress on a new MgO:$LiNbO_3$ modulator, designed to avoid photorefractive losses caused by intense, visible intra-cavity radiation in this upconversion laser, should lead to substantially higher output power.

In the second part of this work, examination of the upconversion excited by 1.06 μm irradiation of Tm-doped fibers revealed the dependence on input power shown in Figure 3. Emission intensity in this figure is directly proportional to 1.06 μm absorption from the $^3F_4$ state of Tm^{3+} and clearly indicates that absorption increases non-linearly at this wavelength as excitation is increased. The figure also gives preliminary evidence of a threshold for this behavior at very low intensity.

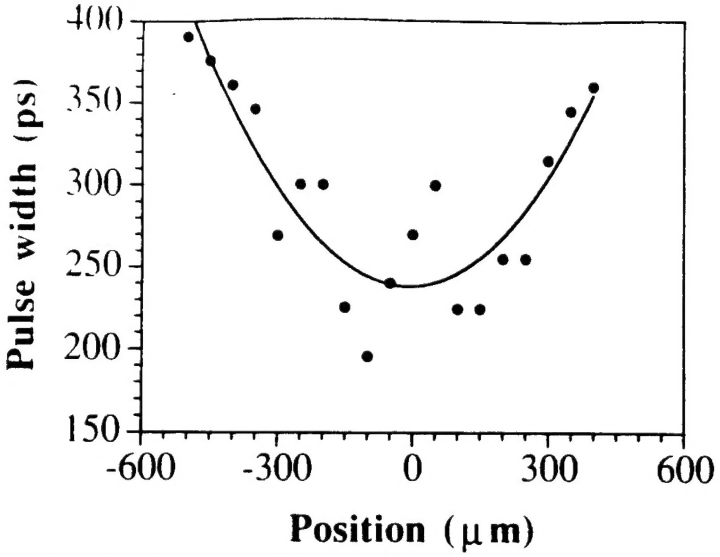

Figure 2. Mode-locked pulse width versus position of the output coupler. The solid curve is the best fit of a quadratic regression.

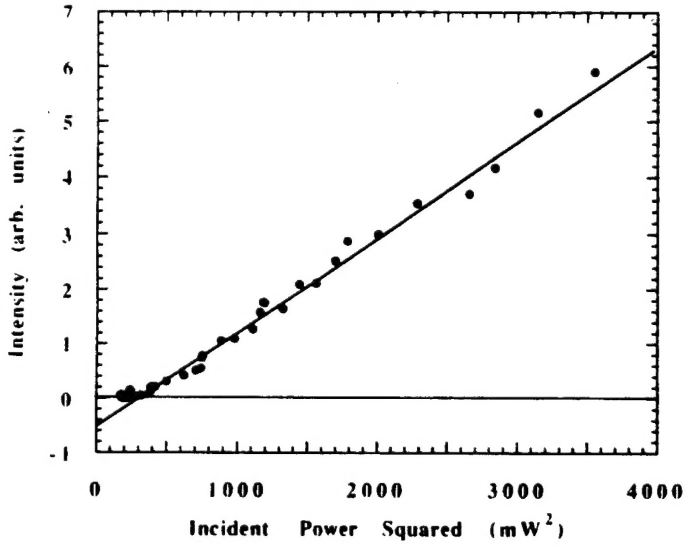

Figure 3. Fluorescence intensity at 480 nm ($^1G_4 \rightarrow {}^3H_6$) from Tm^{3+} impurities excited at λ_{ex}=1.06 μm with a Nd:YAG laser focused into a silica fiber. Core diameter of the fiber was 5.1 μm and dopant concentration was 20,000 ppm. The core/cladding index difference was 0.00675.

DISCUSSION

The results of Figures 1 and 2 were obtained by actively mode-locking a gain medium with an inversion sustained entirely by upconversion of infrared radiation. They demonstrate the viability of this novel approach to direct generation of short pulses in the visible spectral range from solid state sources. Significant improvements can be anticipated from the use of modulators which avoid photorefractive damage and from the identification of room temperature upconversion materials.

In addition to providing stimulated emission at new frequencies, cooperative upconversion processes also give rise to optical nonlinearities which may be useful in novel schemes for passive mode-locking.

For instance, the data in Fig. 3 reveal nonlinear absorption with an apparent threshold of 20 mW and quadratic intensity dependence on incident power, indicating that such nonlinearities may even be useful in heavily-doped fiber lasers. Saturation of an ordinary 3-photon ESA process seems an unlikely mechanism for Fig.3 data at the power levels of this experiment. We tentatively conclude that avalanche absorption, a cooperative effect, accounts for this interesting behavior at the Nd^{3+} laser wavelength. While three photons are required to reach the $^1G_4$ state in principle, upconversion should indeed be quadratic in the presence of an avalanche, since the onset of strong cross relaxation effectively saturates the first optical transition [6]. Drawing on these results, and on the recent report of instabilities mediated by delocalization of excitation in upconversion lasers [9], we now discuss new ways in which cooperative nonlinearities in laser gain media may furnish passive mode-locking.

First, with their unusual property of increased absorption with increased pumping, avalanche processes can be expected to suppress cw laser action and promote short pulse generation in a simple way. One might consider for instance a Tm,Nd co-doped fiber laser in which Tm impurities serve to introduce significant losses (above avalanche threshold) for cw laser operation at 1.06 μm, restricting operation to a short pulse regime characterized by saturation of the ESA at 1.06 μm. In such an application, the repetition rate need not be limited by the avalanche decay time but rather by the ESA saturation recovery time which is typically much shorter.

Internal gain suppression at 1.06 μm by cooperative absorption of Tm could also be used to promote laser operation (cw or mode-locked) at alternative Nd wavelengths with lower gain cross sections, such as 0.9 or 1.3 μm. At these wavelengths, ellipse rotation caused by (off-resonant) avalanche-induced birefringence would be experienced by intra-cavity light [10]. This effect could then mediate self mode-locking in "nonlinear mirror" fiber laser designs [11], avoiding avalanche absorptive losses at the lasing wavelength.

Finally, pulsing instabilities due to delocalization of rare earth excitation in cooperative upconversion lasers have recently been reported [9]. Their repetition rate is dependent on the upconversion rate, lifetimes of the active ion, and the photon density. Population pulsations due to this mechanism have been predicted to occur even in upconversion media without feedback. Hence instabilities of this type are self-starting in principle and have a calculable primary frequency. A self-starting, cooperatively mode-locked laser could take advantage of this mechanism to provide short wavelength sources. Such a device might be realized by matching the cavity round trip time to the pulsation period.

The authors wish to acknowledge sponsorship by the U.S. Air Force Office of Scientific Research (H. Schlossberg) and partial support by the National Science Foundation's Science and Technology Center for Ultrafast Optical Science (STC PHY 8920108).

References:

1. L.F. Johnson and H.J. Guggenheim, Appl. Phys. Lett. 19, 44(1971); P. Xie and S.C. Rand, Opt. Lett. 15, 848(1990).
2. R.C. Stoneman and L. Esterowitz, Opt. Lett. 17, 816(1992).
3. P. Xie and S.C. Rand, Opt. Lett. 17, 1116(1992).
4. P. Xie and S.C. Rand, Opt. Lett. 17, 1198(1992).
5. J. Chivian, W. Case and D. Eden, Appl. Phys. Lett. 35, 124(1979).
6. H. Ni and S.C. Rand, Opt. Lett. 16, 1424(1991).
7. M. Monerie, T. Georges, P.L. Francois, J.Y. Allain, D. Neveux, Electron. Lett. 26, 320(1990).
8. L.F. Johnson and H.J. Guggenheim, Appl. Phys. Lett. 20, 474(1972).
9. P. Xie and S.C. Rand, "Nonlinear Dynamics of Cooperative Upconversion", J.O.S.A. B, Feature Issue on Upconversion Lasers (submitted).
10. Q. Shu and S.C. Rand, Cooperative Kerr Effect in Avalanche Media (to be published).
11. M. Hofer, M. Fermann, F. Haberl, M. Ober, and A.J. Schmidt, Opt. Lett. 16, 592(1991).